Chapter 2

PHYSICAL CHARACTERISTICS OF INTERPLANETARY SPACE[1]

S. N. VERNOV, Yu. I. LOGACHEV

Scientific Research Institute of Nuclear Physics, Moscow State University, USSR

AND

N. F. PISARENKO

Institute of Space Research, Academy of Sciences USSR, Moscow

THE SUN

The properties of interplanetary space are determined, to a considerable extent, by the central body of the solar system—the Sun—which is the source of powerful streams of corpuscular and electromagnetic radiation, and is responsible for the structure of the interplanetary magnetic fields.

Many phenomena on the Earth are closely related to processes occurring on the Sun. The mechanism of this relationship is not yet fully understood, but it is clear that the solar wind, the corpuscular streams, and short-wave electromagnetic radiation of the Sun play a prominent role in these processes. Before describing the manifestations of Sun-Earth relationships, the elements of solar activity should be discussed.

Solar Activity

Solar activity, a combination of various phenomena occurring in the atmosphere of the Sun, is distinguished by significant changes in the physical characteristics of the various strata of the solar atmosphere. The close relationship between the active processes in the photosphere (spots, faculae), chromosphere (flares, flocculi), and corona (protuberances, condensation, radiating areas), and the decisive role of the magnetic field in these processes are obvious.

The magnetic fields, the presence of which has been detected everywhere in the solar atmosphere, play a significant, and in many cases the primary role in the physical processes on the Sun. A general magnetic field of the Sun has also been detected; the field of the Sun is different at different latitudes. In the polar areas ($|\phi| > 55°$), its intensity is about 1 G, and differs slightly from a dipole field. The magnetic field force lines over the poles, judging from the configuration of the coronal rays, diverge more slowly

[1] Translation of, Fizicheskaya Kharakteristika Mezhplanetnogo Prostranstva, Volume 1, Part 1, Chapter 2, of *Osnovy Kosmicheskoy Biologii i Meditsiny* (*Foundations of Space Biology and Medicine*), Moscow, Academy of Sciences USSR, 1973, 149 pages.

The authors acknowledge with appreciation the significant work by J. Van Allen in the preliminary preparation of data for this chapter, as well as A. G. Aiken. They also sincerely thank S. L. Mandel'shtam, Yu. I. Gal'perin, K. I. Gringauz, O. L. Vaysberg, T. N. Nazarov, Ye. V. Gorchakov, and S. N. Kuznetsov for help in compiling the review. Contributors from the USSR were R. I. Ivanov and M. Sugiura; from the USA, W. M. Alexander, S. J. Bauer, J. P. Heppner, W. N. Hess, C. W. McCracken, G. D. Mead, N. Ness, R. Palmeira, G. Pieper, and I. A. Zhulin.

than for an ordinary dipole, and show no tendency to bend in the direction of the Equator. This field with about 1 G intensity observed near the poles of the Sun in the photosphere decreases to 0.5 G at an altitude of about $3 \cdot 10^5$ km. High-resolution measurements have shown that the overall field consists of a multitude of fine elements of different polarities and sizes. The field intensity in some of these elements reaches 10–20 G, with one polarity usually predominating. Coarse observations show a weak field of one sign due to averaging.

In the moderate and low latitudes ($|\phi| < 50°$), local magnetic fields which generally coincide with active formations on the Sun are observed. Large-scale local formations include bipolar (BM), which are most frequently observed and unipolar (UM) magnetic areas. The field intensity in these areas varies over broad limits from 0.2 G to hundreds of G, the sign of the field differing in different parts of the area. The field intensity in a BM area and the area dimensions are inversely related. The area follows a certain cycle of development from the beginning to the end of its existence (several months); the greatest intensity is observed after about 27 d, then it decreases as the area begins to increase in size, possibly reaching about 0.3 $R_\odot$.

Within a BM, there may sometimes be a group of spots ranging in field intensity from about 500 to 4000 G. The BM areas are apparently the primary cause of groups of spots developing. BM fields and spots are usually stretched out along a parallel, corresponding with the direction of general Sun rotation. The first parts of regions and of spot groups are called the leading ones and are designated by the letter "r," and the latter ones are called the closing ones and designated by the letter "f." Fields of leading spots and BM fields have opposite polarity in the northern and southern hemispheres of the Sun and change their sign at the beginning of each new cycle of solar activity (Hoyle polarity laws). These polarity laws are more closely followed for BM areas than for spots.

The unipolar magnetic (UM) areas have weaker field intensity, greater area, and longer life than the BM areas; field intensity is ≤ 2 G, dimensions are about 0.1 $R_\odot$, and lifetime is about 6–8 months. UM fields apparently terminate in high-latitude fields and are the remainders of disappearing BM areas. The development of BM and UM areas, preceded by the appearance of active areas on the Sun, is terminated after their disappearance.

Observations using modern, high-resolution instruments have revealed short-lived small-scale magnetic fields, intermediate in intensity between the BM group fields and the fields of the spots. They are related to the flocculi, pores, small spots, and other active formations in the atmosphere of the Sun.

Sunspots, the dark areas on the surface of the Sun, consist of umbras and penumbras. Granulation is observed in the area of an umbra, while the area of a penumbra consists of radial fibers. The umbra of a sunspot is below the photosphere, while the penumbra forms a sort of funnel. The effective temperature of the umbra is about 4270° K; that of the penumbra about 5380° K. Gas flows from the center of the spot into the penumbra (Evershed effect) at about 2 km/s, the motion disappearing at the edge of the penumbra. The outflow velocity decreases with altitude and changes its direction at the limits of the chromosphere, so that the gas at this point is flowing back toward the center of the spot. There are some indications of rotary motion of the spot as a whole. A light ring forms around the penumbra which is 3%–4% brighter than the photosphere. The diameters of spots range from thousands to tens of thousands of km. The smallest spots, pores, which have no penumbras, make up the majority of all spots. Spots are rarely individual, but usually observed in groups stretching to 100 000 km.

Groups are classified according to polarity: unipolar (type α, 10% of all groups)—spots of identical polarity; bipolar (type β, 90%)—two main spots of opposite polarity; and complex (type γ, about 1%)—spots of different polarities scattered without order. Groups of spots are observed in the so-called "regal zones" ($5° \leq |\phi| \leq 45°$).

The number of spots visible on the surface of the Sun changes cyclically with a mean period of about 11.2 years. The measure of the number of spots is the relative number of spots (Wolf

number): $W = k(10g + f)$, where g is the number of groups of spots, f is the number of individual spots, and k is a reduction factor on the order of 1. Information on the number of sunspots is published [72, 131].

The placement of spots on the visible disk of the Sun changes with the phases of the solar activity cycle, although the position of a spot changes little during its existence. At the beginning of the cycle, spots arise at latitudes of $\pm 35°$, near the maximum at latitudes $\pm 16°$, while at the end of the cycle—at about $\pm 8°$ (Sperer law). Some refinements have been made to this regularity in recent years.

The magnetic field at the center of a spot's umbra is almost vertical and never less than 200 G, reaching 2000–4000 G during the maximum phase of development. In the penumbra, the field is horizontal in direction and at the edge is about 300 G. The role of convective transfer of energy, slight in the photosphere, apparently increases in the area of the spots. Groups of spots are usually extended along parallels, but the leading spot is located near the Equator. A typical group begins to develop with the appearance of pores, from which the spots develop; their area and magnetic field increase for several days. The group reaches its maximum development and begins to break out in 2–3 weeks. The tail spot and most of the smaller spots disappear first, and the group becomes unipolar; the leading spot is retained until its diameter becomes less than 30 000–45 000 km, after which it breaks up rapidly. A group may exist for a few hours to a few months.

Faculae

Sunspots are always accompanied by faculae, light fibrous formations in the photosphere, which also may exist independently of spots. Faculae appear before spots and remain for several revolutions of the Sun after the spots disappear. The range of their latitudes is somewhat greater than that of spots. In white light, faculae are not visible at the center of the disk. For 3–4 d, faculae may be observed near the eastern and western edges of the disk; the upper parts of the faculae are hotter than the surrounding photosphere by about 200°–300°, the lower parts are cooler. Faculae are localized in areas where the magnetic field intensity $H > 2$–5 G. At latitudes around $\pm 70°$, polar faculae are observed, which are smaller (about 2000 km), shorter lived (about 0.5 h), and circular in form.

Flocculi

The upper layers of photospheric faculae become chromospheric faculae or flocculi, which can be observed in the violet lines of ionized calcium H and K (calcium flocculi) and in the red line of hydrogen H (hydrogen flocculi). The latter are smaller and less stable. Flocculi are heterogeneous formations with great fluctuations in brightness, temperature, rate of movement, and magnetic field intensity at various points. The lifetime is greater than that of spots, from a few days to a few months. Flocculi are also observed without spots, but they are less stable. In contrast to spots, they are located throughout the visible disk, but near the poles are less bright, unstable, and rounder. The fine structures of flocculi are closely related to the magnetic fields; most of their fibers are oriented along the lines of forces of the magnetic field. The intensity of flocculi increases on days of appearance and disappearance of spots.

Solar flares, the most active formations on the Sun, appear suddenly over a small area (tens of thousands km). Weak flares last 5–10 min; powerful flares last several hours. They appear in the upper chromosphere or corona, always above a field of faculae near complex groups of type γ spots and near neutral lines of the longitudinal magnetic field, where high field gradients are observed. Large flares correspond to gradients of 0.1 G/km. The number of grade 1 flares is an order of magnitude higher than the number of grade 3 flares. The classification of flares is shown in Table 1 [73].

A flare is accompanied by sporadic UV, x-ray, and radio radiation and by the ejection of particles of various energies up to high-energy solar cosmic rays (see section, THE INTERPLANETARY MEDIUM). Apparently, the generation of high-energy particles is a basic characteristic of flares. Hard x-rays arise in the area of flares or above them as a result of bremsstrahlung of electrons

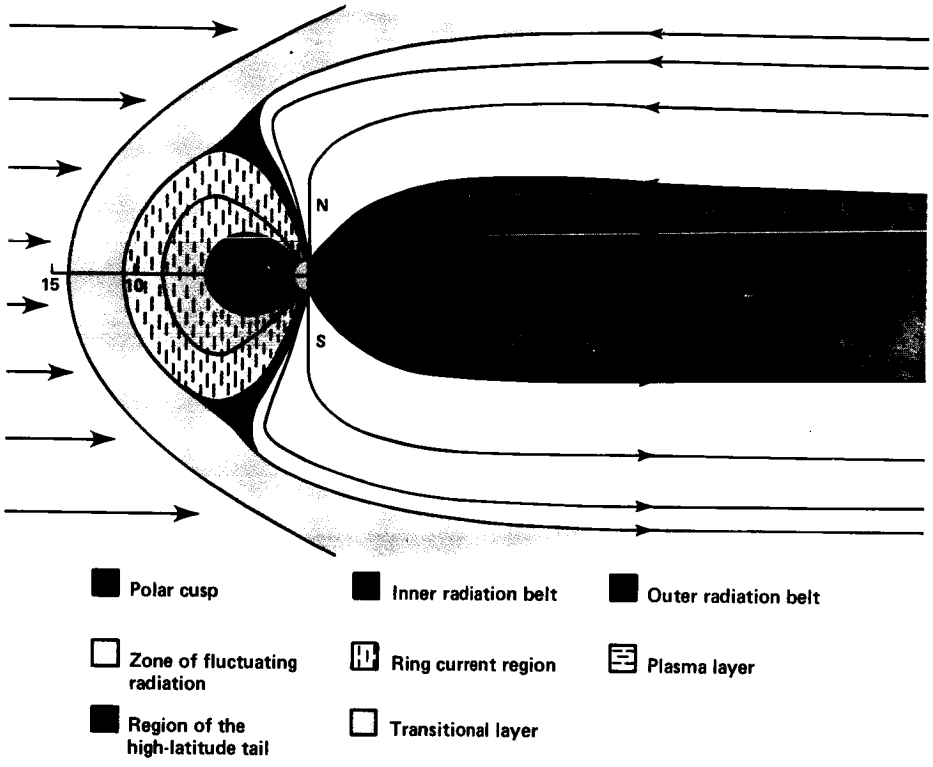

Profile of the magnetosphere of the Earth.

accelerated in the flare, while a cm-band radio burst occurs simultaneously as a result of synchrotron radiation of the same electrons.

The ejection of matter apparently is a characteristic of all flares. The most frequent type of ejection of matter is a protuberance which returns; ejection velocity is 50–5000 km/s, and the stream of matter falls back to the Sun. Ejection of matter into interplanetary space must occur at velocities greater than the escape velocity, which is determined by the Sun's gravity.

The emission of solar cosmic rays at high energies has almost always been observed with very strong flares. It has been discovered that, in addition to rare cases of high-energy particle emission, the Sun radiates low-energy particles much more frequently, also related to flares.

Type IV radio radiation (continuous) and sudden disturbances in the terrestrial ionosphere usually accompany the generation of energetic protons during proton flares. This results from increased ionization of the lower portion of the D area of the ionosphere by solar x-rays with $\lambda \leq 5$ Å. The total energy of solar cosmic rays ejected by a powerful flare reaches $10^{31}-10^{32}$ erg.

The relationship between complex phenomena in flares and the generation of solar cosmic rays has not yet been explained. The appearance of flares is assumed to be related to instabilities near the neutral lines with high field gradients of complex configuration in the chromosphere, which results in conversion of the magnetic energy to other forms [127, 128]. After a flare, the magnetic field is usually simplified, the gradients are decreased, and the field is weaker. Energy estimates have shown that neutralization of a field of 50–100 G is sufficient to compensate for the energy liberated.

TABLE 1.—*Classification of Flares*

Estimate of relative brightness	2.0 Subflare	Adjusted area in square degrees			
		2.1–5.1	5.2–12.4	12.5–24.7	24.7
f—faint	sf	1f	2f	3f	4f
n—normal	sn	1n	2n	3n	4n
b—bright	sb	1b	2b	3b	4b

Protuberances are masses of comparatively cold, dense gas ($n \approx 10^{10}-10^{11}$ cm^{-3}), rising over the chromosphere. At the edge of the disk, protuberances are visible as light clouds; at the center of the disk they appear as dark fibers called hydrogen fibers. Near the Equator, they are located along the meridians; at high latitudes they fall along the parallels. Three types of protuberances are distinguished: quiet, active, and eruptive. Quiet protuberances are encountered at the boundaries of active areas primarily on the high latitude side, but sometimes within the area. These are about 100 000–200 000 km in length with a height of several thousands of km and a thickness of about 10 000 km. Their lifetime is several months and the rate of movement of individual streams is about 10 km/s. Active protuberances are small, encountered within active areas, frequently near spots, and related to flares. Their shape is varied and changes rapidly; their lifetime is several hours or days. The rate of movement of individual elements is up to 100 km/s. Eruptive protuberances, a rare type, are distinguished by extremely rapid development, instability of shape, sudden increase in velocity of motion of hundreds of km/s and sudden disappearance. Their lifetime is but a few minutes.

The temperature of protuberances is about 10^4 °K; their density is about 100 times greater than the surrounding coronal gas. This indicates that protuberances may condense from the coronal matter as a result of cooling related to a decrease in the magnetic field at the base of the corona, or may be formed by compression of a certain volume by some external force, for example a magnetic field. Figure 1 shows various elements of solar activity across the disk of the Sun [21].

Centers of Activity

The development of various active formations throughout the solar atmosphere is a single process, which can be looked upon as development of a center of activity (centers of activity were formerly called active areas, and referred only to a facular area with spots and flares). The development of a typical center of activity can be divided into four stages:

Stage 1, which lasts several days, is characterized by the appearance of a weak (or complex configuration) UM field, plus a bright facula and development of flocculi in the chromosphere. At the brightest point of the flocculi, dark spots (pores) appear, from which spots develop. The field area increases and becomes BM.

Stage 2, which lasts several weeks, is the active state characterized by rapid and unstable development. During this time, the size and intensities of the M areas and flocculi reach their maximum, flares appear, and active protuberances are seen. After a month, the group of spots begins to break up while the flocculi grow but become darker.

Stage 3, the stable state, lasts several months. The group of spots becomes unipolar and disappears; faculae and flocculi gradually weaken although quiet protuberances and a significantly weakened M area are temporarily retained.

Stage 4 lasts several months. The protuberances disappear and the BM area is converted to a UM area before it dissipates.

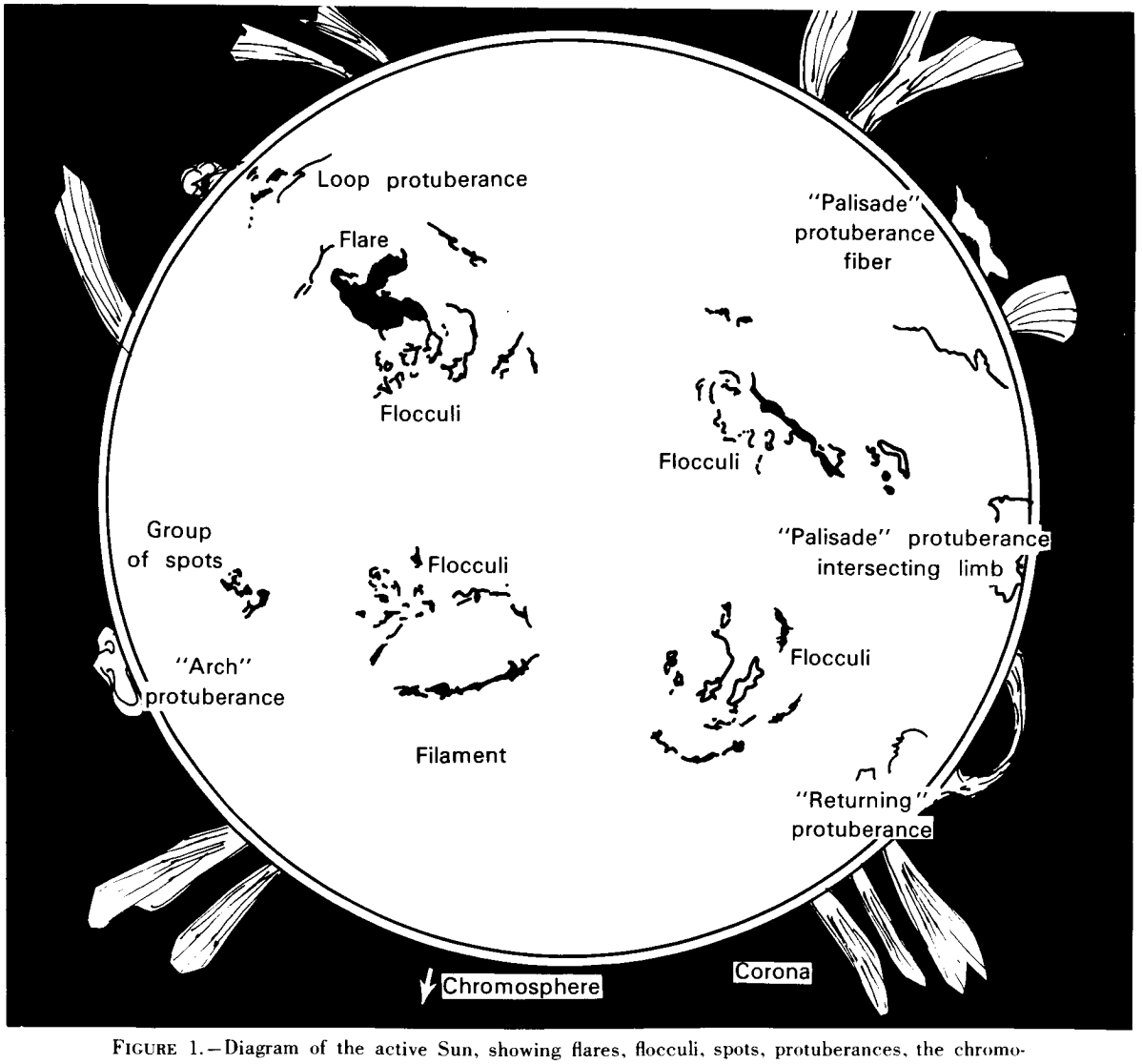

FIGURE 1.—Diagram of the active Sun, showing flares, flocculi, spots, protuberances, the chromosphere, and corona.

Centers of activity are unevenly distributed in the solar atmosphere. The primary latitudes are the "regal zones," but during the years of maximum activity, centers also appear at latitudes of more than $\pm 40°$, although they are less stable here. The intervals of longitude in which centers of activity most frequently develop are called "active longitudes."

The active longitudes are retained for two or more 11-year cycles, although they fluctuate in different directions, obviously unaffected by the presence of differential motion in the layers of the atmosphere. Consequently, the active longitudes characterize the physical state of the deep internal photosphere layers, where the differential rotation is replaced by rigid rotation.

Solar activity can be characterized by various indices [72, 122, 131]:

1. index of the relative number of spots—the Wolf number
2. index of the summary area of groups of spots
3. index of the maximum magnetic field intensity of the spots
4. flare index
5. index of the summary area of protuberances
6. corona index (mean intensity of lines)
7. index of the flux of radio radiation at a given wavelength (from over 1 m to cm); most commonly used is, $\lambda = 10$ cm.

Cycles of Solar Activity

Solar activity is also characterized by cycles of various lengths; those of greatest interest are the 11- and 22-year cycles which have perturbations, and the 80-year cycle.

The 11-year cycle of solar activity is most clearly seen by measuring the number of groups of spots. The cycles are numbered beginning with the zero cycle in 1745. The 11-year cycles, which vary in length (7–17 years) with a mean length of about 11.2 years, are asymmetrical; the transition from the maximum number of spots to the minimum (descending branch) occurs at an average 6.7 years, while transition from the minimum number of spots to maximum (ascending branch) occurs in about 4.6 years. The cycles also differ in mean annual maximum values of Wolf number ($W = 46–190$); in late 1957, the mean quarterly Wolf number was $W = 235$. The intensity of the cycle is related to its length: the more powerful the cycle, the shorter its length; the shorter the growth branch, the greater the asymmetry of the cycle and the higher the latitudes at which its first groups of spots appear. In weak cycles, the ascending branch is almost equal to the descending branch; in very weak cycles, the normal proportion may even reverse. The polarity of the leading spots in the northern and southern hemispheres changes from cycle to cycle. Eras of the maximum in the hemispheres sometimes differ by 1 or 2 years. The most powerful phenomena of solar activity are usually not observed in the year of the maximum of sunspots, but at the end of the ascending branch or at the beginning of the descending branch.

The 22-year magnetic cycle is characterized by a change in sign of the overall magnetic field and the fields of magnetic areas and spots. In odd cycles, the leading spots and the overall field have positive signs in the northern hemisphere and negative signs in the southern hemisphere. The 22-year cycle begins with an even 11-year cycle. Apparently, the 22-year cycle also governs the index of mean area of groups of spots, the index of frequency of flares, and the sum of mean annual Wolf numbers.

The 80-year cycle is a quasi-periodic change in maxima of the 11-year cycles. The maxima of 80-year cycles have fallen approximately in 1775, 1855, and 1930; the minima, in 1815, 1900, and next to be in 1980. The next few minima in the 11-year cycle of solar activity are expected to be deeper than the past few. Studies and descriptions of solar activity are the subject of an extensive literature [41, 46, 57, 58, 93, 121].

Electromagnetic Radiation of the Sun

The spectrum of solar electromagnetic radiation extends from the radio range to the x-ray area. The shortwave boundary of the spectrum usually lies at a few ångströms (1 Å $= 10^{-8}$ cm; the energy of a quantum with wavelength $\lambda = 1$ Å is 12.4 keV) under "quiet" Sun conditions and may shift to several hundred keV during flares.

The solar constant outside the Earth's atmosphere is $1.36 \cdot 10^6$ erg/cm² s, or 1.95 cal/cm² min. Direct measurement of the solar constant considering the short wave portion of the spectrum was first achieved in late 1967. The accuracy of this determination is about 1.0%. Distribution of energy in the various areas of the solar spectrum is presented in Table 2. The general form of the solar spectrum outside the Earth's atmosphere is presented in Figure 2 [85].

The Earth's atmosphere fully absorbs solar radiation at wavelengths of less than 2900 Å. From 3000 Å to 40 000 Å, the atmosphere is transparent (the so-called "optical window"). The next window of transparency begins at millimeter wavelengths and extends to approximately 15 m (the so-called "radio window"). Radio radiation is significantly attenuated by the ionosphere at wavelengths longer than 15 m and fully cut off at a wavelength of about 40 m.

Visible Light

Most of the visible light is emitted from the surface of the photosphere in the form of a continuous spectrum, onto which the Fraunhofer absorption lines are superimposed. The light that arises deep within the Sun in the form of high-energy x-ray photons after traveling the path from the deep layers to the solar atmosphere, generates the continuous spectrum of radiation in the process of multiple energy exchange by radiation and absorption over a broad range of frequencies. The energy of the visible light ($\lambda = 3800$–7600 Å) represents about 20% of the total energy of solar radiation.

The matter of the photosphere has a high coefficient of radiation absorption and becomes practically nontransparent at a depth of about 300–400 km. Tens of thousands of Fraunhofer absorption lines are superimposed on the con-

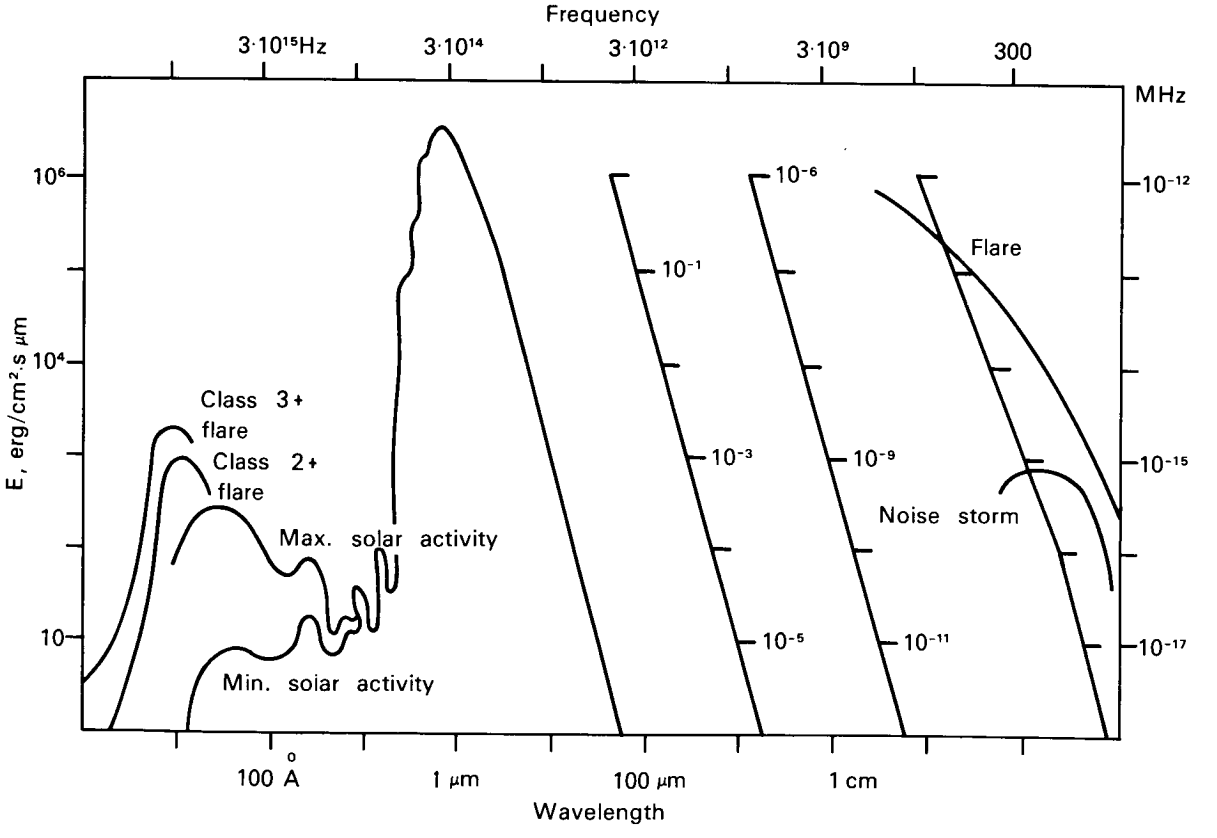

FIGURE 2.—Distribution of energy in the spectrum of the Sun.

tinuous spectrum, most of which are formed in the upper layers of the photosphere, some in the chromosphere. The absorption lines significantly change the distribution of energy in the spectrum of solar radiation. Thirteen elements have over 100 absorption lines each, two of these (Ti and Cr) have over 1000, and one, Fe, over 3000 absorption lines. The observed erosion of the Fraunhofer lines generally results from the combined influence of the Doppler effect and various types of attenuation (Table 3).

Radiation in the visible area is almost constant; in the UV and radio areas it changes about every 11 years. The Earth's atmosphere, opaque to a significant portion of the radiation, also distorts sunlight in the form of extinction (the general weakening of the spectrum, stronger at the violet end), telluric lines, and molecular absorption bands, the density of which also increase toward the violet end; in the red area they even predominate over the solar absorption lines.

TABLE 2.—*Spectral Distribution of Solar Radiation at the Upper Boundary of the Earth's Atmosphere for Mean Sun-Earth Distance*

λ(Å)	f_λ, $\frac{erg}{cm^2 s Å}$	Relative energy, %, for area shorter than λ
10	10^{-6}	10^{-9}
100	10^{-3}	10^{-5}
1000	10^{-3}	10^{-4}
2000	1.4	10^{-2}
3000	61	1.3
5260	196	26
6070	178	36
6880	148	46
10 000	73	73
20 000	11	95
30 000	2.7	98
50 000	0.4	99.8

TABLE 3.—*Strongest Fraunhofer Lines in the Visible Area*

Å	Atom	Å	Atom	Å	Atom
3820.44	Fe	4226.74	Ca	5172.70	Mg
3933.68	Ca^+	4340.48	H_γ	5185.62	Mg
3968.49	Ca^+	4383.56	Fe	5889.97	Na
4045.82	Fe	4861.34	H_β	5895.94	Na
4101.75	Hδ	5167.33	Mg	6562.81	H_α

Shortwave Radiation of the Sun

Radiation with wavelengths shorter than 3000 Å, corresponding to energy of quanta over 4 eV, is generally called shortwave radiation. Compared to the corpuscular ionizing radiation of solar flares, the energy of shortwave radiation quanta is low. However, the energy flux of shortwave radiation is thousands of times greater than the maximum energy flux of other types of ionizing radiation recorded in space. The shallow penetration depth of shortwave radiation can significantly change the surface properties of various structural materials. Thus, when space conditions are simulated under laboratory conditions, detailed knowledge of energy fluxes in various areas of the Sun's spectrum of shortwave radiation is required.

The photosphere makes the primary contribution to the shortwave radiation of the Sun down to 1600–1500 Å; the intensity of this radiation remains practically unchanged with time. In the area of the spectrum with wavelengths shorter than 1500 Å, the primary contribution is made by the chromosphere and the corona, while at wavelengths less than 300 Å, by the corona of the Sun. Radiation with wavelengths shorter than 1300 Å and in particular, shorter than 100 Å, changes sharply depending on the level of solar activity.

Variations in solar radiation flux during the 11-year cycle of activity are known, as well as 27-day variations caused by the visible movement of active areas across the disk as the Sun rotates. The greatest increase in radiation flux, particularly near the shortwave boundary of the spectrum, is observed during brief x-ray bursts, which frequently accompany chromospheric flares. The length of these bursts, depending on class and on the wavelength of the x-ray radiation, is from a few minutes to some hours. For example, in the spectrum area shorter than 10 Å, bursts lasting some tens of minutes are observed, comparable in duration to chromospheric flares. However, in the area shorter than 1 Å, the duration is generally not more than a

few minutes. The development of a characteristic x-ray flare with time is shown in Figure 3 [151].

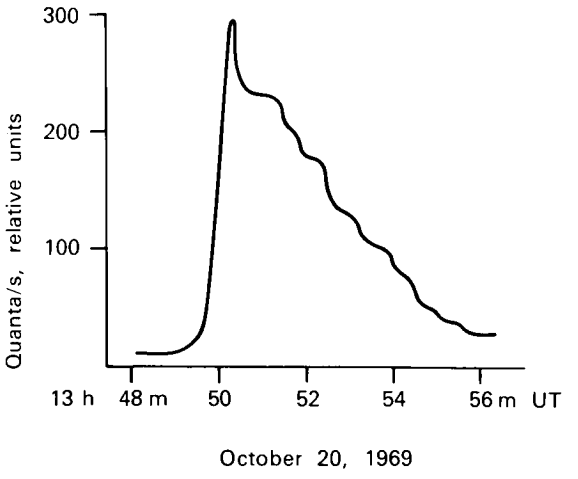

FIGURE 3.—Development of x-ray flare in the spectral area shorter than 1 Å (observed October 20, 1969 at 13:50).

Table 4 shows the absolute values of the radiation flux in the area of the spectrum shorter than 3000 Å when there are no flares ("quiet Sun"), near the minimum phase of the 11-year activity cycle. Between the minimum and the maximum of the 11-year cycle of solar activity, the summary flux shorter than 1300 Å increases by a factor of 2–3 times. During each 27-day period of variation, the summary flux shorter than 1300 Å may change by 1.5–2 times. The flux in the most intensive hydrogen line L_α at 1215.7 Å varies by from 3–6 erg/cm² · s. Brief changes in radiation flux in the area shorter than 1300 Å are apparently slight.

The flux in the spectrum area shorter than 100 Å apparently varies from 0.1 to 1 erg/cm² · s during each 11-year solar cycle and may vary from 3 to 5 times within a few hours or days. The flux of the "quiet" Sun in the area of the spectrum shorter than 10 Å increases by two orders of magnitude from the minimum to the maximum of the solar cycle and may change dozens of times during a 27-day cycle; during solar flares, the flux may reach $5 \cdot 10^{-2}$ erg/cm² · s. The flux in the area shorter than 5Å for the "quiet" Sun apparently reaches 10^{-6} erg/cm² · s and may increase by almost three orders of magnitude during flares. In the spectral area shorter than 1 Å, the flux during flares may reach 10^{-4} erg/cm² · s.

The distribution of energy in the shortwave spectrum of the Sun is shown in Figures 4 and 5, [22]. Figure 5 relates to the "quiet" Sun near the

TABLE 4.—*Flux of Solar Energy and Shortwave Area of Spectrum* ($\lambda < 3000$ Å) *Above the Earth's Atmosphere at a Distance of 1 AU*

Boundaries of intervals, Å	Energy flux, erg/cm² s	Boundaries of intervals, Å	Energy flux, erg/cm² s
3025	3050	1100	0.09
2975	3150	1050	0.17
2925	2600	1000	0.13
2875	1700	950	0.14
2825	1200	900	0.18
2775	1100	850	0.12
2725	1250	800	0.10
2675	1000	750	0.05
2625	700	700	0.05
2575	560	650	0.13
2525	380	600	0.10
2475	390	550	0.07
2425	340	500	0.08
2375	320	450	0.06
2325	360	400	0.13
2275	350	350	0.41
2225	310	300	0.19
2175	240	250	0.23
2125	145	200	0.36
2075	90	180	0.39
2025	70	160	0.07
1975	55	140	0.04
1925	41	120	0.02
1875	28	100	0.06
1825	19	80	0.05
1775	12	60	0.04
1725	8.2	40	0.02
1675	5.0	30	0.005
1625	3.2	20	0.002
1575	1.7	10	0.00001
1525	0.95	< 10	
1475	0.50		
1425	0.26		
1375	0.26		
1325	0.18		
1275	0.37		
1225	5.10		
1200	0.19		
1150	0.10		
1100			

minimum of the 11-year cycle of activity and shows the most intensive lines, their ordinates being numerically equal to the energy flux in a line (erg/cm² · s). Near lines are combined; the ordinate here corresponds to the summary flux.

Experimental material on shortwave solar radiation is still limited. The data in Table 4 were produced at various times by various methods. Some of the measurements were made by rockets and the results extrapolated beyond the Earth's atmosphere. Thus, the data must be looked upon as approximate, and will be refined in the future. Shortwave radiation of the Sun is the subject of several works [8, 9, 23, 69, 109, 129].

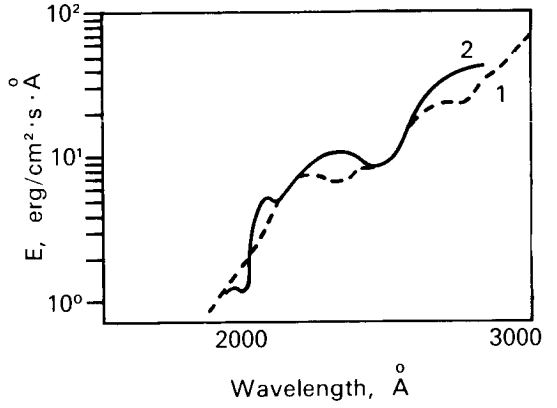

FIGURE 4.—Distribution of solar energy in the spectral region 2000–3000 Å.
1—April 19, 1960 [129];
2—January 13, 1967 [22].

Radio Radiation of the Sun

The radio radiation of the Sun can be observed on the surface of the Earth only in the radio window at wavelengths from $\lambda = 8$ mm to $\lambda = 15$ m. The shortwave boundary is determined by absorption by molecules of H_2O and O_2; the longwave boundary, by the critical frequency of the ionosphere.

The Sun is a variable radio star. Radio waves are radiated by the solar atmosphere, basically by the chromosphere and the corona, i.e., by a plasma varying in temperature from 10^4 to 10^7 °K with electron concentration 10^7 to 10^4 cm^{-3}. The Sun emits three types of radio emission:

1. constant continuum of the quiet Sun (background), observed throughout the entire spectrum

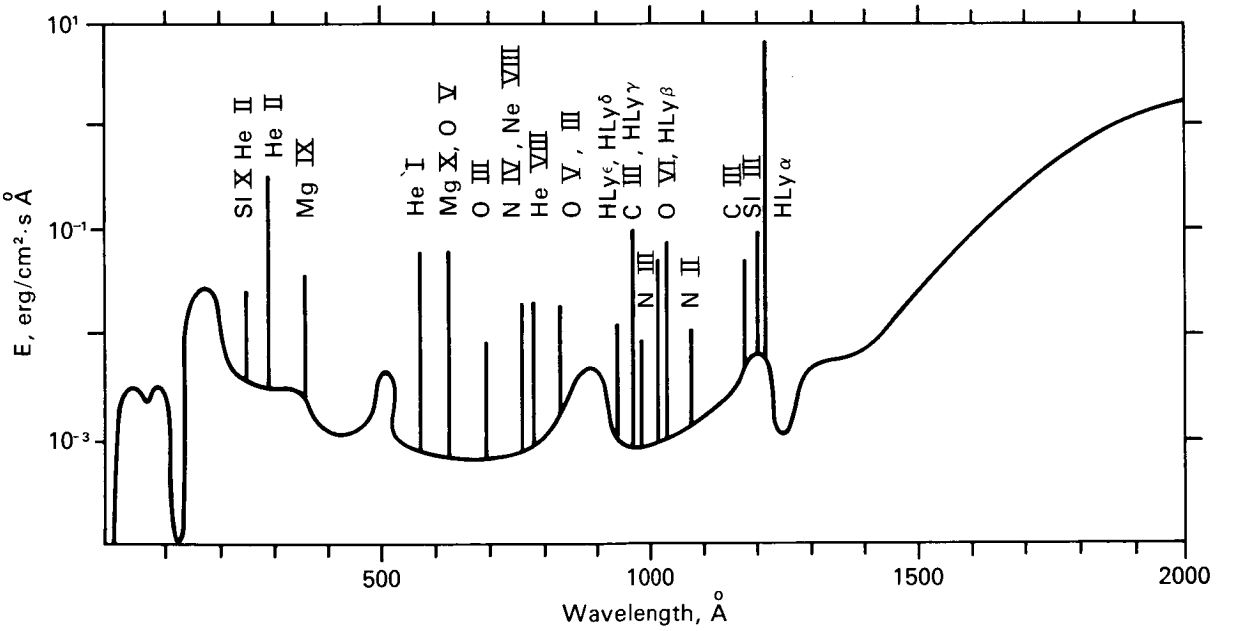

FIGURE 5.—Distribution of solar energy in the spectral region shorter than 2000 Å.

2. slowly changing component, best observed at wavelengths of 3–60 cm, related to spots and flocculi
3. sporadic radio emission—noise storms, five types of microwave bursts and the decimeter continuum; the sources are related to centers of activity, and certain types of bursts correlate directly with flares.

In the equilibrium high temperature plasma of the quiet Sun, radiation of electrons is thermal and incoherent. Nonthermal radiation appears with a deviation from the Maxwellian distribution of velocities and is related to active formations on the Sun and plasma oscillations. For thermal radiation, the influence of the general magnetic field of the Sun can be ignored. Sporadic nonthermal radio emission is related to the areas of the solar atmosphere where strong local magnetic fields are present; therefore, it is polarized and observed in the form of ordinary and extraordinary components.

Electrons generate three types of solar radio emission: bremsstrahlung, magnetic bremsstrahlung (for relativistic electrons called synchrotron radiation, for nonrelativistic electrons—cyclotron radiation), and Cherenkov radiation, which make different contributions to different types of solar radio emission.

The concept of "effective" or "brightness" temperature T_{eff} (λ) is frequently used for thermal and nonthermal radio emission, but it is not always identical to the temperature of the source of the radiation. Rather, it is a measure of the intensity of the radiation, since the observed radiation may contain contributions from various layers of the solar atmosphere.

The placement of thermal radiation sources is different for the different wavelengths. The chromosphere and corona, transparent for visible light and short radiowaves, become nontransparent for the wavelengths which they themselves radiate. The observed radiation at millimeter wavelengths comes from the lower chromosphere, at centimeter wavelengths—from the chromosphere, and at meter wavelengths—from the corona. The radius of the "radio Sun," near the radius $R_\odot$ of the optical disk at millimeter wavelengths, increases with increasing λ and in the meter waveband reaches about (1.5–3.0) $R_\odot$.

Radio emission of the "quiet" Sun (background or B component), observed throughout the entire wave range from millimeter to meter waves, is the lower boundary of radio emission of the Sun and is determined during the time of least solar activity. The frequency spectrum, characterized by T_{eff} (λ), varies from $6 \cdot 10^3$ °K for millimeter waves to about 10^6 °K in the meter waveband. T_{eff} (λ) is a nonmonotonic function, with a maximum at $\lambda = 4$ mm, and a minimum at $\lambda \simeq 6$ mm. It then increases strongly to the meter waveband. The question of 11-year variations of the B component is still undetermined. The B component is thermal, is not polarized in the stationary atmosphere of the Sun, and is basically electron bremsstrahlung with some Cherenkov radiation. As the millimeter waves are generated in the lower chromosphere, the height of the area of generation increases with increasing λ, and the meter waves come from the corona. The B component is a continuum of radiation types, i.e., it is stable and has a broad frequency spectrum, indicating a noncoherent mechanism of generation.

The slowly changing component (S component) of continuum type is observed in the wavelength $3 \leqslant \lambda \leqslant 50$ cm and at a few percent in the millimeter waveband for up to 30 d as a smooth increase in the signal received above the "quiet" Sun level. Periodicity of 27 d is observed, correlating well with the Wolf number and with the overall area of spots; i.e., it is related to the cycle of solar activity. Its sources are local areas on the disk of the Sun at a height of about 0.03 $R_\odot$ from the surface of the Sun, i.e., at the boundary between the chromosphere and corona; it is closely related to the spots, particularly the flocculi and, apparently, is located at spots in the areas of high electron concentration in the lower corona over the centers of activity containing spots and flocculi. The slowly changing component exists longer than the flocculi with which it is associated. Observations of the S component over active areas can be used to predict proton flares. Most proton flares occur when the ratio of flux densities of S component at $\lambda = 3.2$ cm and $\lambda = 7.5$ cm is higher than 1.

The sporadic radio emission of the Sun is related to solar activity, is heterogeneous in composition and most intensive and varied in the meter waveband. For classification, it is best to assume a dynamic spectrum of radio emission (dependence of frequency on time), which facilitates the search for mechanisms of generation.

Solar activity is related to: the slowly changing component (S component), noise storms and type I, II, III, and IV bursts, microwave bursts, and the decimeter continuum.

If the slowly changing component, related to centers of activity, is generated during the stable mode of the Sun and is thermal radiation, all other types of sporadic radio emission would arise during the "active" phase of development of centers of activity and would be nonthermal radiation.

Noise storms and type I bursts are continuum-type radio emissions with superimposed narrow bursts. They are observed primarily in the meter waveband, are less frequent and less intense in the decimeter band. The greatest intensity observed is at $\lambda = 2-4$ m, with a frequency interval range not over 250 MHz. The increase in flux during bursts may be 10^2-10^3 times greater than at the mean quiet level. The continuum usually arises gradually, is observed for several hours or days, and has many brief type I bursts with lengths of a fraction of a second to a minute.

The emissions of noise storms and type I bursts are strongly polarized, do not drift in frequency and are nonthermal in type. The mechanism of their generation is not exactly known; it may be incoherent magnetic bremsstrahlung. It is assumed that the area of noise storms generation forms a sort of reservoir, which retains energetic particles in a "trap" formed by the BM fields of the spots. Type I bursts appearing against the background of a noise storm can apparently be explained by additional acceleration of fast electrons over a limited area of the corona. Another possible source might be plasma waves, which have an attenuation time comparable to the lifetime of type I bursts.

Type II bursts (slowly drifting in frequency) are powerful bursts of radio emission in the meter and decimeter bands lasting a few to tens of minutes. Type II bursts arise at high frequencies, $f \approx 200$ MHz, then shift to lower frequencies; the majority attenuate at a frequency $f = 25$ MHz ($\lambda = 12$ m). The frequency drift rate is about a fraction of a MHz/s. The intensity is 100–1000 times greater than the background. Type II bursts are among the rarest phenomena in the radio emissions of the Sun; even during the period of maximum activity, an average of one burst is observed each 50–100 h. Type II bursts usually arise during large grade 2 and 3 flares. The delay of a type II burst relative to the maximum of an optical flare averages about 7 min. The width of the frequency band of a burst at each moment is about $0.3f$, where f is the frequency of maximum intensity. Polarization is slight.

Type II bursts are clearly distinguished by the appearance of a second harmonic (in 75%–80% of cases); the structure of the bursts at the main frequency and second harmonic is identical. They appear simultaneously and at great altitude in the corona, although the second harmonic is apparently generated deeper in the corona than the main tone.

The frequency drift in the direction of low frequencies, visible in the dynamic spectrum of type II bursts, can be explained by the "plasma" hypothesis of movement of an agent from the area of a flare through the corona. The "plasma" hypothesis relates the frequency of radio radiation to the natural frequency of oscillations of the plasma. With increasing distance from the photosphere, the concentration of electrons decreases; consequently, the frequency drift of a type II burst will be in the direction of lower frequencies. Type II bursts might be caused by shock waves in plasma with a magnetic field frozen in. These arise in the explosive phase of a flare and move at a speed of 10^3 km/s. Bursts are generated in the process of passage, of the leading edge of the shock wave which runs before the bundle of plasma, through the corona.

The relationship of type II bursts to the ejection of material from the area of a flare and to solar geoactive streams is confirmed by the appearance of geomagnetic perturbations 1 to 2 d after strong type II bursts and the agreement of the velocity of a bundle and of these streams. The A_p and K_p indices increase 1.5–2.2 d after type II bursts; magnetic storms and polar auroras begin only after 45% of type II bursts.

Type III bursts (rapidly drifting bursts) are observed in the meter waveband. Similar to type II bursts, they consist of nonthermal radiation, created upon transformation of plasma waves into electromagnetic waves in a system consisting of a corpuscular stream and the coronal plasma. The corresponding stream of particles, which leave the area of the flare, moves through the corona at about 10^5 km/s.

The main difference between type III and II bursts is that type III bursts drift rapidly in frequency, i.e., develop about 100 times more rapidly than type II bursts, and have a duration of about 3–15 s. The velocity of the agent causing type III bursts in the corona is two orders of magnitude higher than in type II. Type III bursts are observed much more frequently than type II bursts; for each 100 hours observation, an average of 300 type III bursts are observed, compared with less than one type II burst. The beginning of a type III burst is usually related to the beginning, not the maximum of an optical flare. Type III bursts frequently appear in groups. About half of all bursts are strongly polarized (30–70%). Type II and III bursts are closely related; 60–80% of type II bursts are accompanied by type III bursts, with a mean delay of 5.5 min.

The U burst is one variety of type III burst, which occurs when the direction of motion of the exciting agent reverses, so that the frequency drift first is downward toward lower frequencies, then toward higher frequencies. This type of burst rarely appears and results either from a special configuration of the magnetic field of bipolar groups of spots, or from local heterogeneities in the corona.

Type IV bursts frequently (about 70%) follow type II bursts, are related to strong flares, and reach a maximum 10 to 30 min after the flash phase of the optical flare. Type IV bursts are radiation of the continuum type, covering a wide frequency band (sometimes more than 8 octaves). The length, from minutes to several hours, and the intensity gradually decrease. The greatest intensity is in the meter waveband ($\lambda > 1.2$ m). A gradual frequency drifting in the direction of low frequencies is observed.

These bursts differ from the continuum of noise storms (with which they are generally not observed) by their more stable nature, briefer duration, broader range of frequencies (in the high-frequency direction), close relationship to type II bursts, mechanism of generation, and movement of the generation area in the corona over distances greater than approximately 6 $R_\odot$.

The structure of type IV bursts is very complex; they are divided into several subtypes, but as yet there is no standard classification. The dynamic spectrum frequently has three maxima: in the meter waveband (type IV m), decimeter waveband (type IV dm), and centimeter waveband (type IV cm). In the meter waveband, two subtypes are differentiated, stationary and moving, which differ in the distance of motion of the source. There are two classes of type IV bursts related to the chromospheric or coronal flares.

The great correlation of type II and IV bursts and movement of their areas of generation at approximately the same velocity indicate that apparently both phenomena are caused by the same agent, for example, shock waves in plasma, moving in the corona from a flare area at a velocity of 10^3 km/s. Although the defining factor for type II bursts is the velocity of the shock wave, type IV bursts are generated by the synchrotron radiation of relativistic electrons behind the shock wave front and are related to ambient magnetic fields. The acceleration of electrons to the necessary energies may occur directly within the bundle during the existence stage of the type II burst. Polarization of radiowaves confirms the hypothesis of the synchrotron mechanism of generation.

Type IV bursts have narrow directionality and are less frequently observed away from the center of the solar disk. Type IV bursts correlate well with various phenomena: geomagnetic storms with sudden onset, appearance of solar cosmic rays, and polar blackouts. The probability of appearance of a magnetic storm increases if a type IV burst follows a type II burst. The time of onset of polar blackouts is determined by the geometry of the magnetic fields in the solar atmosphere and in interplanetary space, and, under favorable conditions, begins about

40 min after a type IV burst. At times they may begin simultaneously with the magnetic storm, i.e., within 1 or 2 days.

Type V bursts consist of broad, continuous radiation in the meter waveband. The frequency band ranges from tens to hundreds of MHz. They are observed only at frequencies less than 150 MHz ($\lambda \geq 2$m), with the maximum intensity usually $\lambda \geq 3$ m. The lifetime of a burst is about 0.5–3.0 min with no observed frequency drift. The velocity of motion of the source is about $3 \cdot 10^3$ km/s. Type V bursts differ from type IV in their close relationship with type III bursts, are about two orders lower in intensity, and consist of directed radiation. They follow type III bursts, excited by streams of fast particles (apparently electrons) moving at about 10^5 km/s. Possibly these particles serve as the source of type V bursts, when they reach the higher layers of the corona, by synchroton radiation of the electrons captured between points of reflection of an arc-shaped magnetic field. A close correlation has been found between type III and V events, centimeter bursts and flares.

Microwave radiation, continuous-type radiation primarily in the centimeter waveband, is more varied and has been less studied than the radiation in the meter waveband. It is divided into three types as a function of the form, duration, and dimensions of the area of generation:

Type A—rise and fall rapid, lifetime, 1–5 min, generation area, small (diam 1–1.6 min), polarized;
Type B—fast rise and slow fall, lifetime—several min to several h, generation area, large (greater than 2.5–3.0 min);
Type C—rise and fall gradual, lifetime about 30 min to several h, generation area, small (0.8 min).

These three types may exist individually or be superimposed on one another. The most powerful bursts are of type A or B and are accompanied by a decimeter continuum.

The sources of emission are localized in three regions of the disk of the Sun, from which the slowly changing component originates. The radiation may be nonthermal for strong bursts and thermal for weaker bursts. The assumed mechanisms of generation are: type A—magnetic bremsstrahlung of energetic electrons appearing in a flare in the local magnetic fields of a center of activity; types B and C—the combined action of magnetic bremsstrahlung and bremsstrahlung mechanisms in the corona over a portion of centers of activity.

Powerful microwave bursts are closely related to flares, and the x-radiation of the Sun, which in turn are related to geophysical phenomena observed practically simultaneously with events on the Sun (sudden ionospheric disturbances, and polar blackouts). The polar blackouts are more closely correlated with microwave bursts than with type IV bursts; they practically always follow a microwave burst.

A direct dependence has been established between the flux of protons recorded after a flare and the intensity of microwave bursts in the range of $\lambda = 3$–10 cm; however, this dependence is at times masked by the propagation conditions of protons in interplanetary space.

An overall picture of sporadic radio emission can be represented approximately as: the centers of activity (flocculi, groups of spots) stimulate the formation of areas of increased plasma density in the lower corona, serving as sources of the slowly changing (S) components, detected primarily in the centimeter waveband. In the higher layers of the corona, to which the strong magnetic fields of the spots penetrate, noise storms with gradual onset and type I bursts are generated in the meter waveband. During flares, noise storms arise near active groups of spots that have rapid onset, reinforcing existing sources of noise storms. Streams of charged particles apparently are accelerated, generating type III bursts, which drift rapidly in frequency as they move through the less dense layers of the corona at about 10^5 km/s. Type III bursts are accompanied by x-ray and microwave bursts in the centimeter band.

A large flare is accompanied by an intensive microwave burst, the spectrum of which extends into the decimeter waveband; a type III burst appears simultaneously in the meter waveband. Radio emission then continues as type II bursts, drifting slowly in frequency over the meter waveband, apparently created by shock waves

574-269 O - 76 - 5

in plasma with magnetic fields "frozen in," spread from the area of the flare into the corona at about 10^3 km/s. An intensive type IV continuum is immediately emitted by the area of the bundle of charged particles moving in the corona. The appearance of the two types of radiation, either one of them or neither, depends on the intensity of the field in the bundle and its velocity. Figure 6 shows an idealized dynamic spectrum of the sporadic radio emission. The radio emission of the Sun has been described [41, 46, 110, 120, 148].

Corpuscular Radiation of the Sun

The corpuscular radiation of the Sun can be divided into constant, continuous emission of particles—the solar wind—and sporadic expulsion of intensive streams of plasma and charged particles—the corpuscular streams and solar cosmic rays. This division is arbitrary, reflecting the time-dependence of these types of radiation, emphasizing the constant existence of the solar wind, variations in its velocity and density never falling below minimum values, of 250 km/s and 0.5 particles/cm^3, respectively, at the level of the Earth's orbit. The stronger streams of solar plasma observed sporadically, i.e., the reinforced streams of the solar wind, are generally considered separately as solar corpuscular streams. This concept was introduced to science before the discovery of the solar wind, to explain various geophysical phenomena which correlated with certain phenomena on the Sun. The solar corpuscular streams reach velocities of about 1600 km/s at particle densities up to 100 cm^{-3}. After their formation, these intense streams move through the quiet, slow portions of the solar wind, disrupt the stable structure of interplanetary space, and cause various disturbances (described below). The solar wind and corpuscular streams are the most important components of solar corpuscular radiation, and determine conditions in interplanetary space. The solar wind, solar corpuscular streams, and solar cosmic rays

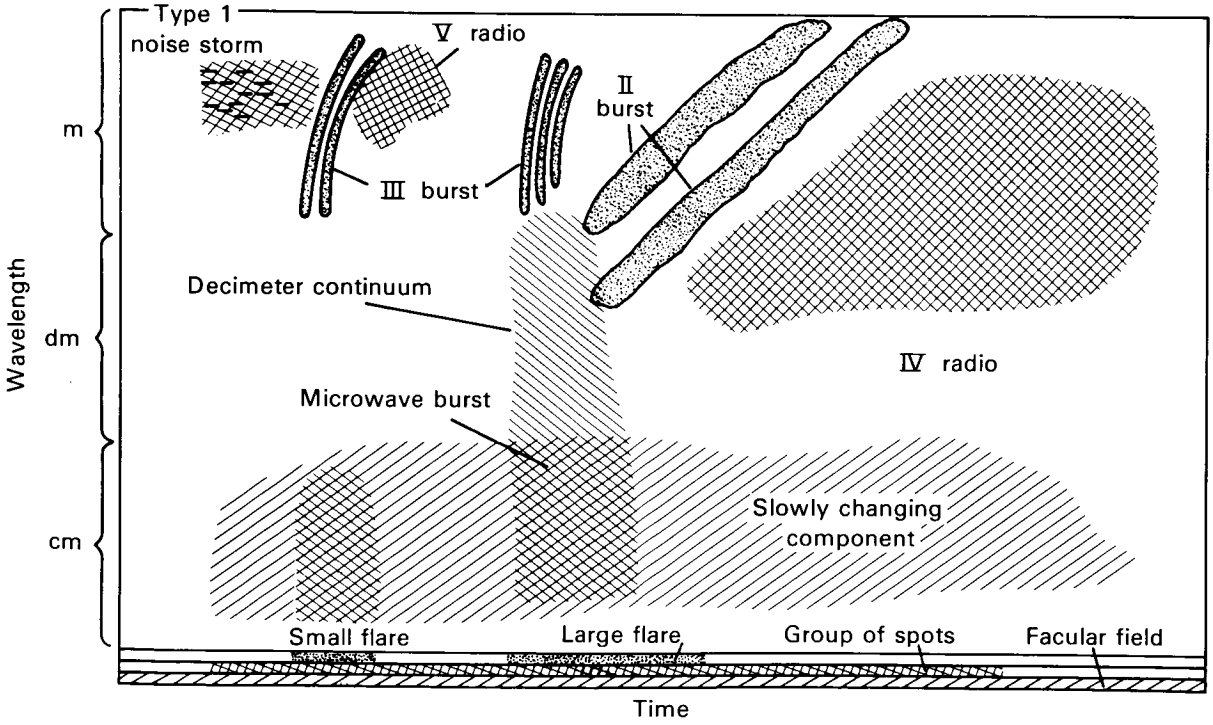

FIGURE 6.—Idealized dynamic spectrum of sporadic radio radiation from a center of activity.

will be described in detail in a subsequent section, THE INTERPLANETARY MEDIUM.

Solar corpuscular radiation causes the Sun to lose an average of a million tons of matter per second, which corresponds to 10^{-22} solar masses per second, assuming spherical symmetry of the solar wind. The basis for this assumption is experimental data produced by Biermann [17], who observed type I comet tails. However, other published data indicate that the solar wind is not spherically symmetrical [123].

Another type of corpuscular radiation, solar cosmic rays, consists of high-energy charged particles (from 30–50 keV/nucleus to several GeV/nucleus). Recent studies indicate that every bright chromospheric flare on the Sun probably generates solar cosmic rays.

Solar cosmic rays are apt tools for the study of interplanetary space; they illuminate the solar system and allow determination of various of its characteristics. After large solar flares, great fluxes of solar cosmic rays sometimes represent a serious radiation danger for space flight.

THE INTERPLANETARY MEDIUM

Properties of the interplanetary medium must be considered during flights in space. The most important are the characteristics of interplanetary plasma (solar wind), magnetic field, galactic and solar cosmic rays, and micrometeorite material. Another component of the interplanetary medium is the electromagnetic radiation of the Sun, stars, and galaxy, which will be briefly analyzed.

The Solar Wind and the Interplanetary Magnetic Field

The general concept of the existence of solar corpuscular streams (the solar wind) was based on many geomagnetic observations, studies of gaseous tails of comets deflected from the radial direction away from the Sun, and variations in galactic cosmic rays [17, 18]. Comets have been observed in various parts of the sky, indicating that corpuscular streams fill all of interplanetary space. The theoretical basis for streams of solar plasma was adduced by Parker [105, 107], who showed that the solar corona can provide the constant presence, in interplanetary space, of streams of solar plasma moving away from the Sun at supersonic speeds. The main reason for the expansion of the corona is its high temperature (about 10^6 °K).

The first direct observations of the solar wind were made by the Soviet lunar spacecraft Luna 2 and 3 and Venera 1 interplanetary space station [60, 64]. According to these data, the flux of the solar wind was about 10^8 cm^{-2} s^{-1}, a result which was confirmed [21]. The solar wind arrives from the Sun at a velocity of about 300 km/s [21]. Numerous studies of the parameters of the solar wind have produced an extensive literature [123].

The coronal plasma distorts the lines of force of the solar magnetic field during its supersonic expansion. The conductivity of the plasma is very high; the magnetic field frozen in the plasma is carried away by the solar wind, forming the interplanetary magnetic field. The dynamic state of the solar wind can be arbitrarily divided into quiet and perturbed, according to modern concepts.

The Quiet Solar Wind

This term, the quiet solar wind, relates to the average dynamic and kinetic characteristics of the stable flux of solar plasma, without the influence of individual active processes on the Sun. The time picture of density, velocity, and temperature of the solar wind, as well as the magnetic field for various periods of solar activity, have been studied [123]. Table 5 presents the mean macroscopic parameters of the solar plasma under quiet conditions and with strong perturbations at a distance of 1 AU from the Sun.

The chemical composition is an important characteristic of the solar wind. The solar corona chemical composition determined by spectroscopic measurements, includes protons (90%), helium nuclei (~ 9%) and heavier ions (^{16}O, ^{14}N, ^{56}Fe) in quantities of less than 1%. Observations of the chemical composition of the interplanetary plasma are quite preliminary. Measurement of charge composition, using electrostatic analysis and selection of velocities, shows that protons and helium nuclei are recorded with good resolution (Fig. 7 [11]). The mean ratio of helium to hydrogen for 1962–1967 was about 4.5%,

fluctuating between 1.5% and 5%. The ions of oxygen, nitrogen, and carbon, i.e., elements with identical mass-to-charge ratio, cannot be differentiated by this method. In a very quiet, unperturbed solar wind with low temperature (less than 10^4 °K), individual peaks of ^{3}He can be resolved, as well as singly or doubly ionized atoms of nitrogen, oxygen, and carbon. Stronger perturbations, such as shock waves from chromospheric flares, frequently increase the content of helium in the interplanetary medium, at times raising it to 20%.

Interplanetary Magnetic Fields

Measurements of the interplanetary magnetic fields have led to determination of the mean unperturbed picture of the magnetic field in space and its distortions during various types of solar activity [28, 29, 97, 99, 101].

TABLE 5. — *Mean Macroscopic Parameters of the Solar Plasma*

Parameters of solar wind and magnetic field	Quiet conditions at 1 AU	With strong perturbations at 1 AU	Dependence on distance from Sun
Velocity, solar wind, km/s	320–400	to 1600	weak
Density, solar wind, cm^{-3}	8–10	to 100	$\sim r^{-2}$
Mean temperature, ions, °K	10^4	to $5 \cdot 10^4$	weak
Mean temperature electrons, °K	10^5	to $5 \cdot 10^5$	weak
Magnetic field intensity, gammas	5	to 50	$H_r \sim r^{-2}$ $H_\phi \sim r^{-1}$

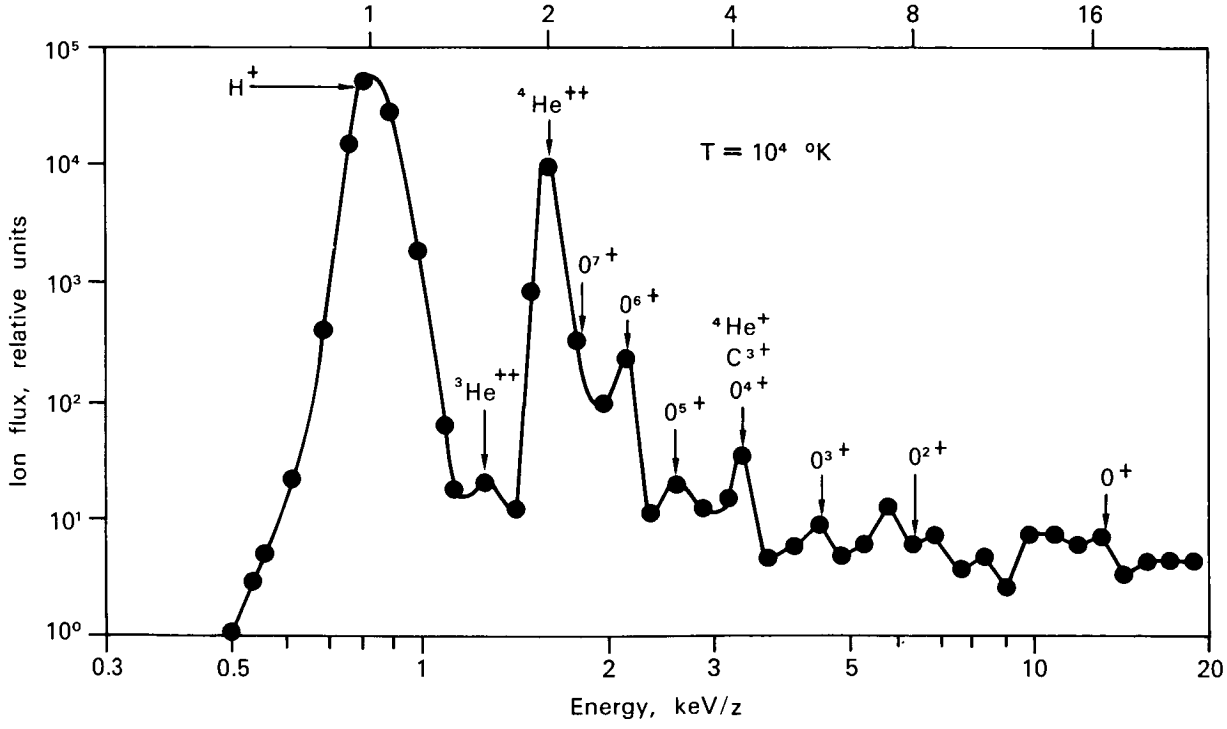

FIGURE 7. — Charge composition of the solar wind, determined October 8, 1965, by the Vela–2A satellite. Arrows indicate peaks of ions of each type. Oxygen, helium, and carbon ions with identical mass to charge ratio are not separated.

The coronal plasma, during supersonic expansion extends the lines of force of the solar magnetic field due to its high conductivity. At the orbit of the Earth, the energy density of the interplanetary field is much less (about 1%) than the kinetic energy density of the solar wind. The geometry of the unperturbed interplanetary magnetic field is reminiscent of an Archimedes spiral. Radio fading and radio transmission studies have shown that at 15–20 Sun radii, the magnetic field has an energy density much less than the kinetic energy density of the plasma, and its direction is almost radial, i.e., even at these distances the interplanetary field is determined by the dynamics of the solar plasma flow.

The radial and tangential magnetic field components H_r and H_ϕ are defined from the condition of conservation of magnetic flux considering the rotation of the Sun:

$$H_r = H_{r_0}\left(\frac{r_0}{r}\right)^2 \tag{1}$$

$$H_\phi = H_{r_0}\frac{r_0\Omega}{u_r}\left(\frac{r_0}{r}\right)\sin\theta \tag{2}$$

r_0 is the minimum distance, at which the velocity of the plasma is supersonic; u_r is the supersonic radial velocity of the wind; Ω is the angular speed of rotation of the Sun; θ is the angle between the line of force and the radial direction.

The angle between a line of force and the radial direction at the orbit of the Earth, $\theta = \arctan r\Omega/u_r$. For $r=1$ AU and $u_r=400$ km/s, angle $\theta=47°$ ($\Omega = 2.9\cdot 10^{-6}$ rad/s). At distances of less than 1 AU, the field is primarily radial; at the orbit of Jupiter, the field is basically tangential.

Sectorial structure. During low solar activity, a sectorial structure to the interplanetary field (Fig. 8) is formed by elongated areas in which the interplanetary field is regular either from the Sun or to the Sun. These sectors, with an appearance related to the large active local magnetic areas in the photosphere, where there are large areas of directed field, rotate at a rate determined by the rotation rate of the Sun around its axis. The sectors differ in size, averaging 100° in the plane of the ecliptic, and correspond to a 6- to 7-d time of passage of one sector near the Earth. Recent measurements have shown the sectorial structure to be defined by the number of areas on the Sun's surface in which the magnetic field is of the same sign; the number of sectors may change. The sectorial structure is only a large-scale picture of the interplanetary field. Variations in velocity of the solar wind tend to wash out the precise boundaries of a sector.

The data of IMP–1 (December 1963–February 1964), indicate a certain structure within the limits of each sector (Fig. 9 [97]). The plasma density is maximal near the leading (western) boundary, and inversely correlates with velocity, so that generally, the flux of the solar plasma is conserved. The magnetic field reaches its maximum during the second day, but does not totally vanish even at the boundaries. Since these observations are true for the orbit of the Earth, the measured parameters may differ significantly from corresponding parameters near the Sun. Figure 10 shows a model of the development of a sectorial boundary based on the pictures of the lines of force in the corona [115]. At the boundary of a bipolar area, the magnetic field prevents acceleration of the plasma. As distance from the

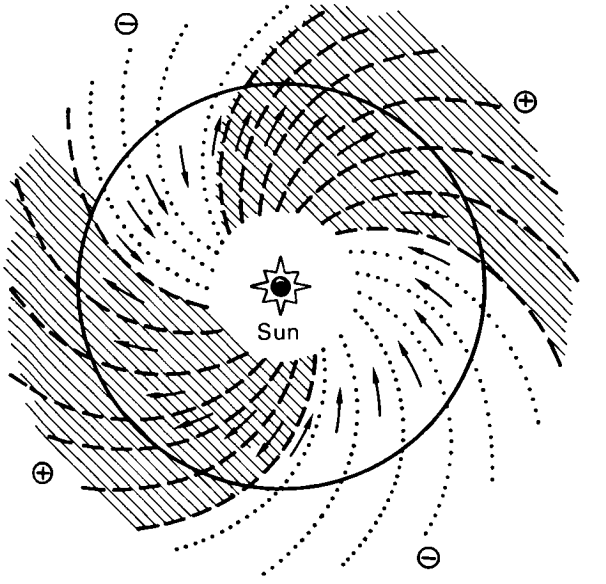

FIGURE 8.—Schematic of sectorial structure of the interplanetary magnetic field during periods of low solar activity.

boundary increases, the field can no longer hold the plasma. Since the dimensions of bipolar areas represent a small fraction of the total area of the solar disk, the magnetic fields probably can only form streams with different acceleration in the overall quasi-radial flow of the solar wind. In regard to the distribution of the flux parameters within a sector, the density maximum near the sector boundary might be created when a rapid stream (about 500 km/s) catches up with a slower stream (about 300 km/s).

At distances >5 AU, the sectorial formations and interaction of streams with different velocities apparently form large-scale magnetic heterogeneities with dimensions of 1 AU and greater. Information on the dynamics of these fluctuations in the field can be produced by analyzing long-period variations (such as the 11-year variations) in galactic cosmic rays in the energy area $E_p \approx 10^9$ eV. Measurements of spectral density of the fluctuations in the magnetic field at distances of ≤ 2 AU show a very low-frequency branch of the spectrum ($f \approx 10^{-6}\,s^{-1}$), which may indicate the presence of large-scale field variations ($L > 1$ AU).

Perturbations in the Solar Wind

In this case, unstable behavior of the interplanetary plasma is observed; various types of

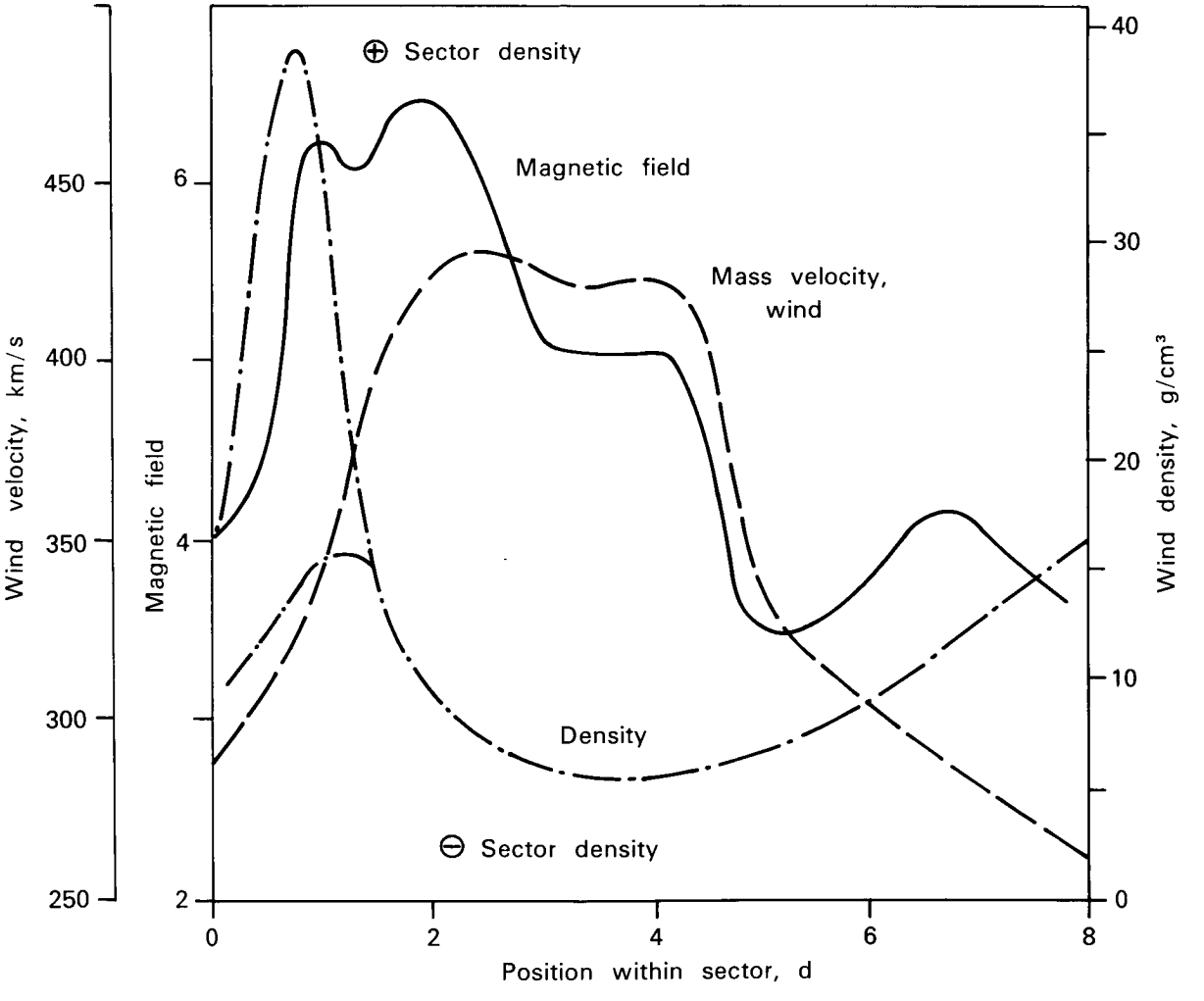

FIGURE 9.—Mean values of interplanetary magnetic field intensity, density and velocity of solar wind produced by the method of superimposition of eras.

magnetohydrodynamic perturbations such as hydromagnetic waves, nonspherical rapid jet flows, fast streams of plasma from chromospheric flares, and so forth, propagate with the supersonic stream from the wind. In these cases, the rapid development of solar activity such as chromospheric flares, the actions of individual active areas, and jet flows in the corona is predominant.

Such concepts as the corpuscular flow no doubt relate to the perturbed solar wind. The term "corpuscular flow" arose before discovery of the solar wind and has come to mean a strong flow of plasma, moving in the solar wind after bursts or as a recurrent phenomenon.

The section of reinforced solar wind or corpuscular flow is distinguished by the slightly greater velocity or density of the plasma and the increased magnetic field. An increase in the velocity and density of the plasma leads to reinforcement of the effects of the solar wind on the magnetosphere of the Earth, whereas the strengthened magnetic field slightly decreases and modulates the flux of galactic cosmic rays in those areas in space experiencing corpuscular flows. The clearest manifestation of unstable perturbations in the solar wind are shock waves, which will be described in more detail.

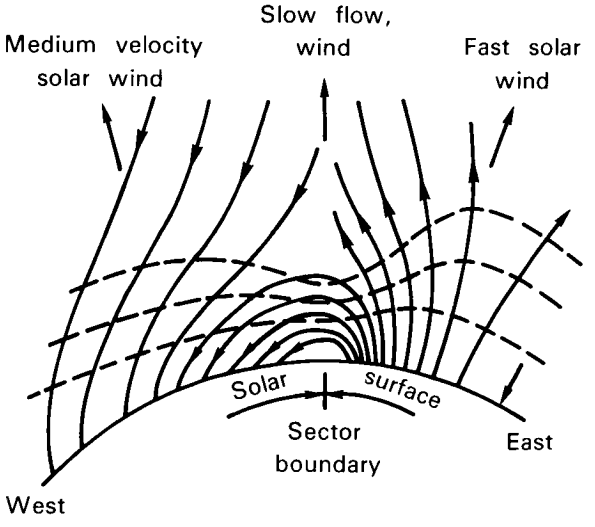

FIGURE 10. — Possible conditions for development of sectorial structure of interplanetary field in the corona. Dashed lines show isothermal surfaces. Solid curves with arrows show lines of force of the coronal magnetic field.

Shock Waves in Interplanetary Space

The stable state of the supersonic flow of the solar wind is disrupted during strong eruptions of the coronal plasma, which result from chromospheric flares on the Sun. Sharp expansion of the plasma in a flare region leads to formation of shock waves, usually having velocities of 1000 km/s, indicated by the type II radio radiation observed. The shock waves in interplanetary space propagate through the stable solar wind. Shock waves at distances of 0.7–1.5 AU from the Sun are now firmly established; they have sudden changes in macroscopic and kinetic parameters of the plasma, energetic particles, and deep modulation of the galactic cosmic rays, called Forbush effects.

The shock wave is characterized by the movement of matter through the discontinuity (wave front); the pressure is discontinuous, while all the laws of conservation of mass, momentum, and energy are observed. The density, velocity, and temperature behind the leading edge of the wave are greater than before the leading edge in the unperturbed area of the plasma. Analyses of the plasma parameters and measurement of low-energy solar protons penetrating the interplanetary magnetic field over the past 11-year cycle have shown that near 1 AU, the interplanetary shock waves can be characterized by values of relative velocity $U_{\text{wave}}-U_{\text{wind}}$ of 50 to 200–300 km/s, and by doubling of the density, temperature, and the magnetic field intensity of the plasma across the wave front (see Fig. 11-a, b) [70]. There are discussions in the literature of two physical concepts of shock waves.

One concept, based on the possibility of unambiguous identification of cosmic phenomena (plasmas, fields, and increasing intensity of cosmic rays of solar origin) with events on the Sun (flares), assumes that a flare generates a strong shock wave (velocity 1000–3000 km/s in the corona) which, as it propagates, undergoes significant deceleration, so that at the Earth's orbit, waves of weak or moderate intensity are measured (with Mach No. 2–3). The area of space containing the shock wave is a trap for solar protons with energies of ≤ 30 MeV, which are recorded simultaneously with arrival of the shock

wave. Processing of experimental observations based on these assumptions shows that the velocity of the shock wave decreases very rapidly ($\approx r^{-3}$), which means that some strong dissipative mechanism must be present. In this case, it is assumed that the shock waves are spherically symmetrical and propagate radially from the Sun.

The other concept [71] assumes that shock waves in interplanetary space usually have moderate intensity, do not decelerate significantly during propagation from the Sun to the Earth's orbit and cannot be identified precisely with events on the Sun. In other words, the shock waves observed near 1 AU may be generated either on the Sun (perhaps by several weak flares) or in interplanetary space at distances of 20–100 $R_\odot$, as a result of the action of plasma fluxes ejected from the corona. This concept is based partially on experimental estimates of the energy of flares from optical observations, measurements of radio and x-ray radiation, which determine the total energy of grade 2B–4B flares as around $2 \cdot 10^{31}$–$5 \cdot 10^{32}$ erg, and partially on results of gas dynamic studies of various flow modes of unstable gas streams in a medium, the density of which decreases as r^{-2}.

Many researchers have found that solar flares only indicate active regions on the Sun, some of which are responsible for geomagnetic activity. Geomagnetic perturbations should not always be related to shock waves propagating through the solar wind; frequently, they result from passage of a sectorial boundary contact surface in the interplanetary magnetic field.

Contemporary experimental and theoretical ideas on plasma phenomena in the interplanetary medium do not allow preference for either concept. Physical interpretations have not yet gone beyond the level of working hypotheses, but a number of important qualitative conclusions may be drawn and quantitative estimates made. The conditions of propagation of collision-free shock waves in interplanetary space are largely determined by the dynamics of the coronal plasma during a flare and status of the solar wind plasma before a flare. Optical observations and measurements of x-ray and radio radiation from the Sun indicate that the nature of a flare plasma flow may vary quite widely, and result in a highly complex process of shock wave generation in

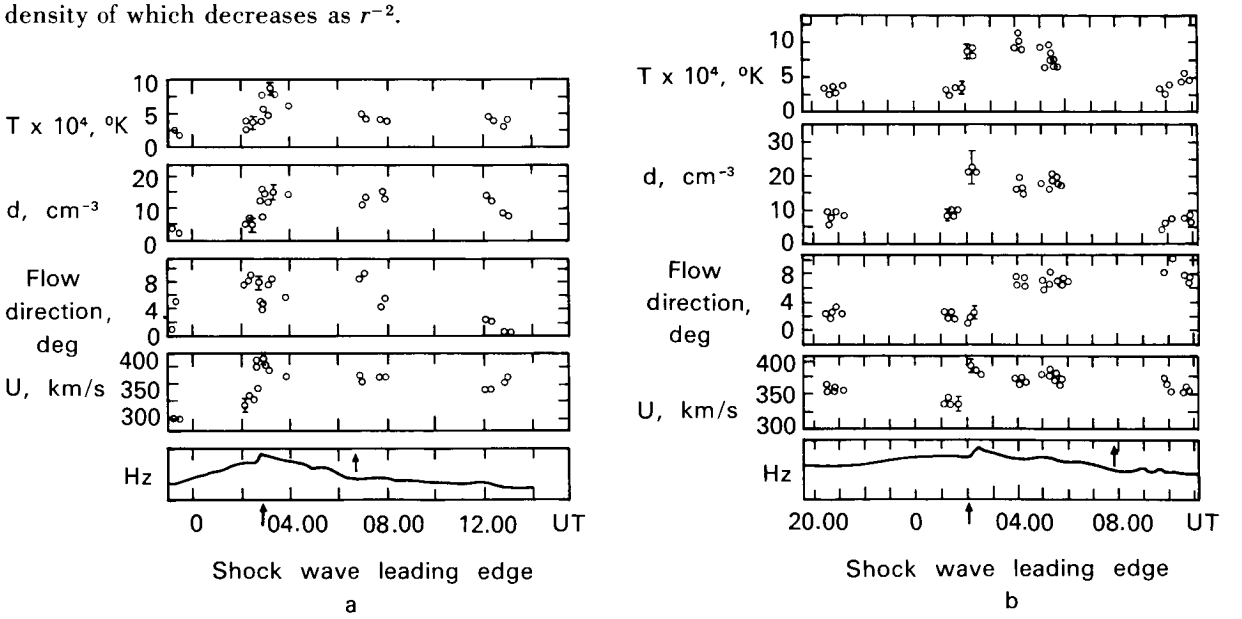

FIGURE 11.—Changes in temperature, density, direction, and velocity of solar wind protons: (a) for October 4–5, 1965, according to measurements of Vela–3B satellite; (b) for January 19–20, 1966, according to observations of Vela–3A satellite. Bottom graphs show sudden change in horizontal component of terrestrial magnetic field H_z, indicating sudden onset of magnetic storm. Direction 0° corresponds to radial flow from the Sun. Typical measurement errors are indicated.

the solar wind. Combined study of perturbations in the interplanetary medium following powerful flares (about 3B) permits sketching the dynamics of plasma flow at the Earth's orbit in many cases.

The event of February 15, 1967, was related to a grade 4B flare with coordinates 20° N, 10° W, which occurred on February 13. On February 15, the Earth satellites Vela 3A and Explorer 33 simultaneously recorded the first jump in plasma parameters and field intensity, which was interpreted as arrival of the leading edge of the shock wave (see Fig. 12). The geometric position of the satellites and the simultaneity of recording the shock wave showed that the direction of propagation of the leading edge of the wave (normal to the leading edge) made an angle of about 60° with the plane of the ecliptic. Measurements of the interplanetary field and recording the sudden beginning of the geomagnetic perturbation (SC) by surface geomagnetic stations permitted measurement of the mean direction of the normal to the leading edge of the shock wave. This also indicated an angle of about 50°–70°, forcing the assumption that the plasma flow following the flare was not spherical.

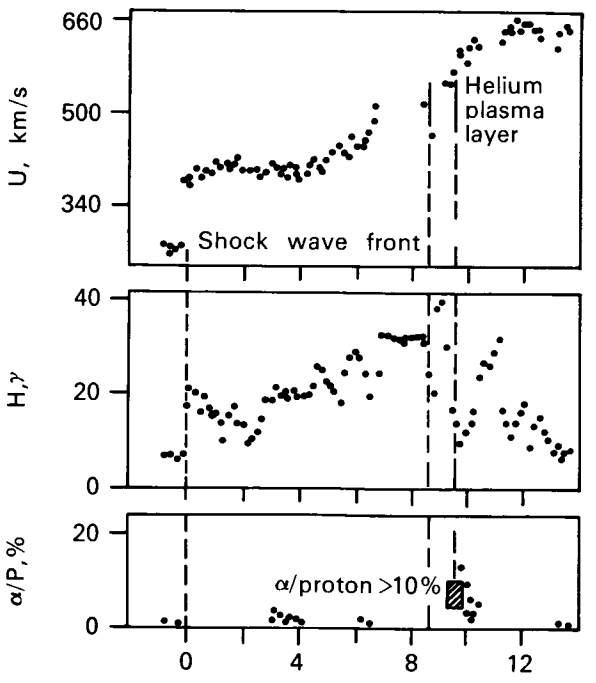

FIGURE 12.—Perturbations in the interplanetary medium following a chromospheric flare. U, velocity of solar wind; H, intensity of interplanetary magnetic field; α/P, percent content of helium in the solar wind in relation to hydrogen.

Measurements of the velocity, density, and magnetic field on February 15 and 16 (see Fig. 12) showed that the shock wave was pushed by the expanding coronal plasma. The "pusher" or, as it is more commonly called in gas dynamics, the "piston," was recorded about 9 h after passage of the leading edge of the wave and was saturated with helium. The plasma analyzers of Vela 3A showed a fivefold increase in content of α-particles [70]. Measurements of the structure of the interplanetary field by Explorer 33 showed that between the leading edge of the shock wave and the leading edge of the helium layer there was a tangential discontinuity. These important experimental facts have been noted by other researchers, who found that the shock wave is frequently accompanied by several tangential discontinuities and a three- to fivefold change in the relative content of helium to hydrogen. This increase in the content of helium in the interplanetary plasma has been observed repeatedly, but no single theoretical interpretation of it has been developed.

Based on analysis of parameters of solar proton plasma and fluxes during 1965–1970, data on shock waves in the interplanetary medium can be summarized:

- flares on the Sun can be precisely identified with shock waves in interplanetary space in some cases;
- shock waves generally propagate with Mach numbers 2–5, while the density, temperature, and magnetic field in the shock wave usually double in comparison with the unperturbed status of the interplanetary medium;
- the shock wave is often pushed by a "piston" of dense plasma, rich in helium;
- plasma flows in which the propagation of shock waves is not spherically symmetrical have been observed;
- the plasma area between the leading edge of the shock wave and the leading edge of the helium piston generally contains one or more tangential discontinuities, and rotary discontinuities may develop;
- aspherical shock waves are frequently

interpreted as propagation of a spherical wave with a displaced center.

Galactic Cosmic Rays

Galactic cosmic rays, the most energetic component of corpuscular flow in interplanetary space, consist of nuclei of chemical elements, primarily hydrogen, of very high energies. Galactic cosmic rays (except the neutrino) exceed all other types of radiation in penetrating capacity. The mean energy of the primary particles observed near the Earth is about 10^{10} eV; the energy of some individual particles may reach 10^{20} eV and higher. The energy spectrum of galactic protons at energies over 10^4 MeV can be represented as:

$$\frac{dN}{dE} = 2.14 \cdot 10^9 E^{-2.7} \, (\mathrm{m^{-2} \cdot s^{-1} \cdot sr^{-1} \cdot MeV^{-1}}) \quad (3)$$

where E is expressed in MeV.

For lower energies, the flux of the particles depends on solar activity: at the maximum and minimum of solar activity, the total flux of galactic cosmic rays with energies $E > 30$ MeV (nucleon is about 2000 $\mathrm{m^{-2}\ s^{-1}\ sr^{-1}}$ and 6000 $\mathrm{m^{-2} \cdot s^{-1} \cdot sr^{-1}}$ respectively).

The chemical composition of galactic cosmic rays in the high-energy area is sufficiently known (see Table 6). The flux of nuclei represented in Table 6 relates to particles with energies $E > 2.5 \cdot 10^3$ MeV/nucleon.

The chemical composition of primary cosmic rays differs slightly from the composition of elements in the Earth's crust, meteorites, solar atmosphere, and atmosphere of certain stars, which is known from spectroscopic analysis. Cosmic rays are characterized by relatively lower content of hydrogen and helium, and predominance of the heavier elements, particularly noticeable in the area of light nuclei (Li, Be, B group), where the difference reaches several orders of magnitude. This doubtless reflects the nature of the sources of cosmic rays, mechanism of their acceleration, and status of interstellar space, which the cosmic rays penetrate on their path to the Earth. It serves as a serious argument in favor of the theory of the origin of cosmic rays and their subsequent fragmentation upon collision with nuclei of interstellar material. In addition to the nuclei of the chemical elements, the galactic cosmic rays contain a slight flux of electrons and gamma quanta.

TABLE 6.—*Flux of Nuclei*

Nuclei, groups	Symbol	Charge	Mean number, nucleons/nucleus	Flux of particles $\mathrm{m^{-2} \cdot s^{-1} \cdot sr^{-1}}$	Percent total flux
Proton	P	9	1	1500	≈94
Helium nuclei	α	2	4	90	5.5
Light	L	3–5	10	2	
Medium	M	6–9	14	5.6	
Heavy	H	10–19	30	1.9	0.6
Very heavy	VH	20–28	48	0.7	

The energy spectra of various particles observed in interplanetary space at a distance of 1 AU from the Sun are shown in Figure 13. As distance from the Sun increases, the flux of

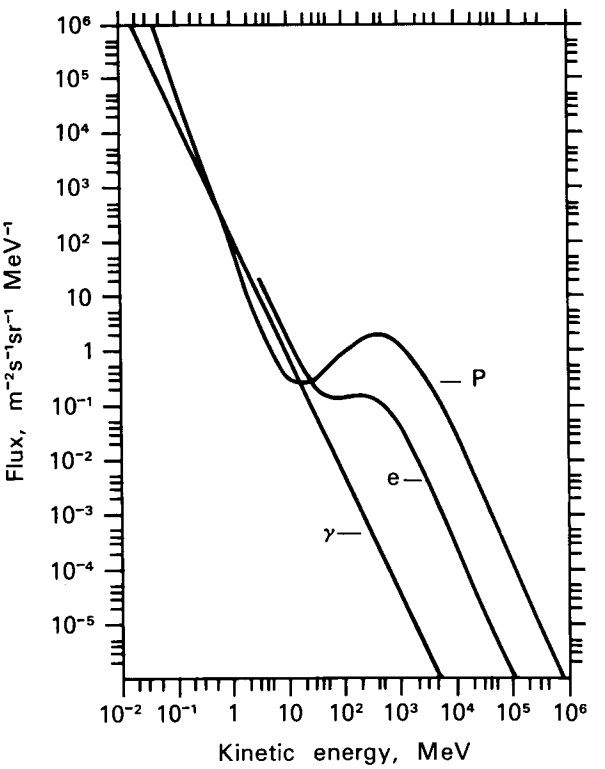

FIGURE 13.—Idealized spectrum of galactic protons, electrons, and γ-rays.

galactic cosmic rays can only increase, because the magnetic fields in the solar system, carried away from the Sun by the solar wind, prevent penetration of cosmic rays into the inner areas of the solar system. This same mechanism, the modulation mechanism, causes the difference in fluxes of particles in different phases of the solar activity cycle. Increased flux of cosmic rays cannot continue without limit. At some distance from the Sun, the solar wind density or interplanetary magnetic field intensity will no longer exceed the corresponding parameters of interstellar space and at these distances, modulation of galactic cosmic rays will cease. The area of modulation of galactic cosmic rays is estimated to be about 10–30 AU.

The differential energy spectra of charged particles have a minimum in the area of 30–60 MeV (Fig. 14). It is assumed at present that particles with energies less than 30–60 MeV are of solar origin, i.e., can be considered solar cosmic rays. Experimental and theoretical aspects of galactic cosmic rays have been widely studied [45, 55, 94, 117, 118, 141].

Solar Cosmic Rays, Definition and Classification

The Sun is a source of corpuscular radiation over a broad range of energies. Solar cosmic rays form the high-energy portion of the Sun's corpuscular radiation. Fluxes of protons and electrons observed in interplanetary space, with energies of tens of keV to several hundred MeV, and originating in various forms of solar activity will be discussed here.

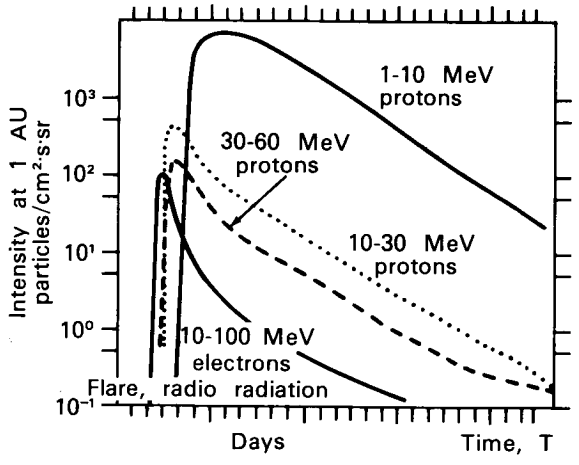

FIGURE 14.—Typical increase in flux of solar cosmic rays observed immediately after a major chromospheric flare.

The study of high-energy particles generated by the Sun began in 1942. Until early 1957, only five events were studied when high-energy particles reached the Earth. Since then, experiments performed at high altitudes using balloons, satellites, and rockets, and observations with rheometers, have shown that fluxes of solar protons with energies of 100–300 MeV appear in the area of the Earth approximately once a month during the time near the solar maximum. Since 1964, practically continuous (monitor) observations using Earth satellites and spacecraft have been made outside the terrestrial magnetosphere. During this time, the energy threshold of recording protons has been significantly reduced to a few hundred keV and the installation of low- and medium-energy electron detectors on spacecraft began. Experiments beginning in 1967 have shown that electrons with energies from 10 keV to several MeV and protons with energies of tens of keV to several hundred MeV are generated by the Sun during flares [134].

Fluxes of charged particles observed in interplanetary space at about 1 AU from the Sun can be divided arbitrarily, according to their relationship to various forms of solar activity, into these groups.

1. Increases in protons with energies up to several hundred MeV and high-energy electrons with energies up to 10 MeV, immediately follow large (class 1B and higher) solar flares. These show a rapid increase in the intensity of particles, and arrival of the particles from the Sun at the point of measurement according to their velocity, i.e., the more energetic particles appear before less energetic particles. At the maximum of large flares, the intensity of the proton flux with energy $E_p > 1$ MeV reaches values of about 10^5 particles/cm$^2 \cdot$ s. The drop of these streams usually shows a characteristic exponential shape with a time constant τ of about 10–30 h.

2. An increase in low-energy electrons with energies of 10 to several hundred keV is generally observed following small flares. These increases differ from increases in group 1 and therefore are considered separately.
3. Long-lived streams of protons and electrons of low and moderate energies, apparently form after large flares and rotate with the Sun. These streams, when observed by spacecraft, have a relatively smooth rise and fall; the duration of recording these streams (characterizing their angular width in the plane of the ecliptic) is 6–30 h. Some streams, particularly during minimum solar activity, may exist for several solar revolutions, and are called recurrent streams.
4. Streams of protons and electrons are observed near the Earth simultaneously with shock waves from large solar flares. The passage of these particles has not yet been definitely established. It is possible that these particles move with the shock wave from the Sun in a trap, or are accelerated in the shock wave itself as it moves through interplanetary space or, if they exist for some time, are transferred by the shock wave with tubes of force lines to the point of observation. Since it has been assumed in some studies that these particles are accelerated behind the leading edge of the shock wave (causing a magnetic storm on the Earth), the electrons and protons in these streams, in earlier works, were frequently called "energetic storm particles."
5. A minimal background flow of protons with energy $E_p < 20$ MeV and, possibly, electrons with energy $E_e < 3$ MeV, not directly related to flares, change slowly with changes in the overall level of solar activity.

Properties of Solar Cosmic Ray Events During Large Flares

Large flares characteristically occupy a vast area of the Sun's surface and are observed in the Hα line for long periods (about 2 h). These flares are accompanied by intensive x-ray and complex microwave bursts, frequently followed by type II and IV radio radiation.

During a solar flare, particles are ejected from the Sun, which, at a distance of 1 AU, is observed as a time change in the flux, with a rapid increase to its maximum value and a slow, exponential drop. The development of events in time for these situations is shown in Figure 14.

The maximum fluxes of particles, for example protons with energies >1 MeV, recorded in interplanetary space following large solar flares, reach 10^5 particles $\cdot$ cm$^{-2} \cdot$ s$^{-1} \cdot$ sr^{-1}. These fluxes are observed rarely and only after the largest flares. The fluxes of protons usually observed are 10^2–10^3 particles $\cdot$ sm$^{-2} \cdot$ s$^{-1} \cdot$ sr^{-1}. The number of events recorded increases with decreasing intensity.

Electrons from flares with energies of 10 to several hundred keV were first observed, 1965–1966, in interplanetary space. Streams of electrons with energies of 40 keV $\leq E_e \leq$ 300 keV, recorded in mixed electron-proton events, act differently from protons and relativistic electrons. The properties of streams of low-energy electrons will be considered in detail separately; this section deals with the properties of streams of protons and electrons with energies at $E > 1$ MeV.

In spite of the serious interest in solar cosmic rays, detailed study of the chemical composition has been performed with photographic plates launched on rockets for only four flares. The flare of November 12, 1960, was most thoroughly studied, during which several research rockets were launched and hardness spectra were produced for protons, helium nuclei, and nuclei with charge $6 \leq Z \leq 9$. The spectra are in Figures 15 and 16 [19]. Within limits of accuracy, all three groups of nuclei have identical dependence on hardness. The ratio of fluxes of helium nuclei and nuclei of group "M" ($6 \leq Z \leq 9$) remained constant during measurement, whereas the relative flux of protons changes, which is evident from comparison of the scales of Figures 15 and 16.

During the flare of July 18, 1961, an upper limit of the ratio of fluxes of "L" nuclei ($3 \leq Z \leq 5$) to "M" nuclei of 0.07 was produced. The relation-

ship between the flux of helium nuclei and that of group "M" nuclei remained the same as in the flare of November 12, 1960. The mean ratio of these fluxes for all measurements was 62 ± 7. Figure 17 shows the charge spectrum of solar cosmic rays [20]. The relationship of fluxes of nuclei of oxygen and carbon differs from this ratio in primary cosmic rays and agrees well with the composition of the photosphere of the Sun.

Increases in Fluxes of Particles

Near the Earth, an increase in intensity of solar cosmic rays is most frequently recorded following flares near longitudes of 60° W. These longitudes serve as the sole origin for the lines of force of the interplanetary magnetic field

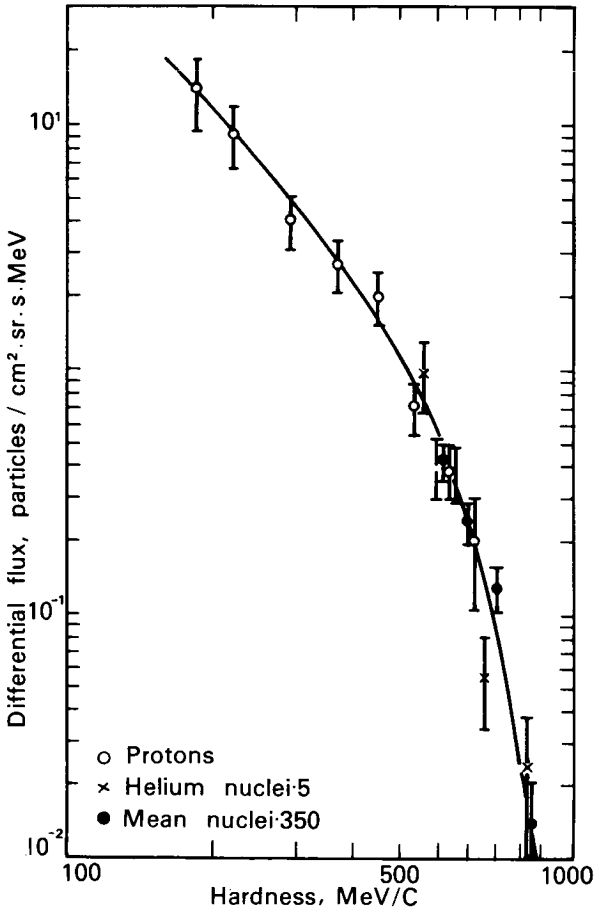

FIGURE 15.—Hardness spectrum of solar protons, helium nuclei, and nuclei with charge $6 \leq Z \leq 9$, measured during flare of November 12, 1960, at 18:40 UT [19].

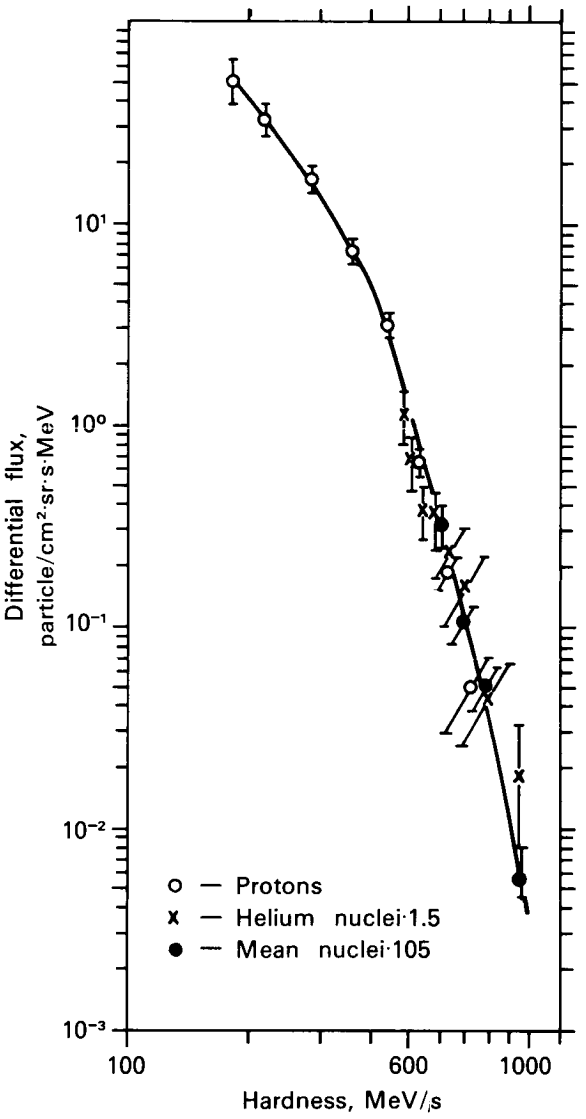

FIGURE 16.—Hardness spectrum of solar protons, helium nuclei, and nuclei with charge $6 \leq Z \leq 9$, measured after flare of October 12, 1960. Data relate to 16:03 UT, November 13 [19].

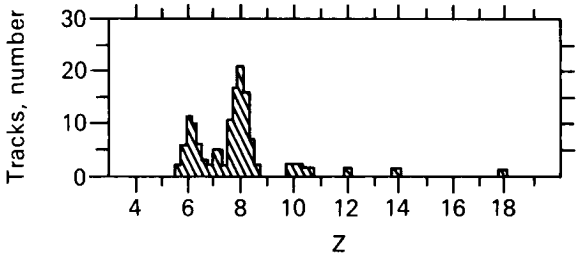

FIGURE 17.—Charge spectrum of solar cosmic rays for flare of November 12, 1960 [20].

passing by the Earth at the mean velocity of the solar wind $u \approx 400$ km·s. However, this does not mean that particles generated in flares outside of these longitudes are not recorded near the Earth. The increases caused by eastern and western flares, as well as flares at higher latitudes greater than 15–20° are also observed near the Earth. The rise front in these events is usually less steep ($t \approx 5-10$ h) than for increases produced by flares at low latitudes of the Sun and at longitudes of 50°–60° W.

Solar Flares with Various Levels of Activity

Solar particles in interplanetary space depend directly on the activity of the Sun. During years near the minimum solar activity, large flares are rare; likewise, generation of cosmic rays. Spacecraft flying during 1964–1965 often did not record a single event for months.

The statistics of proton ($E_p > 15$ MeV) increases measured at the beginning of the 20th cycle of solar activity by the IMP series satellites are shown in Figure 18 [83]; the number increased sharply in 1966–1967. High-energy electrons appear more frequently in interplanetary space during years near the maximum of solar activity. For observations in near-Earth orbits, the time required to reach the maximum is usually a half to several hours following the beginning of a flare, indicating the mean distance traveled by

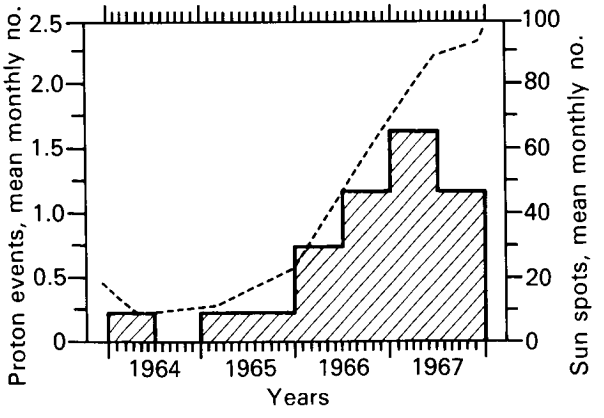

FIGURE 18.—Number of proton increases $E_p > 15$ MeV recorded by IMP satellites as a function of mean number of sunspots. ---- —number of sunspots; —— —proton events.

most particles is greater than 1 AU. This is particularly noticeable in a flare at the base of force lines of the interplanetary magnetic field not connected with the Earth, for example in the far western and eastern longitudes, or the far southern or northern latitudes.

Figure 19 shows the dependence of observed particle fluxes in various energy intervals on the path traveled by these particles for the flares of July 7, 1966 (a) [83], February 25, 1969 (b) [13], and September 28, 1961 (c) [141]. These figures show that the points for protons of various energies and relativistic electrons, within the limits of measurement error, fall on the same curve. This agreement indicates that protons and relativistic electrons travel the same path from the moment of acceleration to the moment of recording. The mean length of this path, determined on the basis of the maximum of the increase, is near 8–10 AU.

A curve for low-energy electrons is shown in Figure 20. These electrons arrive at the point of observation before the protons and relativisitic electrons, which is characteristic for such mixed electron-proton events. The intensity of the fluxes of protons and electrons in impulse events decreases with time according to an exponential rule with $\tau_0 \approx 0.5-1.5$ d. This rule is well fulfilled for times of 5–6 τ.

Energy Spectra of Solar Particles

Measurements of the energy spectra of solar cosmic rays performed in the stratosphere and by remote satellites have shown that the energy spectra of solar protons can be described by an exponential function of the form $N(\geq E) = AE^{-\gamma}$ for a broad range of energies (from several MeV to several hundred MeV), where $N(\geq E)$ is the number of particles with energies higher than E, while A and γ are constants for a specific flare. For various flares, the values of A change over several orders of magnitude; the exponent γ has a range of about 1–5, and is most frequently 3 or 4.

Detailed measurements of the energy spectra are rare, and have been performed by different methods and in different energy intervals. Several examples of energy spectra for various increases in solar cosmic rays are presented below. Figure

20a shows the differential spectrum of protons for the flare of February 25, 1969 [13]. This event has been carefully studied over a broad energy interval. The spectrum presented was produced 14 h after the beginning of the event; its index over a broad energy interval is $\gamma = 2.7$.

Figure 20b [35] shows a spectrum of electrons for the same flare, which also follows the rule $E^{-\gamma}$, where $\gamma \sim 3$–4 as shown in Figure 20b. The index of the integral spectrum of relativistic electrons for most events is $\gamma \approx 4$. Figure 21 [25] shows energy spectra of solar protons for the flares of September 28, 1961, and October 29, 1962, extrapolated in time to the moment of the flare, i.e., the energy spectra formed in the process of acceleration.

The spectra both of protons and of energetic

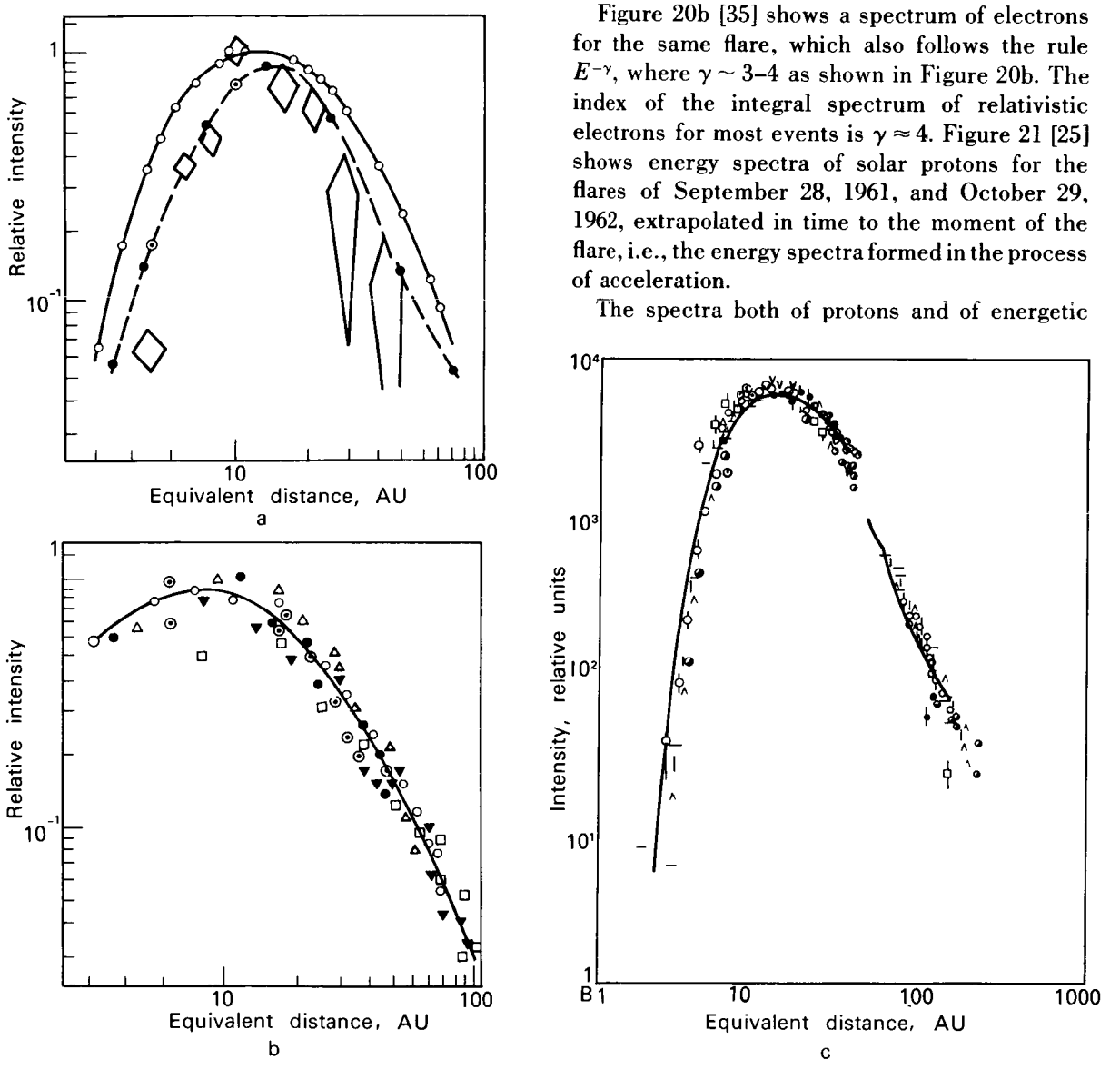

FIGURE 19.—Intensity of particle flux (normalized at maximum) as a function of path traveled by particles of various energies. Path defined as produce of particle velocity by time elapsed between moment of injection and moment of recording.

(a) for protons and electrons of various energies from flare of July 7, 1966 [83]: ○, ≥ 45 keV electrons, with $\beta \approx 0.4$; ◇, 3+12 MeV electrons, $\beta \approx 0.99$; ●, 19+45 MeV protons, $\beta = 0.20 + 0.30$; ⊙, 16+38 MeV protons, $\beta = 0.18 + 0.28$;

(b) for protons of various energies in flare of February 25, 1969 [71]: ⊙, 30 MeV; ●, 45 MeV; △, 67 MeV; ○, 98 MeV; ▼, 160 MeV; □, 282 MeV;

(c) for protons of various energies in flare of September 28, 1961 [140]: ∨, 2.2 MeV; ●, 3.8 MeV; ◑, 5.7 MeV; ○, 7.9 MeV; ⊙, 14.5 MeV; ◒, 87 MeV; —, 135 MeV; |, 175 MeV; ∧, 230 MeV; ⊘, 295 MeV.

electrons, measured some time (about 20–30 h) after the flare, apparently have the same form with $\gamma \approx 3$, regardless of the magnitude of the flare. When solar cosmic rays are observed simultaneously with the arrival of a shock wave, the energy spectra are greatly softened (Fig. 22 [34]).

Anisotropy of streams. Considerable experimental material has been accumulated on the angular distribution of streams of protons and of low-energy electrons. Measurements have not been made of the angular distributions of high energy electrons. If the angular distribution of particles is expressed as

$$F(\theta) = a + b \sin(\theta + \phi), \quad (4)$$

then the quantity $A = a/b$ defines the anisotropy of the stream, while angle ϕ is the anisotropy direction. With more complex angular distribution, the stream may have more than one maximum, and there may be so-called bidirectional anisotropy. If the measurements are performed in two directions, for example, "toward the Sun" and "from the Sun," the anisotropy is

$$A = \frac{n_+ - n_-}{n_+ + n_-} \quad (5)$$

where n_+ is the flux from the Sun; n_- is the flux toward the Sun. Simultaneous measurements of the flux of particles and the direction of the interplanetary magnetic field have shown that there is a strong correlation between the direction of the angular distribution maximum and the direction of the magnetic field at the point of observation (Fig. 23 [87]). Simultaneous measurements of the anisotropy of streams of protons and

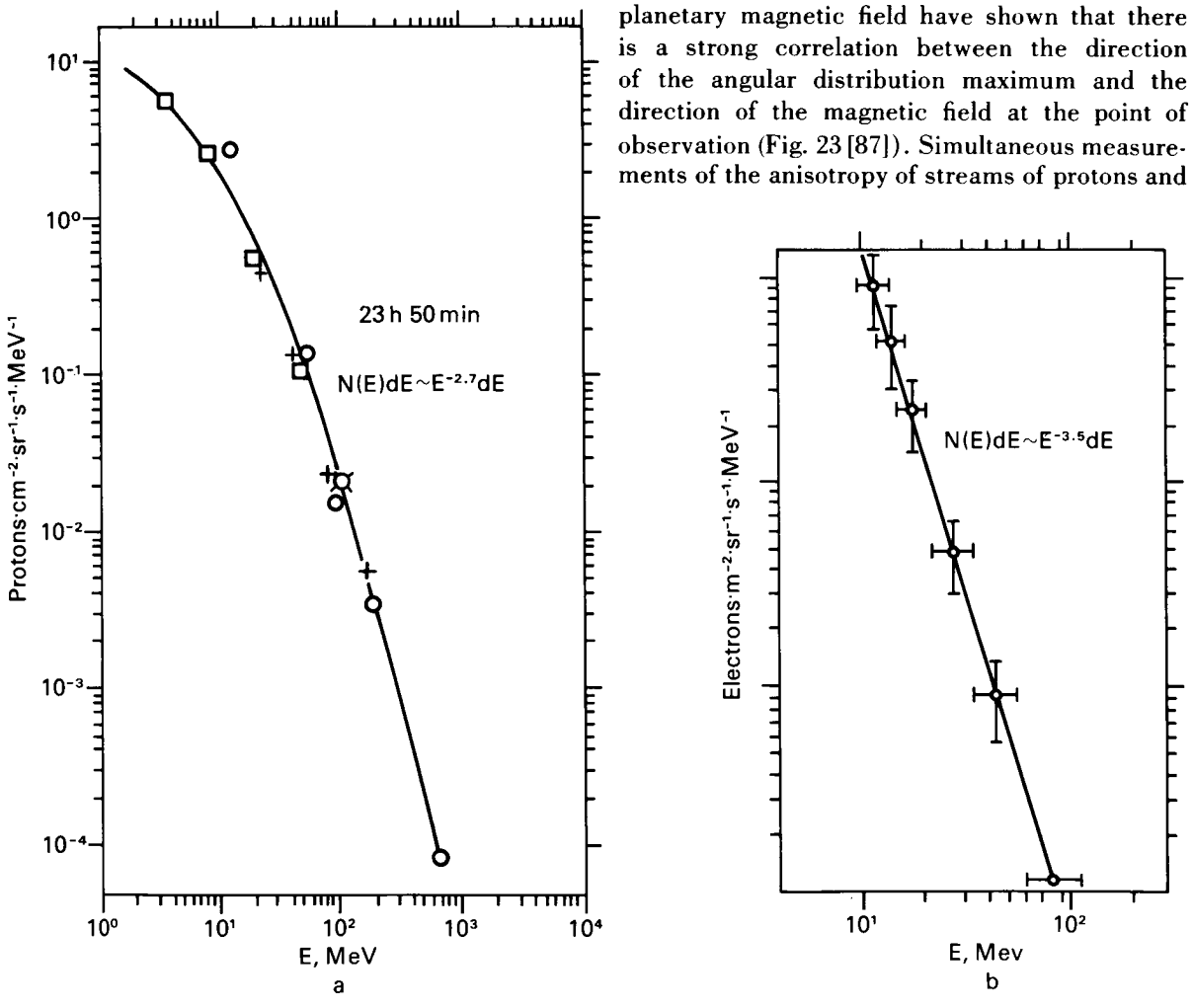

FIGURE 20.—Energy spectra of solar cosmic rays for flare of February 25, 1969. (a) according to [13]; (b) according to [35]

low-energy electrons in mixed proton-electron events have shown that the directions of maximum arrival of protons and electrons coincide. Figure 24 shows an example of such correlation between streams of electrons and protons [104].

The amplitude of anisotropy for low-energy protons and for low-energy electrons in mixed proton-electron events reaches 70%–80%. For events related to eastern flares and far western flares, with a slower rise front ($\tau \approx 10$ hours), the anisotropy is slightly less, $A \approx 30\%-50\%$. The amplitude of anisotropy decreases, after reaching the maximum of intensity, although the maximum of the flux remains directed toward the field.

The time course of intensity of tones with $E = 7.5-45.0$ MeV is presented in Figure 25 [90] for the flare of November 18, 1968, which was near the western limb of the Sun 18° N, 84° W, at 10 h 30 min UT, and was accompanied by types II and IV radio bursts. Figure 26 [104] shows a vector diagram for changes in anisotropy of protons of 0.7–7.6 MeV in the time following a flare. During the initial period $T < 2$ d, during the phases of increase and decrease, the anisotropy reaches 50% (western flare). The direction of the anisotropy is near the mean direction of the interplanetary magnetic field. The value of anisotropy is related to the energy of particles so that A is greater for particles with lower velocity.

During later stages of an event, for times $1-2 < T < 4$ d, when the flux of particles is not great, there is also some anisotropy of protons, with a value directly proportional to the velocity of the solar wind, u, and inversely proportional to the velocity of the particles, v. This anisotropy, as shown below, is caused by transport of particles from the space near the Sun by the solar wind and is called "equilibrium" anisotropy, the area of which is directed radially from the Sun.

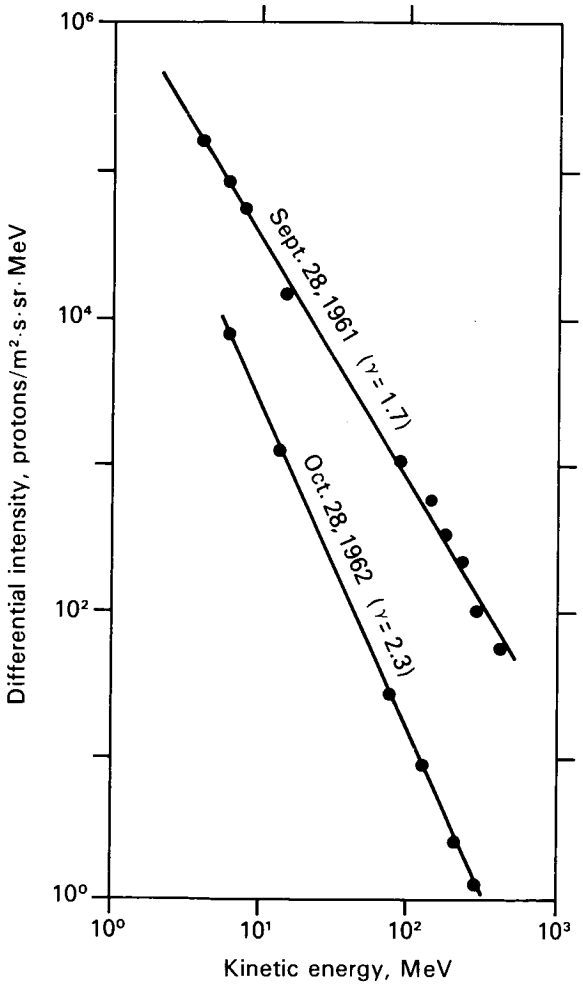

FIGURE 21.—Differential energy spectra of protons extrapolated to moment of flare [25].

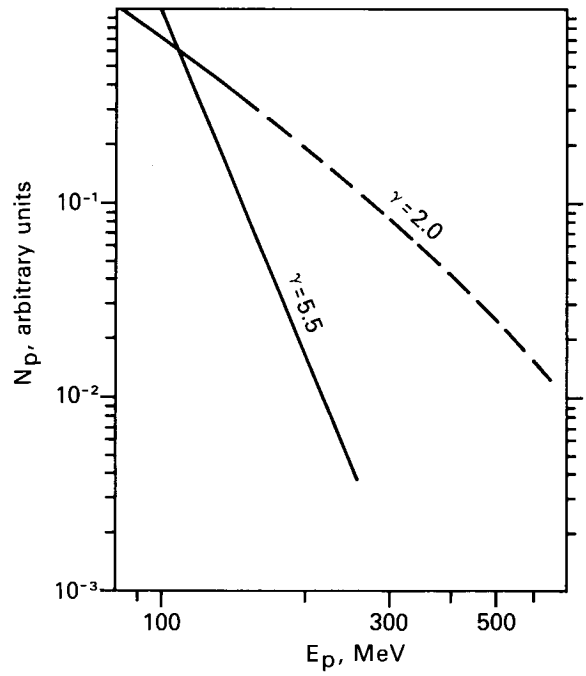

FIGURE 22.—Mean integral spectra of solar protons for energies over 100 MeV during magnetically quiet periods (dashed line) and during magnetic storms (solid line) [34].

In the last phase, decreasing flux of solar protons for $T > 4$ d, the anisotropy becomes eastern making an angle of 45° from the Sun-spacecraft line with a value of anisotropy $A \approx$ 5–10%. Equilibrium anisotropy in this late period is also inversely proportional to the velocity of the particles.

Increases in Fluxes of Low-Energy Electrons

Electrons with energies of 10–100 keV are the most common and most frequently encountered types of particle emitted by the Sun during mild and moderate flares. During the 20th solar cycle, from 1964 to mid-1970, about 230 such events were recorded by spacecraft near the Earth. The properties of electrons emitted by small solar flares are:

1. Streams of electrons can almost always be correlated to an optical flare, which may have small areas, but are bright in the H_α line.
2. The intensity of streams of electrons observed near the Earth after individual flares may reach about 10^4 particles · cm^{-2} · s^{-1} · sr^{-1} for energies $E_e > 40$ keV. In most cases, fluxes of 10–1000 particles $cm^{-2} \cdot s^{-1} \cdot sr^{-1}$ were recorded at the maximum of each event [83]. The electrons are not usually accompanied by significant streams of protons. The energy spectra of solar electrons in interplanetary space in most cases can be represented in exponential form:

$$N(E)\,dE = K \cdot E^{-\gamma}\,dE \qquad (6)$$

where $\gamma \approx 3$ in the interval of energies of 20–45 keV; over 100–200 keV the spectrum falls very rapidly ($\gamma \geq 5$). This means that particles with energies of over 200–300 keV are not present in these streams.
3. The delay of arrival of electrons to the

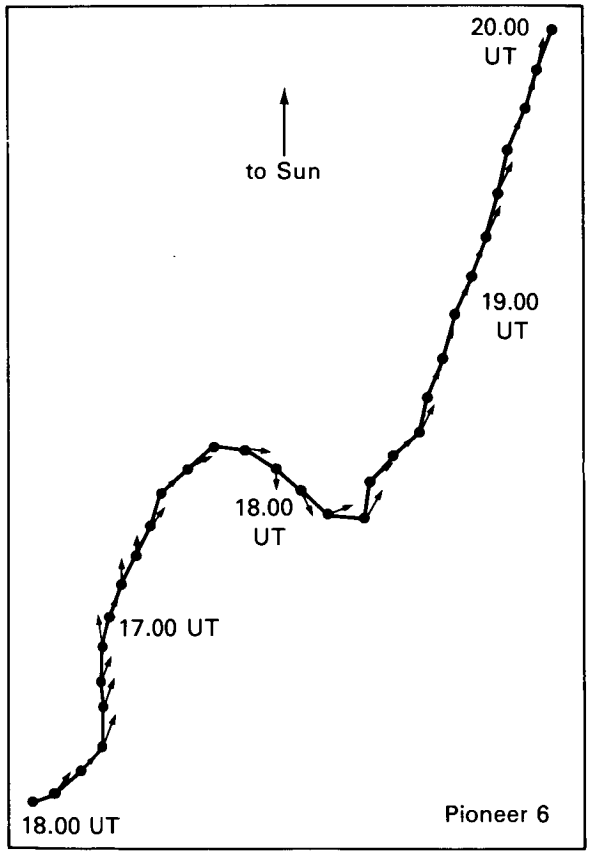

FIGURE 23.—Direction of interplanetary magnetic field in the plane of the ecliptic (azimuth) and anisotropy of cosmic rays during period 16:00–20:00 UT, December 30, 1965 [87].
●—● azimuth of field lines;
●—> direction of anisotropy of cosmic rays.

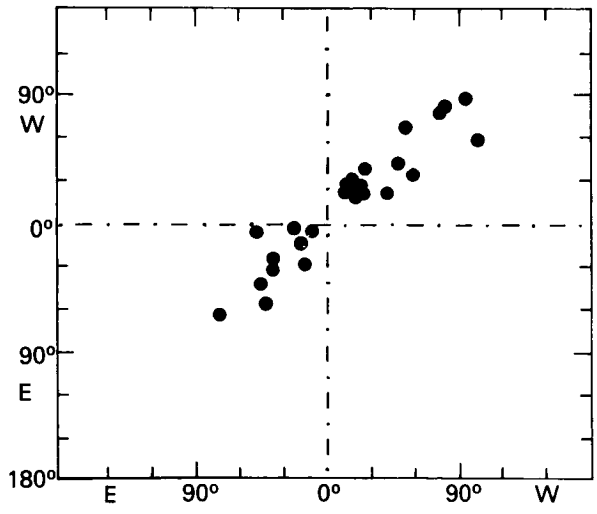

FIGURE 24.—Correlation between direction of arrival of streams of protons and electrons in mixed electron-proton events [104].

Earth in relationship to the burst of x-rays usually is 15–60 min. The rise time to the maximum is much briefer than the rise time of the flux of protons following large flares (usually 5–50 min). The drop in intensity has a dual nature. In some cases, an exponential decrease in intensity is noted from the maximum at $\tau \approx 12$ h [83]. In other cases, there is a rapid drop with τ on the order of the rise time, followed by a much slower drop in intensity as soon as it has reached 10% of its maximum value.

4. When the active area moves across the solar disk, electrons from this area reach the Earth only when the area falls within a certain interval of heliolongitudes. Statistical analysis of the electron increases leads to the conclusion that most of the electrons recorded at the Earth are produced by flares located $60° \pm 30°$ W solar longitude (see Fig. 27 [83]). These conclusions lead to the concept of "cones of propagation," with a width of 30°–90°, within which low-energy electrons propagate in interplanetary space (Fig. 28 [83]). If this is true and the electrons are emitted only in the "cone of propagation," only a portion of all the electron events generated on the Sun can be recorded on the Earth.
5. The anisotropy of streams of electrons has recently been measured. The initial anisotropy is great and directed along the interplanetary magnetic field, after which it falls much lower than the anisotropy of proton events, reaching an equilibrium value of about 2.5%. This indicates

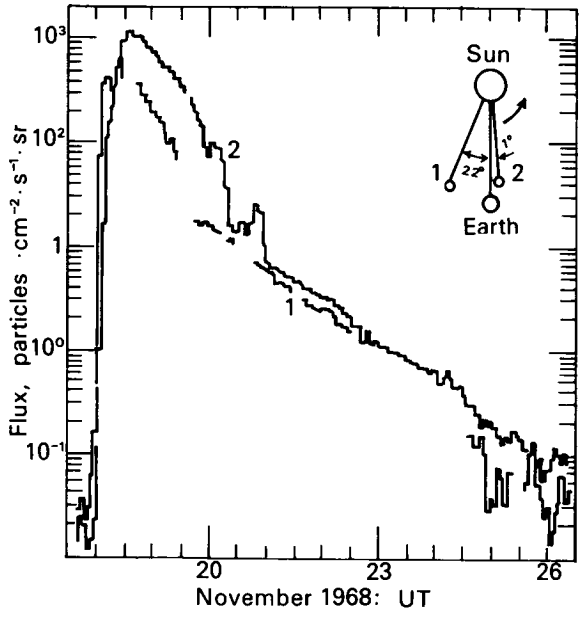

FIGURE 25.—Time behavior of flux of protons with energies $E_p = 7.5$–45 MeV [90].
1—Pioneer 8
2—Pioneer 9

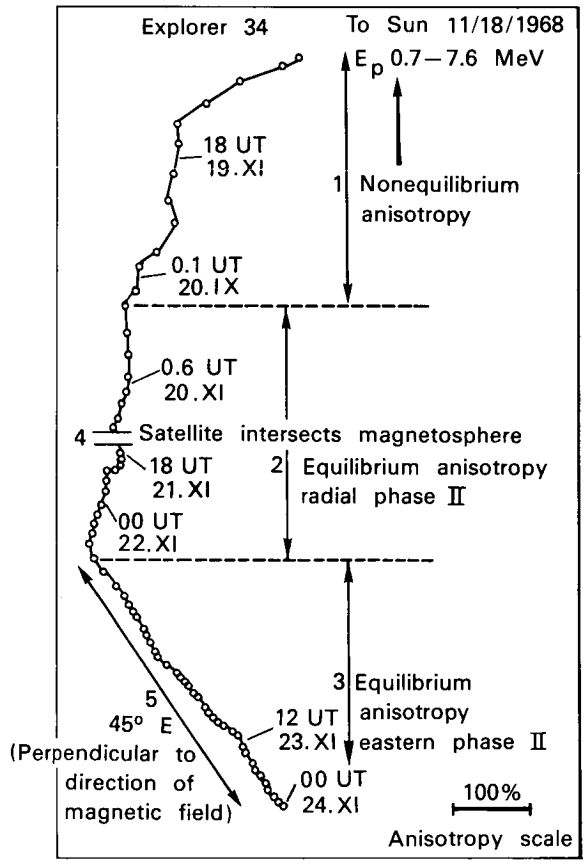

FIGURE 26.—Vector diagram of change in direction of anisotropy with time for flare of November 18, 1968. Anisotropy in initial nonequilibrium phase of event (1–2 d) directed along lines of force of field and value near 50%. Vector diagram construction: each vector represents the mean for a certain interval of anisotropy. The length of each vector corresponds to the amplitude of anisotropy, the direction—to the direction of the maximum flux of particles in the plane of the ecliptic [104].

that the nonequilibrium anisotropy exists for a long time during the phase of decreasing electron flux. The question of anisotropy is still far from answered and requires many more experiments.

Solar Particles Localized in Space

Streams of high-energy particles are almost always related to flares on the Sun. Low-energy particles (protons with energies of 0.3–20 MeV and electrons with energies of 20–100 keV) may appear in interplanetary space at times other than immediately after a flare. An increase in streams of particles is frequently observed which cannot be related to a visible flare, or for which the interval of time between the optical flare and the rise in the flux of low-energy particles is much greater than the direct flight time of the particles. Measurements by spacecraft of such delayed fluxes have shown that the time course of intensity is almost identical for protons with energy $E_p \sim 0.5$ MeV and $E_p \sim 10$–20 MeV. When this type of increase is recorded, the spacecraft is intersecting a stream of particles localized in space, moving with the solar wind. The magnetic field of this area modulates the intensity of the galactic cosmic rays, and causes a Forbush reduction; the flux of plasma, colliding with the magnetosphere of the Earth, may cause geomagnetic disturbances.

These localized areas are usually tubes of force lines extended in space and rotating with the Sun. These "rotating" fluxes are frequently so long-lived that they are observed over several rotations of the Sun as recurrent events, repeating with periods of 27 d. Long-lived streams of protons with energies of several MeV are usually related to active areas on the Sun. The initial sources of long-lived protons are assumed to be solar flares, supporting extended expulsion of plasma after the flare from the same active area. Subsequently, the stream remains attached to the same active area.

The magnetic field frozen in the plasma of the solar wind fully determines the motion of particles in these streams; i.e., the particles move within a certain cone of lines of force of the magnetic field, carried outward from the Sun by the solar wind. Therefore, when the same stream is measured at two points in interplanetary space, a shift in the time of recording the increase ΔT is observed. This is related to the velocity of the solar wind, u, and the distance between the points of observation:

$$\Delta T = \frac{\Delta R + \Delta\phi \cdot R}{u} \cdot \cot\theta = \frac{\Delta R}{u} + \frac{\Delta\phi}{\Omega} \qquad (7)$$

where $\Delta\phi$ is the angular distance between the spacecraft;

ΔR is the radial distance between the spacecraft;

u is the speed of the solar wind;

$\Omega \approx 13.3°/\text{d}$ is the angular rate of rotation of the Sun;

$\cot\theta$ is the angle of inclination of the lines of force of the magnetic field in the plane

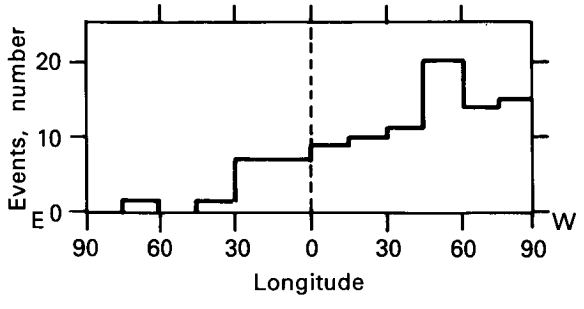

FIGURE 27.—Dependence of recording of electron increases on heliographic longitude of flare [83].

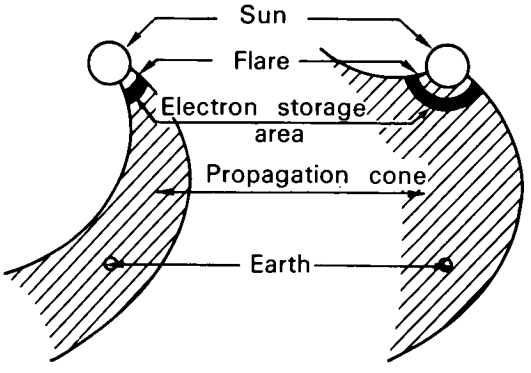

FIGURE 28.—Concept of the "cone of propagation" of electrons in interplanetary space.

of the ecliptic to the radius at the given point;

R is the distance from the Sun.

This shift in recording time of two spacecraft separated in longitude allows an unambiguous increase in particles in rotating streams to be separated from all other types of increase in the case of simultaneous presence of spacecraft at different points in space.

Figure 29 is an example of the recording of such an increase by the Zond–3 and Venera–2 spacecraft [138]. The mutual placement of the spacecraft during recording of the localized stream is to the right.

The properties of such streams, characteristic for most recorded increases, are summarized briefly.

1. The intensity of particles in long-lived streams is usually low: $N \approx 10$–100 $cm^{-2} \cdot s^{-1} \cdot sr^{-1}$. For protons with energies of $E_p \approx 0.5$ MeV and electrons with energies of $E_e \gtrsim 40$ keV, the intensity may sometimes reach 10^4 $cm^{-2} \cdot s^{-1} \cdot sr^{-1}$.
2. The energy of particles populating these streams is usually not great: $E_e \approx 40$–300 keV, $E_p \approx 0.5$–20 MeV. In several cases, electrons of high energies have been recorded in rotating streams (Fig. 30 [88]).
3. The energy spectra of electrons and protons recorded in long-lived streams are usually softer than those of particles observed during flare bursts.
4. The long-lived streams may consist only of protons or electrons, but sometimes both.
5. When streams of protons and electrons are recorded, an electron maximum is frequently followed by a proton maximum [6].
6. Rotating streams sometimes have a broad halo of 70°–90° longitude; the halo is of harder particles of relatively low intensity. At the center of the stream, where the particles have lower energy, the concentration of particles is higher. The duration of recording the central portion of a stream is usually 6–12 h, indicating that the angular width of the central stream is 3°–6°.
7. The anisotropy of long-lived streams is usually low, 10%–20%, sometimes reaching 30%–40%; however, very few reliable measurements have yet been made.
8. A shock wave called a standing shock wave is sometimes recorded simultane-

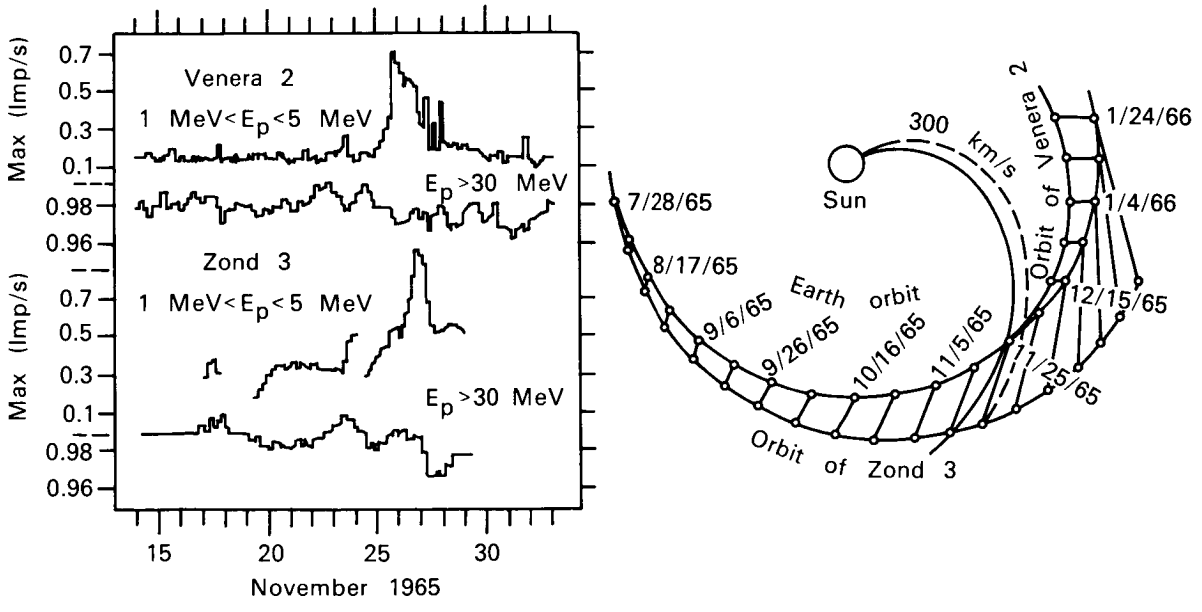

FIGURE 29.—Recording of long-lived flux by Zond 3 and Venera 2 spacecraft [138].

ously with the rotating stream, bounding the stream on the side of the interplanetary medium, and a magnetic storm is observed.

Solar Cosmic Rays and Shock Waves

An increase in the intensity of cosmic rays is frequently observed in interplanetary space, coinciding in time with the passage of a shock wave, generated in a large flare. In relationship to the initial flare, these particles are delayed, like the particles in the long-lived streams. It is possible that both types of increases represent the same phenomenon. The recording of such particles is always accompanied by a Forbush decrease in the intensity of galactic cosmic rays and geomagnetic storms on the Earth, caused by interaction of the shock wave with the Earth's magnetosphere. Figure 31 shows an example of such an increase [136].

The mean propagation velocity of shock waves from flares at 1 AU is about 600 km/s; therefore, the usual delay of such particles appearing at the Earth in relationship to a flare generating the shock wave is 50–60 h. In the case of flares in the central portion of the limb, two phenomena may be superimposed: a rotating stream of particles and those related to the movement of the shock wave. When strong waves with a mean propagation velocity of about 2500 km·s^{-1} are observed, the energetic particles are observed approximately 1 d following the flare. The criterion for selecting such events is the accompaniment by a shock wave, propagating from the solar flare into interplanetary space. The differentiation of a shock wave from all other types of perturbations in the interplanetary medium is difficult and can be achieved unambiguously only by simultaneous measurement of the parameters of the plasma and magnetic field by satellite. A summary of the basic known properties of such streams of particles accompanied by shock waves is presented.

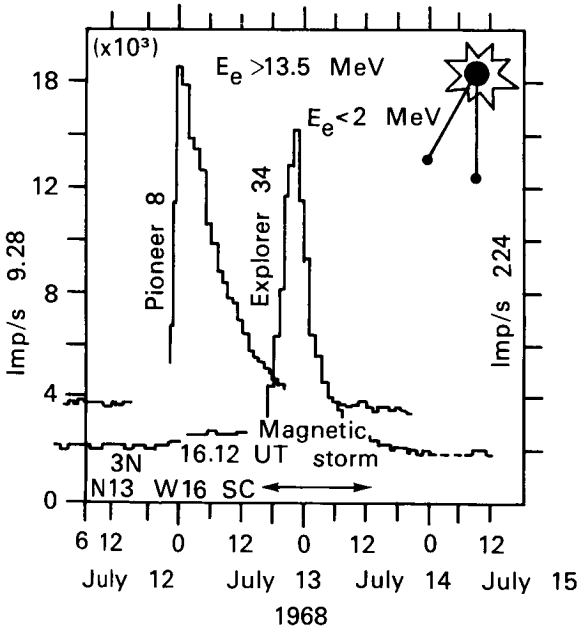

FIGURE 30.—Recording of long-lived stream of relativistic electrons [88].

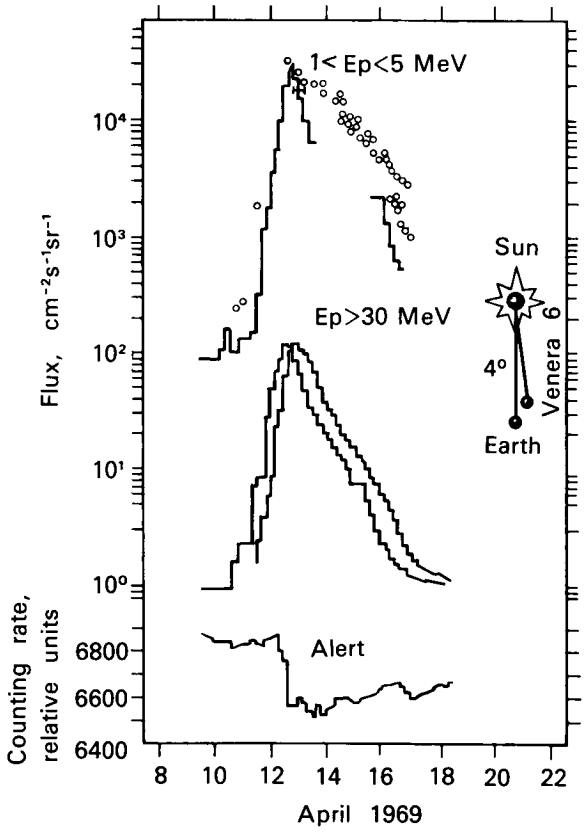

FIGURE 31.—Increase in flux of particles related to shock wave for protons with energy $1 \leq E_p \leq$ MeV and $E_p > 30$ MeV according to data by Venera 6, Molniya 1, and Explorer 34 spacecraft, April 10–15, 1968. Bottom curve shows indications of neutron monitor in alert [138].

1. The rise time is 6–24 hours. Usually, the rise begins before the arrival of the shock wave is recorded. At the moment of passage of the leading edge of the shock wave, an additional narrow burst lasting 10–20 min is recorded.
2. The streams may be either pure proton streams with energies $0.5 \leq E_p \leq 100$ MeV, or may contain electrons with $E_e \approx 40$–300 keV.
3. Simultaneous arrival at the observation point of particles of various energies is observed, with identical rise rates of the fluxes of particles at different energies.
4. The energy spectra of such particles are usually much softer than the spectra of the diffusion components against the background of which they are recorded.
5. The anisotropy of such streams has been insufficiently studied. The anisotropy may be great, but the direction of the maximum arrival of particles changes rapidly with time, apparently synchronously with rapid fluctuations in the magnetic field behind the leading edge of the shock wave.
6. The appearance of particles is always accompanied by Forbush reduction of the intensity of galactic cosmic rays and geomagnetic storms with sudden onset.

Solar Cosmic Rays During "Quiet" Periods

A minimum background flux of protons occurs during quiet periods when there are no solar flares. Low fluxes and the spectra of such particles with energies of 30 MeV against the background of the significantly greater flux of galactic cosmic rays are difficult to measure; therefore, data produced so far are not distinguished by great accuracy. The mean flux of protons with energies $E_p > 1$ MeV, according to various measurements, is about 10^{-2} particles/cm$^2 \cdot$s$\cdot$sr. The differential spectral index for the energy area 0.03–5 MeV is $\gamma \approx 3$.

Generation of solar cosmic rays during flares. There is reason to assume that the generation of solar electrons and protons occurs in two stages, both directly during the period of the explosive phase of a flare, when the brightness in the H_α line is maximum (stage 1), and after the explosive phase, when the hydromagnetic shock wave formed during the large flare explosion interacts with the intensive magnetic fields in the sunspots (phase 2). Thus, there are probably two accelerating mechanisms, acting in sequence, i.e., acceleration in the explosive phase is the injector of particles accelerated in the second phase.

Direct generation of particles during the explosive phase is a possibility which is indicated by observation of type III radio bursts. The velocity of movement of the source of type III bursts is from 0.2 c to 0.8 c; the agent exciting these plasma oscillations can be identified as electrons with energies of 10 to several hundred keV. The movement of such a source of type III radio bursts from the Sun to a distance of 200 $R_\odot$ was observed [119], and it was found that the velocity of motion remained constant, equal to $(0.4$–$0.5) \cdot c$, while the source itself was a compact formation with linear dimensions of 10^6 km. An estimate of the number of electrons causing a type III radio burst in the corona is $N_e \approx 10^{35}$–10^{36}, which is similar to the number of solar electrons (N_i) observed directly in interplanetary space after a flare ($N_i \approx 3 \cdot 10^{33}$–$10^{34}$ for $E_e \geq 22$ keV). This yields a value of 0.1–1% for the effectiveness of departure of electrons from the corona into interplanetary space [83]. With a type III radio burst generated in the corona, there are simultaneous microwave bursts in the cm radio range and x-ray bursts in energies ranging to 100 keV (Figs. 32 and 33). Since type III radio

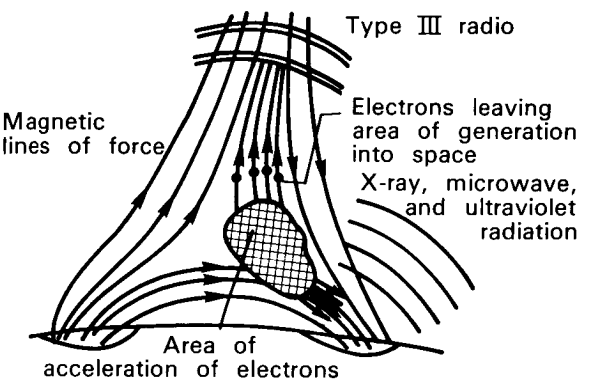

FIGURE 32. – Model of generation of electrons in a flare.

bursts are observed from particles moving outward, microwave bursts may arise as magnetic bremsstrahlung in the chromosphere when a portion of the stream of accelerated particles moves in the direction parallel to the boundary of the chromosphere. The x-radiation of this phase results from bremsstrahlung of electrons moving into the denser layers of the solar atmosphere. That all of these particles belong to the same area of generation shows similarity of the time form of a burst for various types of electromagnetic radiation. The ratio between intensities of these groups of electromagnetic radiation may vary, even to the point that individual forms may be totally absent, depending on the situation and specific conditions of acceleration.

If the acceleration of particles in this phase is achieved by electric fields arising upon dissipation near the zero points of oppositely directed magnetic fields, acceleration to identical hardnesses probably occurs. If the electrons are accelerated to energies of about 300 keV, the protons are accelerated only to 200 eV, i.e., their energy is lower than the kinetic energy of the solar wind. Observations in interplanetary space have shown that after flares of low intensity, only the first phase of acceleration occurs, accelerating mostly electrons. If there is any mechanism of acceleration, for example, accelerating a particle to identical energy, a low energy (up to a few hundred keV) proton component should be observed after a low-intensity flare. The scarcity of experimental data does not yet allow drawing any reliable conclusions in this respect.

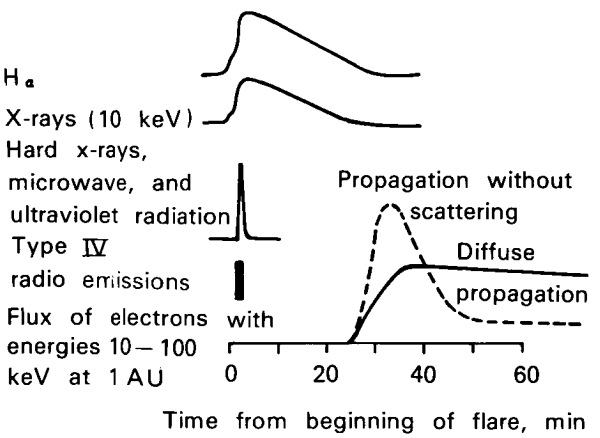

FIGURE 33.–Model of generation of electrons in a flare (time picture).

The primary portion of the protons is accelerated to energies of hundreds of MeV, while the electron component is accelerated to energies of tens of MeV, apparently in the subsequent phase of the flare phenomenon, in which the shock wave formed in the explosion interacts with the strong magnetic fields of the spots. This shock wave is noted on the basis of type II radio bursts several minutes after the beginning of large solar flares. There apparently is an energy threshold of formation of a shock wave, since it generally does not follow low-intensity flares.

Finally, the interaction (mentioned above) causing acceleration of particles is indicated by type IV radio storms, resulting from synchronous radiation of electrons captured in the corona. These storms are varied in form, often last for many hours, and cover areas that drift slowly in the corona. The proton component of solar cosmic rays correlates rather well with the appearance of these type IV radio storms. It has been assumed that the corona, similar to such type IV areas, also contains areas occupied by type I radio storms, a broad continuum of radio noise, sometimes lasting for several days. In type IV radio storms, these regions are occupied by energetic electrons and protons, but in type I radio storms, they consist of captured electrons with energies of tens of keV.

Thus, at a stage in the flare phenomenon in the corona, near the base of the lines of force carried by the solar wind out into interplanetary space, broad regions are formed, populated with charged particles, and frequently quite distant from the location of the flare. At some moment, the particles are liberated and enter the interplanetary magnetic field.

Propagation of Solar Cosmic Rays in Interplanetary Space

The interplanetary magnetic field is the basic factor defining the nature of motion of charged particles in interplanetary space. Protons injected by the Sun propagate in the interplanetary spiral

magnetic field formed by the solar wind. The spectrum of the heterogeneities related to the inconstancy of solar wind parameters is superimposed on this basically ordered interplanetary magnetic field structure. Corresponding to this structure of the interplanetary magnetic field, the motion of a charged particle can be divided into motion along the spiral mean regular field and scattering on magnetic heterogeneities.

With movement in a regular field, changing as a function of R, the magnetic moment of a particle $M=E\cdot 1/B$ is conserved (first adiabatic version), leading to conservation of the value of $\sin^2\alpha/B$, where α is the angle between the direction of the velocity of the particle and the line of force. The intensity of the magnetic field decreases as $B_r(R)\approx 1/R^2$, $B_\phi(R)\approx 1/R$. Since the value of the field at the orbit of the Earth is decreased by 10^4 times in comparison to the intensity at the surface of the Sun, the pitch angle of the particle α would be very slight $\alpha\leqslant 1°$ (even for a particle which departed the Sun at an angle of about 90°), if the particle were not scattered on magnetic field heterogeneities.

When a particle interacts with field heterogeneities, it is scattered, i.e., changes its pitch angle and the direction of motion. The particle is most effectively scattered on field heterogeneities with dimensions ℓ on the order of the Larmor radius of the particle $\rho\lambda=pc/ZeB$ where p is the momentum of the particle, B is the mean intensity of the field in the heterogeneity. Where $\ell\gg\rho\gamma$, particles are scattered on heterogeneities to very slight angles; when a particle moves along the line of force, it either runs around a heterogeneity so that the scattering angle is also slight, or is reflected from it.

Most increases in solar particles recorded in the past 15–20 years (as stated above) have been gradual during several hours from the moment of the first particles at the recording point, to the maximum of intensity with subsequent slower decrease. The solar flares responsible for these increases last from $\frac{1}{2}$ to 3 h; the phase of the flare in which hard x-ray and radio radiation is observed lasts for much less time (Fig. 33). Therefore, the longer leading edges of the time profiles of particles are interpreted as the effect of diffusion of particles.

The model of isotropic diffusion is the simplest model describing the process of propagation of particles when strong scattering is present, which is suggested at the very beginning of the study of solar cosmic rays. This simple model, in the case of an unlimited medium and constant diffusion factor, yields the time-dependence of the flux of particles:

$$n(R, v, t)=\frac{N(v)}{(4\pi\cdot D\cdot t)^{-3/2}}\cdot e^{\frac{-3t_m}{2t}} \qquad (8)$$

where n is the density of the particles;

R is the heliocentric distance to the point of observation;

$D(R, v)$ is the diffusion factor;

v is the velocity of the particles;

$t_m=R^2/6D$ is the moment in time when $n(R, v, t)$ has its maximum value.

Isotropic diffusion. The model of isotropic diffusion assumes that the particle is injected in a pulse over a very short time near the maximum of a flare or the maximum of a burst of x-rays and moves in a spherically symmetrical volume encountering heterogeneities, leading to isotropic scattering of the particles. The density of heterogeneities in space must be such that the length of the free path of a particle λ is much less than the distance L from the source to the point of observation.

The time-dependences of intensity of solar cosmic rays are sometimes fairly well-described by isotropic diffusion, particularly if the source of particles is located in the eastern or central portion of the Sun. Agreement of the time-dependence can be improved by considering the dependance of diffusion factor D on heliocentric distance R.

However, isotropic diffusion does not explain the spatial anisotropy of the flux of solar protons observed in the initial stages of a flare; the maximum of the flux in the process of isotropic diffusion should be observed in the direction from the Sun. Actually, the maximum flux is directed at an angle of $\phi\approx 50°$ to the Earth-Sun line and is displaced to the east. Isotropic diffusion also cannot explain the greater effectiveness of the western half of the Sun from the standpoint of arrival of solar cosmic rays. Measurements in

interplanetary space have indicated that the fluxes of particles in space depend strongly on the heliolongitude of the location of the solar flare, which also does not fit the isotropic diffusion theory.

Furthermore, experiments frequently indicate a free path length for protons with $E_p < 50$ MeV which is comparable to 1 AU, contradicting one of the conditions of applying the diffusion theory [89].

All of this indicates that isotropic diffusion produces an acceptable description of the late stage of an increase, with the exception of the properties of anisotropy. However, it must be recalled that most particles are recorded at the maximum of an increase. Consequently, isotropic diffusion can describe the behavior of not more than 10% of particles emitted by the Sun.

Anisotropic diffusion. Models of anisotropic diffusion have been developed in recent years. Some are based on the assumption that the diffusion of particles occurs not only in interplanetary space, but also in the solar corona, with the relative roles of coronal and interplanetary diffusion depending on the time of observation; when a particle moves along lines of force, scattering predominates over transfer across the lines of force. In other words, the effective diffusion factor along the field $D_{||}$ is significantly greater than $D_{\perp}$—the factor across the lines of force ($D_{||} \approx 100\, D_{\perp}$).

Based on these assumptions, a theory of scattering of particles as to pitch angles has been developed for description of the physical relationship between the scattering of particles and the observed fluctuations in the magnetic field [78, 84]. A theory of anisotropic diffusion has been developed under the same assumptions [54, 56], considering transfer of particles by the solar wind, time behavior of fluxes and anisotropy of solar cosmic rays in the nonequilibrium phase of the phenomenon, when diffusion is significant. It is indicated that the anisotropy $A \approx R/2\ vt$, where R is the distance from the source to the observer along a line of force, v, the velocity of the particle, and t, the time since the moment of injection of the particle into the solar system. Consequently, the anisotropy of electrons, even of low energies ($E_e \gtrsim 100$ keV) should decrease much more rapidly than for protons with $E_p \geqslant 10$ MeV, which agrees with the experimental data [104].

In one model [27], it is assumed that at a certain heliocentric distance R_1 (R_1 is comparable to 1 AU), the nature of scattering of solar particles by the interplanetary magnetic field changes so that particles reaching this distance do not return to the area of diffusion. This boundary condition for the decreasing intensity phase leads to the exponential dependence of particle fluxes on time up to the moment in time $t \gg t_D$, where t_D is the mean time of diffusion of particles from source to boundary. Within the framework of the models studied, the value and direction of "equilibrium" anisotropy observed in the late stage of increases in solar cosmic rays for $T > 2$ d can be produced.

After the increase in solar cosmic rays begins, when the solar particles have propagated by several AU, long-term anisotropy may be caused by: (1) convective transfer of solar protons along lines of force in the magnetic field B, (2) drift of particles due to movement of the magnetic field relative to the particles, where the velocity of drift is directed perpendicular to the magnetic field force line, and (3) constant injection of particles by the Sun. The drift of particles has a very significant effect, particularly for low-energy particles. The radial equilibrium anisotropy existing 1–4 days after a flare, arises because of drift of particles due to convection along field lines B.

The movement of the particles at this time is fully determined by the solar wind. Consequently, a current of particles is perpendicular to the line of force due to drift motion, as well as along the line of force, caused by collision of a particle with magnetic heterogeneities moving along the lines of force of the field at velocity $u \cos \theta$.

The total equilibrium anisotropy is independent of the direction of the interplanetary field vector. For an observer at rest, the anisotropy of the cosmic rays will be directed along the radius and its value $A_{eq} = (2+\gamma)u/v$, where u is the velocity of the solar wind, v is the velocity of the particles, γ is the differential spectral index of the particles.

In the late stage of the increase in solar cosmic rays, for moments more than 4 d after the flare, the equilibrium anisotropy is observed about 45°

to the east of the Sun-spacecraft line. This anisotropy is fully determined by drift movement of solar cosmic rays; the component of the anisotropy parallel to the lines of force of the magnetic field disappears due either to lack of deflection of solar cosmic rays by magnetic field heterogeneities, or to compensation of this anisotropy by the reverse flow of particles accumulated during the first phases of the increase at the periphery of the solar system. In the latter case, a significant positive (i.e., increase of flux of particles with increasing distance from the Sun) radial gradient of solar cosmic rays should be observed. With full compensation of the convective anisotropy, only the drift anisotropy remains, the value of $A = (2+\gamma)u/v \sin\theta$, where θ is the angle between the direction of the lines of force of the magnetic field and the direction to the Sun.

The increase in solar cosmic rays related to the arrival at the point of observation of shock waves caused by flares on the Sun has not been fully determined. The existing hypotheses of the origin of these energetic particles do not describe all aspects of the phenomenon observed. The most natural "trap" hypothesis assumes that the solar particles were accelerated in a flare on the Sun, then moved in interplanetary space with the shock wave from the same flare in a certain adiabatic or diffusion trap. Another hypothesis assumes that within the shock wave, there are conditions capable of accelerating particles to the observed energies. It would follow that the solar cosmic rays observed with the shock wave are not inherently solar, but interplanetary. A third hypothesis states that the particles were created on the Sun, remained near the Sun for a long time and fed a group of force tubes, which the shock wave has pushed outward to the point of observation. The nature of this phenomenon will not be discussed in detail, because there are not sufficient data to support any of the hypotheses listed.

Based on current knowledge of particles of solar origin, the magnetic field of the Sun and the interplanetary magnetic field, a phenomenological picture can be constructed of the propagation of solar cosmic rays.

Particles generated during a flare diffuse in the solar corona far from the point of the flare. The shock wave, propagating in the chromosphere and corona of the Sun, facilitates this diffusion of particles. The particles are then injected along neutral lines into interplanetary space over a broad range of angles, frequently reaching 90°, propagate along the lines of force of the field, forming a "cone of propagation," and dissipate little over the range of 1 AU. The particle population of lines of force departing from the area of a flare, or the area into which the maximum concentration of accelerated particles has diffused, is much greater than in neighboring areas. When the particles have traveled far from the Sun (2–3 AU), they begin to scatter intensively, causing isotropization of flow in the propagation cone and filling the entire space near the Sun with particles, i.e., erosion of the cone. If the injection process lasts many hours, the increased intensity of particles and great anisotropy in the bundle of lines of force departing from the area of the flare will also be retained for a long time. However, the spectrum of such particles will become softer than the first time following the flare, since the more energetic particles disappear sooner at the boundaries of the diffusion volume.

If the shock wave generated in the flare propagates into interplanetary space, it is greatly perturbed and changes the distribution of particles (or serves as a source of reflection of particles, possibly changing their energy). Therefore, when a shock wave passes spacecraft, a change in the characteristics of the particle stream is recorded. After the shock wave passes, the interplanetary medium gradually returns to its quiet state. Since shock waves propagate from the Sun at speeds of 500–800 km/s, 4 to 5 d after a flare, the primary process of propagation of particles will be transfer of particles by the solar wind from the solar system.

Streams of High-Energy Solar Protons

The greatest radiation danger for man and for various materials within spacecraft is the high-energy solar protons which penetrate freely through the skins of contemporary spacecraft. The energies of such protons can be, arbitrarily, 100 MeV. This section provides a summary of the increases in solar cosmic rays during which pro-

tons with energies greater than 100 MeV have been observed.

During the past two cycles of solar activity, over 100 flares of solar cosmic rays containing protons with energies $E_p > 100$ MeV have been observed. The most powerful of these, as well as the integral flux of particles in each flare [67, 92], are presented in Table 7. The values of fluxes in Table 6 were from varied data; the accuracy of their determination can be assumed to be within the limits of a factor of 2. Figure 34 shows the time-dependence of the summary flux of solar cosmic rays over a year, and the time-dependence of the smoothed number of sunspots.

Meteorite Material

Meteor material in interplanetary space consists of a multitude of small bodies moving freely in the Sun's field of gravity and generally unrelated physically to the planets. These bodies range broadly in dimension, from asteroids (tens of km in diameter) to tiny dust particles, comparable in size to the wavelength of sunlight. The number of particles in interplanetary space increases rapidly with decreasing dimensions.

The study of small bodies in the solar system is undoubtedly of theoretical and practical interest. The distribution of small bodies into classes of comets, asteroids, meteorites, and cosmic dust is more deeply based physically than mere differences in dimensions of bodies, phenomena, or related methods of observations, and reflects their characteristic features. Explanation of the physi-

TABLE 7.—*Flares of Solar Cosmic Rays*

Date of flare	Flux of protons with energy $E_p > 100$ MeV/cm² for entire flare
2/23/56	$3.5 \cdot 10^8$
5/10/59	$8.5 \cdot 10^7$
7/10/59	
7/14/59	$3.7 \cdot 10^8$
7/16/59	
11/12/60	
11/15/60	$4 \cdot 10^8$
11/20/60	
8/02/72	
8/04/72	$2.4 \cdot 10^9$ (Estimate for protons with $E > 60$ MeV)
8/07/72	

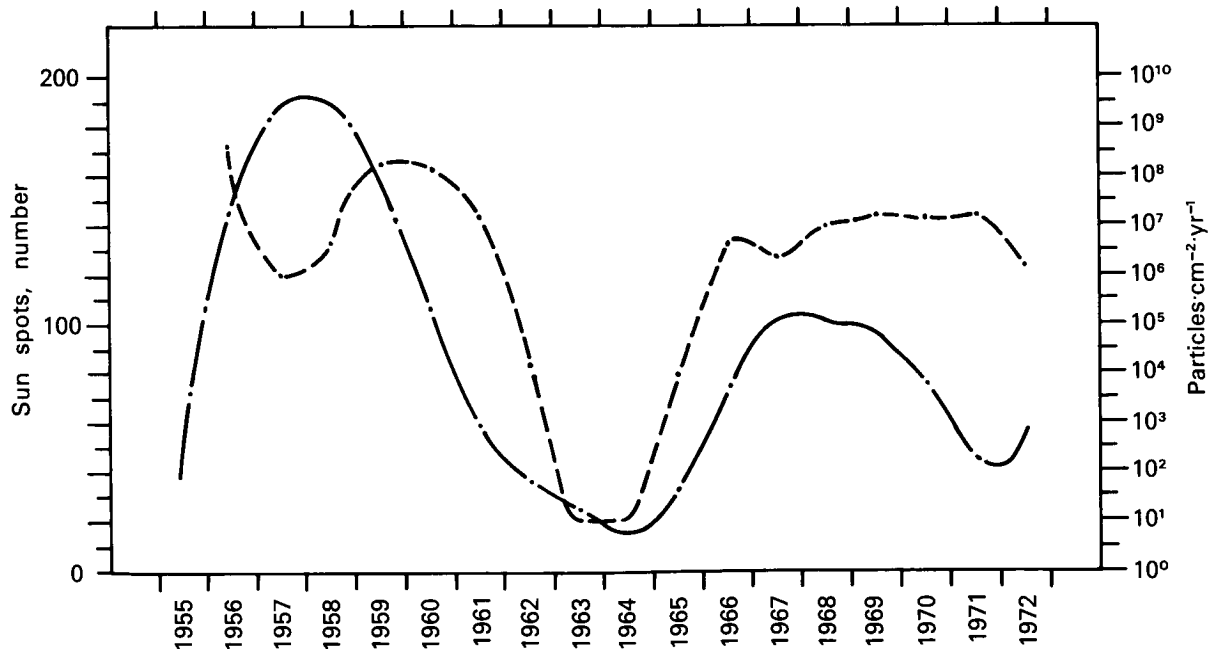

FIGURE 34.—Summary flux of protons from Sun/yr as a function of time (dashed line) and number of sunspots (solid curve).

cal structure and chemical composition of small bodies in the solar system, their origin and age, and establishment of the evolutionary relationships between comets, asteroids, and meteorites may be highly significant for the development of solar system cosmogony.

These problems are frequently interwoven closely with other problems of space physics and the immediate surroundings of the Earth. Investigation of meteorite material interactions and, in particular, comets with fluxes of radiation and corpuscular radiation is an effective means of obtaining information on properties of the interplanetary medium, the solar wind plasma, and magnetic fields in space. A comprehensive study of meteorites can yield important information on the structure of the upper atmosphere and the physical processes within it, as well as on the propagation of radiowaves.

The effects of meteorite bombardment on the surface of the Moon provide a basis for study of the history of the Moon, and to determine the flux of meteorite material and its evolution in the solar system. Analysis of the properties of meteorites reaching the Earth allows judgment of their nature, origin, and age, and the effects and properties of cosmic rays.

Special problems in the study of meteorite bodies and cosmic dust are connected with the problem of meteorite danger for space flights. There are two potential types of danger represented by solid particles for satellites, rockets, and spacecraft. Collision with a sufficiently large particle can cause serious damage to a spacecraft, even in an individual event. On the other hand, continuous bombardment with tiny particles causes erosion of surfaces and may lead, for example, to failure of optical devices or changes in the optical properties of heat exchange surfaces and temperature regulation systems. Determination of the degree of meteorite danger is necessary in the design of spacecraft and the development of protective measures when necessary.

Studies and experience show that the meteorite danger during flights in the region of the Earth's orbit is slight, but extrapolation of these data over a great range of heliocentric distances is unjustified; experimental data must be developed on the meteorite situation for long interplanetary flights beyond the limits of the orbits of Mars and Venus.

Main channels of information on the presence and properties of meteorites in the solar system are from studies of meteors, meteorites, zodiacal light, optical phenomena in the upper atmosphere, stratospheric dust, and meteorite dust reaching the Earth's surface. Most of the information on the meteorite component of the interplanetary medium is from surface investigation.

The development of rocket and space technology over the past two decades has made possible direct studies of micrometeorite particles in the upper atmosphere of the Earth and in space, using special equipment which utilizes various recording principles. In contrast with surface observations, these studies have produced information on individual particles with masses down to 10^{-14} g, their spatial density, physical properties, and chemical composition. The phenomena studied, related solid interplanetary particles, frequently have practical applications. Observations of meteorite tracks are used to determine the direction and velocity of winds in the upper atmosphere, and the ionization created by meteorites is used in some communications systems.

The meteorite material rotating around the Sun at a distance of about 1 AU consists of rock and iron particles primarily of iron, nickel, and iron sulfide. The chemical composition of rock meteorites is reminiscent of that of terrestrial rock. The density of rock meteorites is about 3 g/cm^3, that of iron meteorites about 7.8 g/cm^3. Meteorite bodies may form conglomerates, with very low density, approximately 0.5/cm^3. The velocity of meteorite particles relative to the Earth varies from 12 to 72 km/s. The significant fraction of these bodies is combined into clusters extended along their orbit or concentrated in small sections.

Meteorite bodies which cannot be classified in any meteorite stream are called the meteorite background or sporadic meteorites, which belong to weak meteorite streams not yet defined.

Meteorite matter has been studied using spacecraft in the areas of the Earth, the Moon, and interplanetary space along the spaceflight trajectories to Venus, Mars, and beyond the orbit of Mars in the asteroid belt [86].

Measurements of micrometeorite material by

acoustical methods near the Earth have indicated that the number of micrometeorite particles with masses less than 10^{-6} g is higher, by several orders of magnitude, near the Earth than the interplanetary background level. These results have led to formulation of the hypothesis of a dust belt or dust cloud around the Earth. Two possible sources have been considered for these particles: interplanetary dust particles captured by the gravitational field of the Earth, and dust particles separated from the Moon.

However, careful study of these mechanisms [37, 38, 47, 116] has shown that these phenomena could not support the observed concentration of dust particles. At the same time, doubts have been expressed concerning the experimental reliability of the results produced; many scientists currently believe that the fluxes of powder particles in near-Earth and interplanetary space are the same. However, recent studies using sensors of various types have shown that there is spatial density of particles with masses of $\leq 10^{-7}$ g elevated by approximately an order of magnitude in the area around the Earth in comparison to their similar density in the area of the Moon and in interplanetary space (Fig. 35). The presence of a dust belt of this concentration near the Earth is not difficult to explain. Nevertheless, the accumulation of experimental data to answer this question finally must be continued.

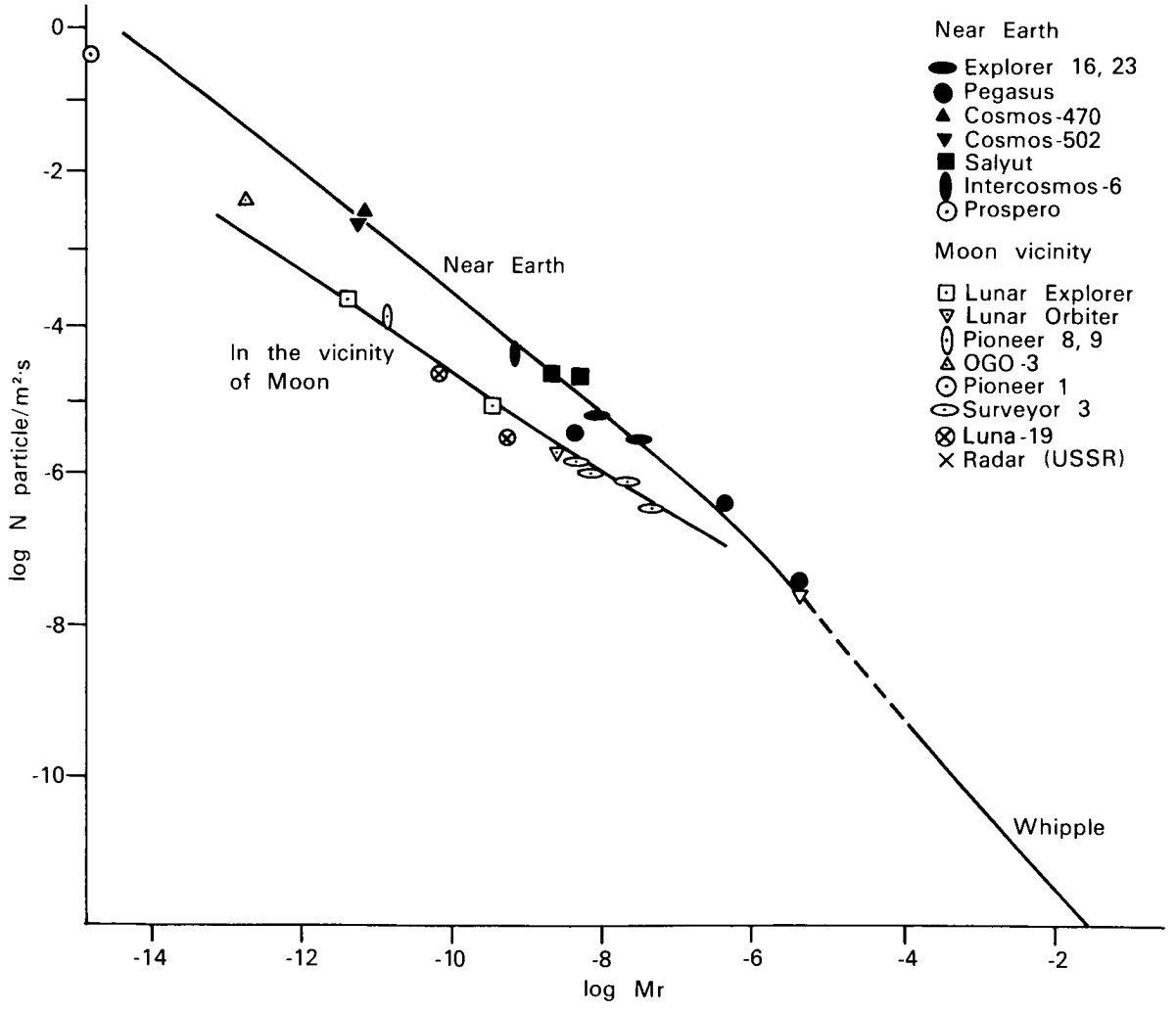

FIGURE 35. – Results of measuring meteor bodies.

In Figure 35, parameter S, characterizing the exponential law of propagation of meteorite bodies by mass, for the mass range $m = 10^{-12} - 10^{-7}$ g, near the Moon and interplanetary space is $S \simeq 0.6$ in comparison to $S \simeq 0.8$ near the Earth, i.e., the shortage of particles with decreasing mass in the area of the Moon and in interplanetary space is greater than near the Earth.

Preliminary results of measurement by Pioneer 10 spacecraft have shown that in the asteroid belt, the flux of particles increases sharply with the main mass of asteroid belt particles having dimensions of 0.01–1 mm. The number of particle impacts with the Pioneer 10 spacecraft has been greater than expected before launch, but there is not great danger of serious damage to the spacecraft [1].

Micrometeorite Matter at the Surface of the Moon

There is no atmosphere around the Moon; therefore, meteorite bodies collide with its surface at high velocities. When a particle impacts with the surface, an explosion occurs, and the mass of soil particles ejected is many times greater than the mass of the impacting particle. Experiments with models in the US have shown that many of the particles ejected in such an explosion have a mass of about 10^{-11} g. Ninety-nine percent of these particles fly over ballistic trajectories at velocities of about 1 km/s, and only 1% achieves a velocity greater than 2.4 km/s, sufficient to depart the Moon. Secondary particles and impacts should not greatly increase the danger of materials penetrating the surface of the Moon due to their primarily low velocities; however, the erosive effect of repeated impacts, even at low impacting particle speeds, might present a problem for operation of individual structural elements.

When large meteorites strike the Moon (a rare occurrence), a great quantity of rock is ejected from the surface. Experiments by the Pegasus, Explorer 16, and Explorer 23 spacecraft have been very valuable for the study of meteorite danger, which used penetration-type sensors recording the penetration frequency of an envelope as a function of its thickness, and considered the specifics of rupture of the envelopes when particles strike at an angle (due to the isotropic model of the incident stream used). These figures are presented in Figure 36, together with the calculated data of Whipple. In the area with thickness of less than 1 mm, the experimental and calculated data agree well.

For medium-range flights in the area of the Earth and Moon, this figure shows that meteorite danger can be ignored, while for long flights (about 1 year or more) in little-studied areas of the solar system, the meteorite danger must be taken into consideration.

The recording of micrometeorites in meteorite streams is of a particular interest; this represents a unique phenomenon in the solar system. The point of view generally accepted is that there is a genetic relationship between meteorite streams and comets, and the processes of rupture of these are the sources for formation of streams and their constant new supply of meteorite bodies. A hypothesis has been set forth and actively developed [81, 82, 138] which assumes that all meteorites, including sporadic ones, are of comet origin, and the breakup of comets and scattering of meteorite streams maintain the quasi-stable state of the zodiacal cloud of cosmic dust. The meteorite streams, like sporadic meteorities, have been intensively studied by surface visual, photographic, and radio observation. There is, understandably, great interest in the study, related to the technical capabilities of direct observation in space, of micrometeorites belonging to meteorite streams by means of satellites and rockets.

Extrapolation of the data from surface optical and radio observations of sporadic meteorites and meteorite streams indicates that the probability is slight of recording small particles with masses of 10^{-8}–10^{-11} g in meteorite streams [37, 38, 82]. This is due primarily to the different distributions of particles by masses of sporadic meteorites and meteorite streams; the contribution must be slight of meteorite streams to the total counting rate of micrometeorites with masses of less than 10^{-6} g. It is important that with decreasing dimensions of particles, the significance of nongravitational forces acting on such particles increases, essentially limiting their lifetime in the solar system. The decrease in the

steepness of the integral distribution of sporadic micrometeorites with masses of 10^{-7}–10^{-11} g to a value of 0.6, compared with mean value $S=1.2$ for meteorites in the optical and radio ranges, is characteristic. The effects of such forces on the particles in streams can lead to selective removal from orbit of particles of small dimensions. This makes the recording of small particles in the streams more difficult.

Based on experiments with micrometeorite material, the mean density of meteorite material in the solar system is about $2\cdot10^{-22}$ g/cm^{-3} and the mean rate of accretion of interplanetary matter by the Earth is 40 t/d.

MAGNETOSPHERE OF THE EARTH

Terrestrial Magnetosphere Structure

The physical conditions near the Earth differ greatly from conditions in interplanetary space because of the terrestrial magnetic field. The structure of the magnetosphere of the Earth, washed in the solar wind, is shown in Figure 37 for the spring and fall (magnetic axis of the Earth perpendicular to the direction to the Sun) [98]. Figure 38 is for June (significant inclination of magnetic axis to Earth-Sun line) [112]. Differentiation can be made on the figures between the stable magnetic field of the Earth (described in this section), and the area perturbed by disturbances (under the subsequent section, SUN-EARTH CONNECTION).

Stable Magnetic Field of the Earth

The terrestrial magnetic field is described in the first approximation by a dipole field with magnetic moments $\vec{M}=8.07\cdot10^{25}$ G·cm^3, placed at the center of the Earth. The axis of the dipole intersects the surface of the Earth at two opposite points with coordinates 78.3° N, 69.0° W, and 78.3° S, 111.0° E. In the second approximation, the magnetic dipole is shifted from the center of the Earth by 436 km in the direction toward the point with coordinates 15.6°N, 150.0°E. A stricter approximation of the geomagnetic field can be produced using an expansion with respect to spherical harmonics.

Some properties of the dipole field should be considered at this point which will be needed in later exposition.

A magnetic line of force is produced by the equation:

$$r=R_e\cos^2\phi \qquad (9)$$

where R_e is the distance from the center of the dipole to the line of force in the equatorial plane ($\phi=0$); ϕ is the geomagnetic latitude; and r is the distance from the center of the dipole.

The unit of distance used is the radius of the Earth R_0, equal to $6.37\cdot10^8$ cm.

Then $L=\frac{R_e}{R_0}$; $R=r/R_0$; the equation for a line of force can be rewritten as

$$R=L\cos^2\phi \qquad (10)$$

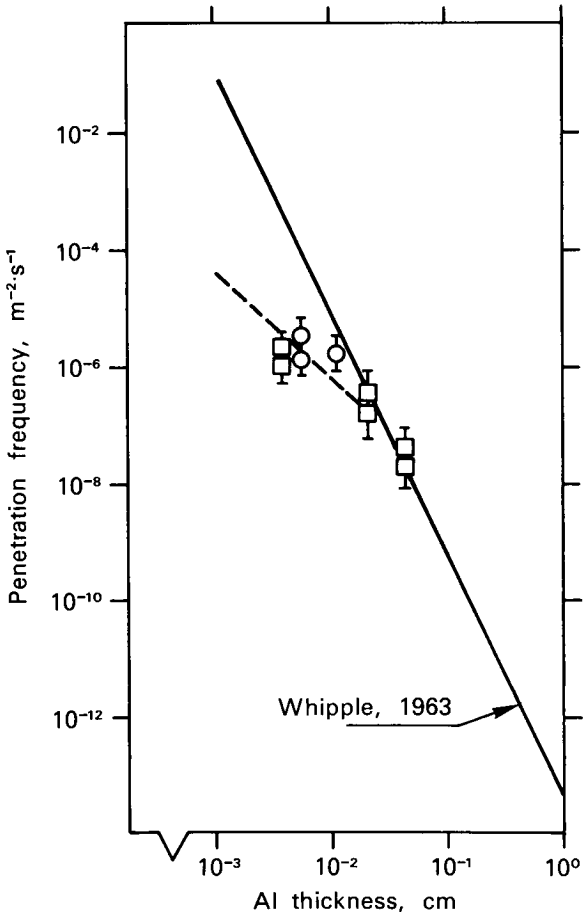

FIGURE 36.—Frequency of penetrations of solid barrier in area of the Earth's orbit.

The intensity of the field in the plane of the equator B_e can be calculated by the formula

$$B_e = \frac{0.312}{L^3} \text{ [G]} \qquad (11)$$

The intensity of the field at any point on a line of force can be determined by the expression:

$$\frac{B}{B_e} = \frac{\sqrt{4-3\cos^2\phi}}{\cos^6\phi} = \frac{\sqrt{4-3R/L}}{(R/L)^3} \qquad (12)$$

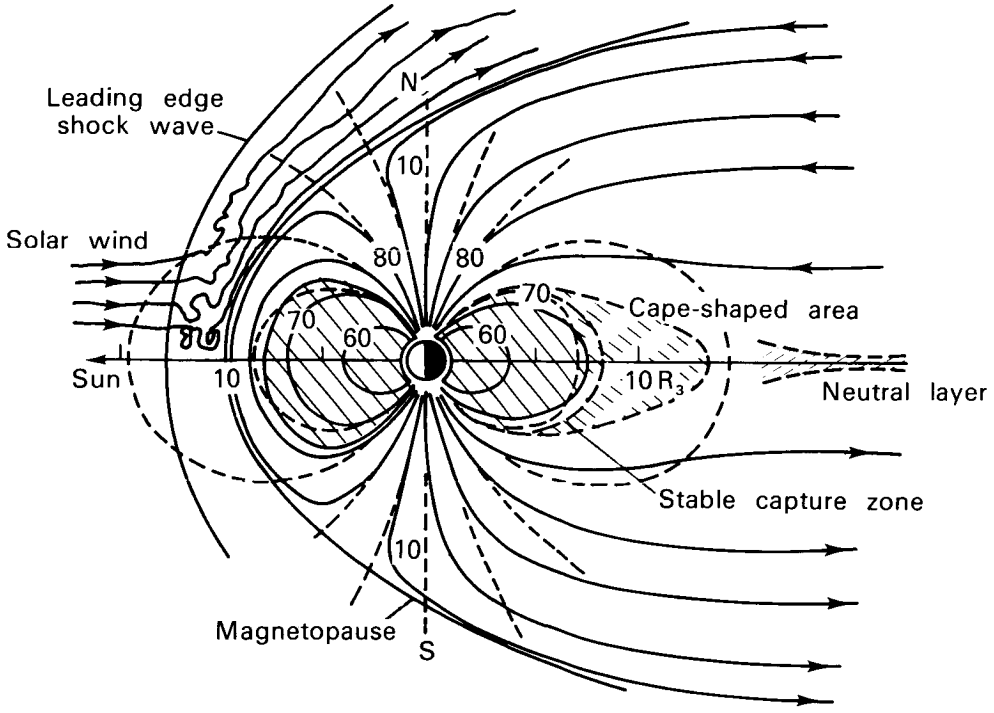

FIGURE 37.—Magnetosphere structure.

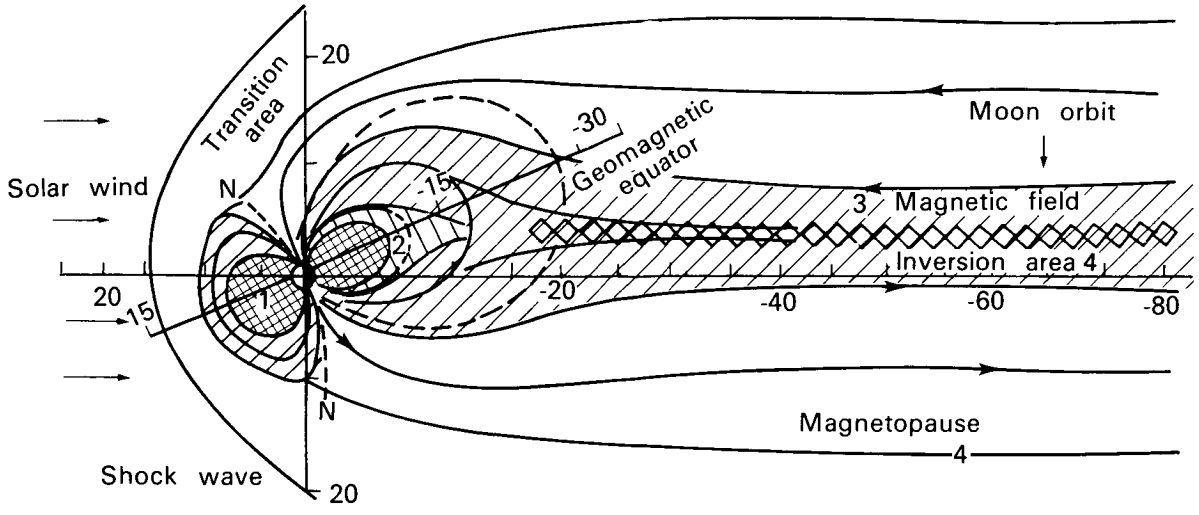

FIGURE 38.—Structure of the Earth's magnetosphere. 1, radiation belts; 2, quasi-capture area; 3, plasma layer; 4, neutral layer.

Angle γ between a line of force and the radius-vector is determined by the relationships:

$$\tan \gamma = 1/2 \cot \phi \qquad (13)$$

The "inclination" of the field $I, = \frac{\pi}{2} - \gamma$.

At great distances, the structure of the geomagnetic field differs significantly from that of a dipole, due to the interaction of the Earth's magnetic field with the solar wind (see Fig. 37).

Movement of particles in the geomagnetic field. The movement of particles with $E <$ GeV can be represented as the superposition of three independent motions [5]: the Larmor rotation of the particle in the plane perpendicular to the magnetic field; oscillations of the instantaneous center of rotation (leading center) along the lines of force; and drift of the leading center around the Earth.

The Larmor rotation has a period of:

$$\tau_1 \approx \frac{7 \cdot 10^{-7}}{B} (E_k + E_0) \text{ [s]} \qquad (14)$$

where: E_k is the kinetic energy of the particles in MeV; E_0 is the rest energy of the particle in MeV; for an electron $E_0 = 0.51$ MeV, for a proton $E_0 = 938$ MeV.

The Larmor frequency $1/\tau$ of electrons near the Earth is about 1 MHz, of protons about 1 kHz, the frequency decreasing as I/R^3 with increasing distance from the Earth. The Larmor radius of rotation of a particle can be determined from the relationship

$$\rho = \frac{33 \sin \alpha}{B} E_0 \sqrt{\epsilon^2 + 2\epsilon} \text{ [M]} \qquad (15)$$

or $pc = 300 B\rho$

where α is the angle between the velocity vector of the particle and the direction of the magnetic field force line (pitch angle), $\epsilon = E_k/E_0$, p_1 is the momentum of the particle in eV/s.

The Larmor radius of electrons in the geomagnetic field does not exceed a few kilometers, whereas for protons it may reach several hundreds of kilometers.

As a particle moves along a line of force, this relationship is fulfilled:

$$\sin^2 \alpha / B = \text{const.} \qquad (16)$$

From this, the intensity at the point of reflection can be determined:

$$B_{ref} = B_e / \sin^2 \alpha_e. \qquad (17)$$

The period of oscillation of a particle between points of reflection is given by the formula

$$\tau_2 = 8.5 \cdot 10^{-2} \cdot L \frac{1+\epsilon}{\sqrt{\epsilon^2 + 2\epsilon}} \cdot T(\alpha) \text{ [s]}, \qquad (18)$$

where $T(\alpha) = 1.3 - 0.563 \sin \alpha_e$.

The longitude drift around the Earth is opposite for particles with opposing charges (electrons move toward the east, protons toward the west).

The period of drift around the Earth τ_3 is defined by the expression

$$\tau_3 = 88 \frac{1+\epsilon}{2+\epsilon} \cdot \frac{K}{L \cdot E_k} \text{ [min]} \qquad (19)$$

where $K = 1.25 - 0.25 \cos^2 \alpha_e$.

For nonrelativistic particles, $\tau_3 = \frac{44}{LE_k}$ [min]. (20)

All three types of motion studied correspond to certain quantities which are conserved approximately constant for the entire time of motion of a particle, if the change in the magnetic field with time characteristic for a given type of motion (τ_1, τ_2, τ_3) is slight in comparison to the value of the magnetic field

$$B \Big/ \frac{\partial B}{\partial t} \gg \{\tau_1, \tau_2, \tau_3\}; \; \rho \frac{(\text{grad } B)}{B} \ll 1 \qquad (21)$$

These quantities are the adiabatic invariants of motion in the magnetic field.

The first adiabatic invariant is the magnetic moment of particle $\mu = P_1^2/2\gamma mB$; (where $v \ll c$, $\mu = E_{k1}/B$), where $\gamma = 1/\sqrt{1-(v/c)^2}$, P_1 and E_{k1} are the components of momentum of the particle perpendicular to the magnetic field.

The second or longitudinal invariant (longitudinal action invariant) is defined as $j = \phi m v_{\parallel} ds = p\phi \sqrt{1 - B/B_{ref}}\, ds$. Using these two invariants, as well as that $E_k = \text{const}$ in a constant magnetic field, it can be shown that particles on one line of force but with different pitch angles describe practically the same envelope as they drift around the Earth as they would in a dipole field. Therefore, the captured radiation can be characterized by a function of two coordinates L and B [91].

Calculation of L, B coordinates is a rather cumbersome task, performed by computer.

If the points of reflection of the captured particles are at low altitudes over the surface of the Earth, the influence of the atmosphere on the captured particles is considered by introducing the parameter h_{min}, representing the minimum altitude over the surface of the Earth at which a particle descends onto a given drift envelope L.

The third invariant ϕ is defined as the magnetic flux through the surface intersecting the drift envelope of a particle around the Earth and the limited trajectory of the point of reflection of the particle. Each L envelope corresponds to a unique value of invariant ϕ. In the case where $B \Big/ \frac{\partial B}{\partial t} \approx \tau_3$, the third invariant is not conserved, but since in this case $B \Big/ \frac{\partial B}{\partial t} \gg \{\tau_1; \tau_2\}$, the first two invariants μ and j are conserved. The magnetic field for a given L envelope will change. In this case $E_k/B = \text{const}$, due to the conservation of μ, also the particle can shift to another L envelope with the corresponding change in E_k. If $B \Big/ \frac{\partial B}{\partial t} \approx \{\tau_1; \tau_2\}$, the equivalent pitch angle of the particle changes, E_k may change and in this case either μ or j is disrupted. Finally, the particle enters the ionosphere. Movement of particles in the magnetic field has been reported [68, 112, 130, 133].

Movement of a Particle in the Presence of an Electrical Field

Many phenomena in the magnetosphere of the Earth can only be explained by assuming the existence of an electrical field perpendicular to the magnetic field in the plane of the Equator. In this case, drift in the direction perpendicular to the electric and magnetic fields is superimposed on the rotation of the leading center around the Earth, with the velocity

$$v_\epsilon = 10^8 \frac{\epsilon}{B}$$

where ϵ is the electric field intensity in v/cm. The trajectory of motion of the leading center in the plane of the equator ($\alpha_e = 90°$) can be calculated on the basis of the rules of conservation of energy and magnetic moment:

$$E_k + V = \text{const}, \quad \mu = \text{const}$$

where V is the electrical potential of the given point in space. The form of the trajectories for a homogeneous electrical field [7] is shown in Figure 39. The trajectories moving at great distances from the Earth are open. The particles in closed orbits belong to the radiation bands. The critical trajectory dividing the two types (open and closed) is shown by the dotted line in Figure 39.

The branching point L_{cr} on the critical orbit can be found by assuming the electrical drift velocity v_ϵ and magnetic drift velocity around the Earth $v_m = \frac{2\pi R_0 L}{\tau_3}$ to be equal. For nonrelativistic particles

$$L_{cr} = 4.75 \cdot 10^{-3} \frac{E_k}{\epsilon}$$

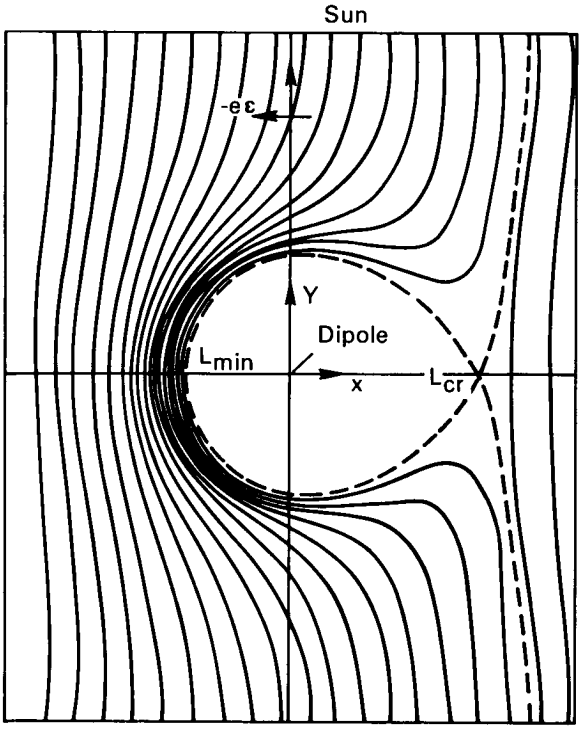

FIGURE 39. — Drift of electrons in equatorial plane of magnetic dipole field with superimposed homogeneous magnetic field in a homogeneous electric field parallel to the equatorial plane. Solid lines show typical trajectories of center of rotation.

From this formula, particles with energies at a given distance can be defined as belonging to the radiation bands. On the other side, particles pass at a minimum distance from the Earth $L_{min}=L_{cr}/1.78$.

Theoretical Models, Earth's Magnetic Field

The coordinates L and B are unsuitable for analysis of captured radiation at $L>6$, where the influence of the solar wind on the Earth's magnetosphere is significant. The effect of the wind causes the trajectory of movement of captured particles to depend on local time. More complex models of the geomagnetic field must be used to study the motion of particles.

The theoretical models of the magnetosphere have the purpose of analytic or numerical description of the area where the source of the magnetic field is the terrestrial magnetic dipole. These models are necessary for qualitative description of various processes occurring in this field. The bases of such processes are the radiation bands of the Earth, polar auroras, dynamics of magnetospheric perturbations, phenomena in the high-latitude conjugate points, and propagation of low-energy cosmic rays.

Two models of the magnetosphere are theoretically best developed; one empirical model has been constructed.

The Williams-Mead model [145] is based on consideration of currents at the boundary of the magnetosphere by spherical harmonics, as well as internal field sources. A plate with a homogeneous point in the plane of the geomagnetic equator on the night side of the Earth imitates the neutral layer of the tail of the magnetosphere.

For this model there are four parameters: R_s—the distance from the center of the Earth to the subsolar point of the boundary of the magnetosphere, R_h and R_f—distances from the Earth to the near and far edges of the plate with the current, and B_t—the field of the plate with the current.

Usually, $R_s=10R_0$, $R_h=10R_0$, $R_f=200R_0$ and $B_t=15\gamma$.

The two-dipole model [7] is based on the possibility of imitating the perturbing effect of the solar wind, under certain assumptions, by an additional dipole. The field of the neutral layer is imitated by the field of a plate with current. Characteristic for this model are: α—the distance from the Earth to the perturbing dipole, β—the value showing the number of times by which the perturbing dipole is greater than the terrestrial dipole $M_{pd}=\beta M_e$. R_h and R_f are the distances to the near and far boundaries of the plate with current from the Earth. B_t is the field of the plate with current. For ordinary conditions, when $R_s=10R_0$, $\alpha=33-40R_0$, $\beta=12.7-27$, $R_h=11R_0$, $R_f=51R_0$, $B_t=16\gamma$.

Empirical model of the magnetosphere [48]. So much data has recently been produced on the magnetic field at distances $>5R_0$, that it is possible to construct an empirical model of the magnetosphere, which has been done by Fairfield [48].

Calculation of various theoretical models has been made to explain the position of certain characteristic points of the magnetosphere and the topology of motion of charged particles in the magnetosphere. In the field and in models in the equatorial plane, the magnetic field is greater on the day side than on the night side (see Figs. 40 and 41). However, in the figure, the value of the field near the boundary is different for all models, in spite of the approximately identical position of the magnetosphere's boundary. The form of the magnetic lines of force near the boundary of the magnetosphere differs notably for different models.

Figure 40a, b, c, shows the meridional cross section of the magnetosphere for all three models in the day-night direction. The qualitative similarity of all the models is evident but the approximation of the infinitely thin plate with current is too rough for description of the field near the neutral layer; also evident is the different position of the neutral points at the boundary of the magnetosphere with the day side of the Earth and their projection over the lines of force on the Earth.

The figure shows good agreement of the line of force configuration for various models, although there is some quantitative divergence.

Envelopes of magnetic drift. The study of the motion of captured charged particles around the Earth indicates that $R \lesssim 5\ R_0$, the influence of

external field sources (currents at the boundary and in the tail of the magnetosphere), can be ignored, and the L, B, coordinates described above can be used. In this case, particles located on a single line of force and having different pitch angles drift around the Earth practically around a single drift envelope. At great distances from the Earth, the drift envelopes split.

Figure 42 shows the distribution of particles of various energies in the magnetosphere of the Earth [113]. Four areas are easily distinguishable.

The area of the polar cap (area I). The lines of force departing from the day side of the Earth at latitudes $\lambda \geq 78°$ and on the night side at latitudes $\lambda \geq 73°$ move out into interplanetary space or close far from the Earth. Here it is primarily a plasma of ionospheric origin with temperature $T \approx 3\text{–}5 \cdot 10^4$ °K, which moves out to great altitudes along the magnetic lines of force and, apparently, can extend into interplanetary space.

The area of the plasma layer on the night side

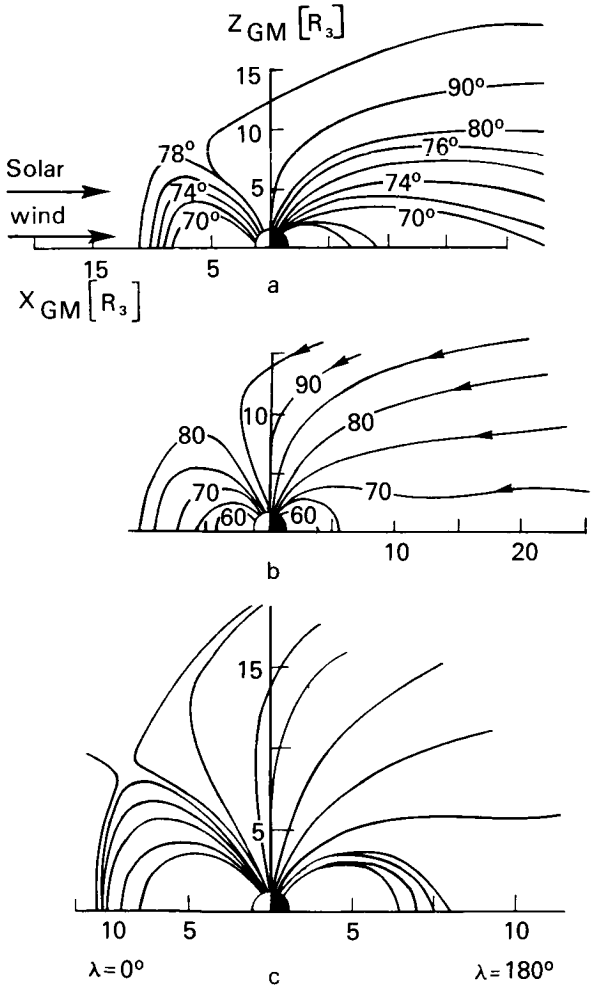

FIGURE 40.—Contours of even geomagnetic field intensity in equatorial plane [2]. (a) For empirical models; (b) for Williams-Mead models; (c) for two-dipole model.

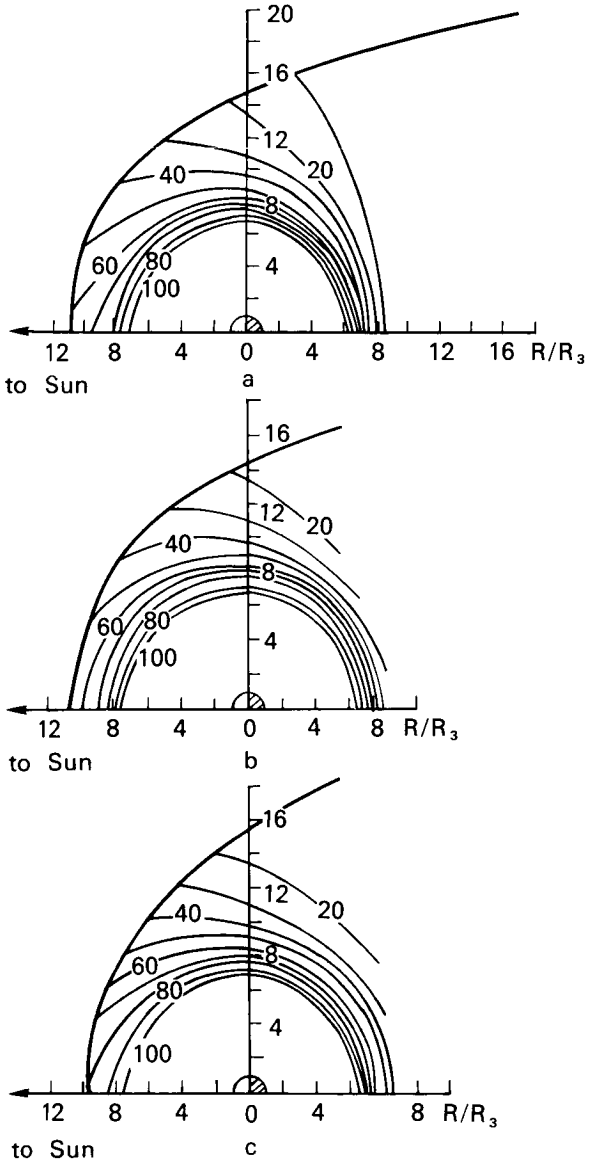

FIGURE 41.—Magnetic field of the Earth, perturbed by solar wind, in meridional day-night cross section. Latitudes of intersection of the surface of the Earth by lines of force—(a) empirical model [48]; (b) Williams-Mead model [145]; (c) two-dipole model [7].

and neutral points on the day side of the Earth (area II). On the day side, this area is located at $\lambda \simeq 76°–80°$, where the neutral point is projected along the magnetic lines of force (latitude of polar drop on the day side of the Earth). On the night side this area is projected along the magnetic lines of force at latitude $\lambda \simeq 68°–73°$ (latitude of polar drop on the night side of the Earth). The source of the plasma of this area is the solar wind, penetrating into the magnetosphere of the Earth. The mean energy of particles in this area fluctuates from a few hundred eV to several keV.

The area of the plasmosphere (area III) is located at the center of the magnetosphere of the Earth, extending from the ionosphere to $4–5\ R_0$, limited on the high latitude end by $\lambda \approx 60°–65°$. This area is characterized by increased concentration of electrons and ions of ionospheric origin. Near the ionosphere, the concentration of ions $N_i \approx 10^5$ cm^{-3}, while at a distance of $4\ R_0$ the concentration decreases to about 10^3 cm^{-3}. The energy of particles is about a few eV.

Area of the radiation belts of the Earth (area IV). The area of the magnetosphere is populated by particles with energies of several tens of keV to hundreds of MeV. A characteristic feature of the particles at these energies is rapid magnetic drift around the Earth in a time much less than the rotation period of the Earth around its axis.

If area I is related to the open lines of force of the geomagnetic field, areas II and III form under the influence of the weak electric field, about $2–4 \cdot 10^{-6}$ v/cm in the plane of the equator, directed from morning toward evening.

The source of ions in area III is within the magnetosphere (ionosphere of the Earth), while the source of ions in area II is outside the magnetosphere (solar wind).

For particles of area IV, the influence of the electric field on their drift trajectories can be ignored. The boundary of this area is at a distance where the electric field carries the particles beyond the limits of the magnetosphere. From the standpoint of dynamics of the magnetosphere and effects on space objects, characteristics of particles in areas II and IV are most important.

The most detailed measurements of plasmas in the tail of the magnetosphere have been performed by the Vela and OGO satellites. Information on direct measurements of the plasma near the neutral point have not yet been published, but data are available on low-energy particles, produced near the Earth on lines of force connecting with the area of the neutral points. Based on these measurements, the position of area II in the magnetosphere of the Earth is shown in Figure 42. On the night side of the Earth, the neutral layer of the magnetosphere tail is surrounded by a plasma layer with a thickness $h \approx 4\ R_0$ near the midnight meridian; closer to the morning and evening sides, the thickness of the layer increases to $h \approx 6\ R_0$. The streams of electrons can reach values of 10^9 electrons/cm^{-2} s^{-1}. The mean energy of electrons fluctuates from about 10 eV to about 5 keV.

During magnetic disturbances, the thickness of the plasma layer first decreases to $h \approx 1\ R_0$, then increases to $h \gtrsim 6\ R_0$ by the end of the geomagnetic disturbance (during which time magnetic disturbances develop at latitudes $\phi \approx 75°–83°$). During this time, electrons appear in the plasma layer with energies of at least 40 keV.

Plasma-layer particles drifting in the crossed electric and magnetic fields may reach the morning, evening, and day sides. From the day side, particles of the solar wind may penetrate into the magnetosphere of the Earth through the neutral points. Although the fluxes of particles have not yet been measured near the neutral points, at altitudes of several hundred to several

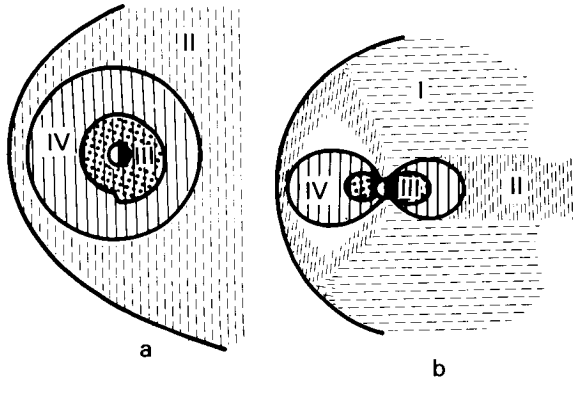

FIGURE 42.—Distribution of charged particles in magnetosphere of the Earth; (a) equatorial cross section; (b) meridional cross section.

thousand kilometers at latitudes $\phi \approx 75°–83°$. electron fluxes have been recorded with $E_e >$ 100 eV, reaching values of N ($E > 100$ eV) $\approx$ 10^8 cm^{-2} s^{-1} sr^{-1} with a spectrum of N ($> E$) $\approx$ E^{-1}. Since the fluxes are isotropic, it can be assumed that they have the same value in the area of the neutral points. The energy density of these electrons corresponds to that of the magnetic field with an intensity of 5 γ.

In area II, electron fluxes with $E_e \gtrsim 100$ keV are also sometimes observed. If electrons at this energy level, observed on the morning and day sides, can be accelerated in the tail of the magnetosphere, the origin of the electrons in the plasma layer is uncertain. Observation of electrons of such energies near the morning side is more probable than near the evening side.

The spectrum of the electrons from the zone of the polar aurora on the night side is frequently similar to the spectrum of electrons in the plasma layer, indicating that this is the same area. The polar auroras are closely related to ionospheric and geomagnetic disturbances caused by various manifestations of solar activity, which will be discussed in the section, SUN-EARTH CONNECTIONS.

Radiation Belts of the Earth

The area of radiation belts of the Earth is shown in Figure 43 (area IV). Since high-energy particles can be recorded outside this area as a result of various physical factors, the placement of electrons with energies of several tens of keV differs from the placement of the areas of the belts. Figure 43 shows schematically the areas of recording high-energy particles in the magnetosphere of the Earth. The area of distribution of electrons with energies >40 keV, noted by the slanted shading, does not belong to the radiation belt, since the drift orbits in this area for particles are open. Therefore, the high-energy particles at great distances from the Earth are not particles of the radiation belts, but are expelled from the magnetosphere in a time less than 1 period of drift around the Earth.

Two areas of radiation belts are mentioned in the literature: the inner and outer radiation belts [68, 130]. Although this separation was initially caused by imperfections in the detectors used to study the radiation belts, it was later found that for certain groups of particles this separation does have a physical sense. This will be discussed in greater detail.

Protons of Earth Radiation Belts

The distribution of protons of various energies, from 100 keV extending to 500 MeV at $L \leq 6$ [144], is shown in Figure 44. For $L \geq 6$, the distribution of particles becomes a function of local time. Figure 44 shows that as the energy increases, the maximum intensity shifts to lower L, at which the spectrum of protons becomes harder. The meridional cross section of the belt of pro-

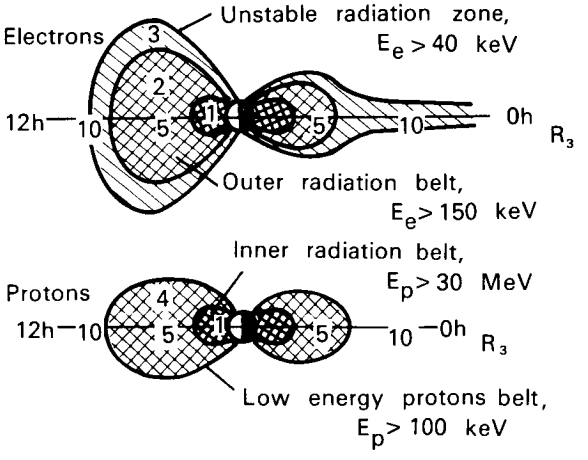

FIGURE 43. – Structure of radiation belts.

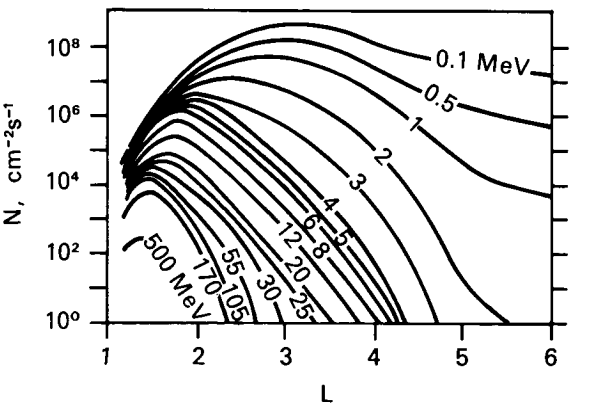

FIGURE 44. – Radial profiles of time-averaged global intensity of protons with energies over a fixed value in the plane of the geomagnetic Equator [144].

tons with energies $E > 1.0$ MeV and $E > 30$ MeV is shown in Figure 45.

Important characteristics of the radiation belts include the distribution in the plane of the Equator, and distribution of particles along lines of force, usually approximated by the function $N(B)_{L=\text{const}} \approx B^n$. Analysis of the data shows that for low-energy protons ($E_p < 30$ MeV), this approximation satisfies the experimental data well, n increasing with decreasing L. For high-energy protons, the dependence of intensity on L is more complex. Protons of these energies are more concentrated in the plane of the Equator; with increasing L, the altitude course increases. Examples of altitude courses for protons with $E > 1$, $E > 30$ and $E > 110$ MeV are presented in Figure 46 [139]. Analysis of the spectra shows that for low-energy protons, the energy spectrum is well-approximated by an exponential function:

$$N(>E) \approx \exp(-E/E_0) \qquad (22)$$

where $E_0 \approx L^{-3}$ (for $L=6$, $E_0 \approx 60$–100 keV). High-energy protons have an exponential energy spectrum $N(>E) \approx E^{-x}$.

At the maximum of the belt ($L \approx 1.5$), $x=1$; at $L=2$, $x \approx 2$.

These peculiarities of high- and low-energy protons are explained by their difference in origin. It is assumed that their origin differs; the source of high-energy protons is neutrons in the cosmic ray albedo, interacting with the atmosphere of the Earth; the source of low-energy protons is the solar wind. The protons of the solar wind are captured by the magnetosphere of the Earth and, diffusing into the magnetosphere, fill the core of the magnetosphere. The area of protons with $E_p < 50$ keV, detected on the evening side of the Earth, can be interpreted as an intermediate stage between the proton belt and solar wind. Figure 47 shows the distribution of protons in the radiation belt and protons with $E_p < 50$ keV as functions of L [144]. The intensity maximum of protons with $E_p < 50$ keV is observed at $L=7$–8. During magnetic storms, the intensity of protons with $E_p < 50$ keV at the maximum increases by an order of magnitude or more, and the maximum is shifted to $L \approx 4$. Protons with $E_p \lesssim 50$ keV at this time cause a D_{st} variation in the magnetic field.

The death of protons is due to ionization losses in the upper layer of the atmosphere.

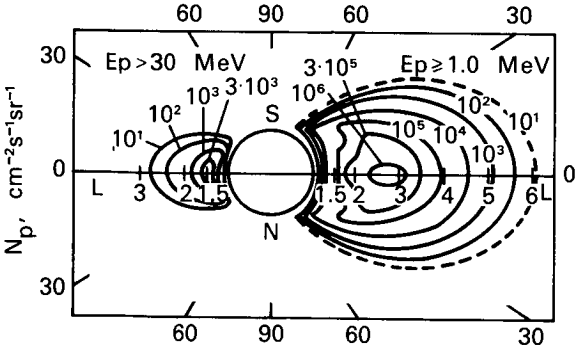

FIGURE 45.—Meridional cross section of belt of protons with energies $E_p > 1.0$ MeV and $E_p > 30$ MeV.

α-Particles in Radiation Belts Around the Earth

Since the solar wind contains both protons and α-particles, it is natural to assume that the radiation belts of the Earth would also contain α-particles. However, their flux should be quite low, since ionization losses of α-particles are greater than those of protons and the concentration of α-particles in the solar wind is 10 times less than the concentration of protons.

A profile of the belt of α-particles, according to Soviet data [53], is shown in Figure 48, while Figures 49 and 50 show the spectrum and relative intensity of α-particles. These figures show the data of other authors as well [144].

Electrons in the radiation belts of the Earth. The distribution of electrons of various energies in the plane of the Equator in 1966 is shown in Figure 51. The area where captured electrons are recorded is divided into the external and internal radiation belts. The boundary between these belts follows approximately $L=3$, where electrons with energies of several hundred keV have minimal lifetimes in comparison to the surrounding L envelopes.

The electron source in the inner radiation belt is neutrons of the cosmic ray albedo, interacting with the atmosphere of the Earth. During the strongest magnetic storms, particles are injected not only into the external radiation belt, but also into the internal radiation belt at $L \gtrsim 2$. Subse-

quently, during the process of diffusion, these electrons may penetrate to even lower L. The data relating to the inner belt (Fig. 51) can characterize the natural electrons of the inner radiation belt [147]. By 1966, electrons with $E_e \leqslant 690$ keV injected by the Starfish explosion had

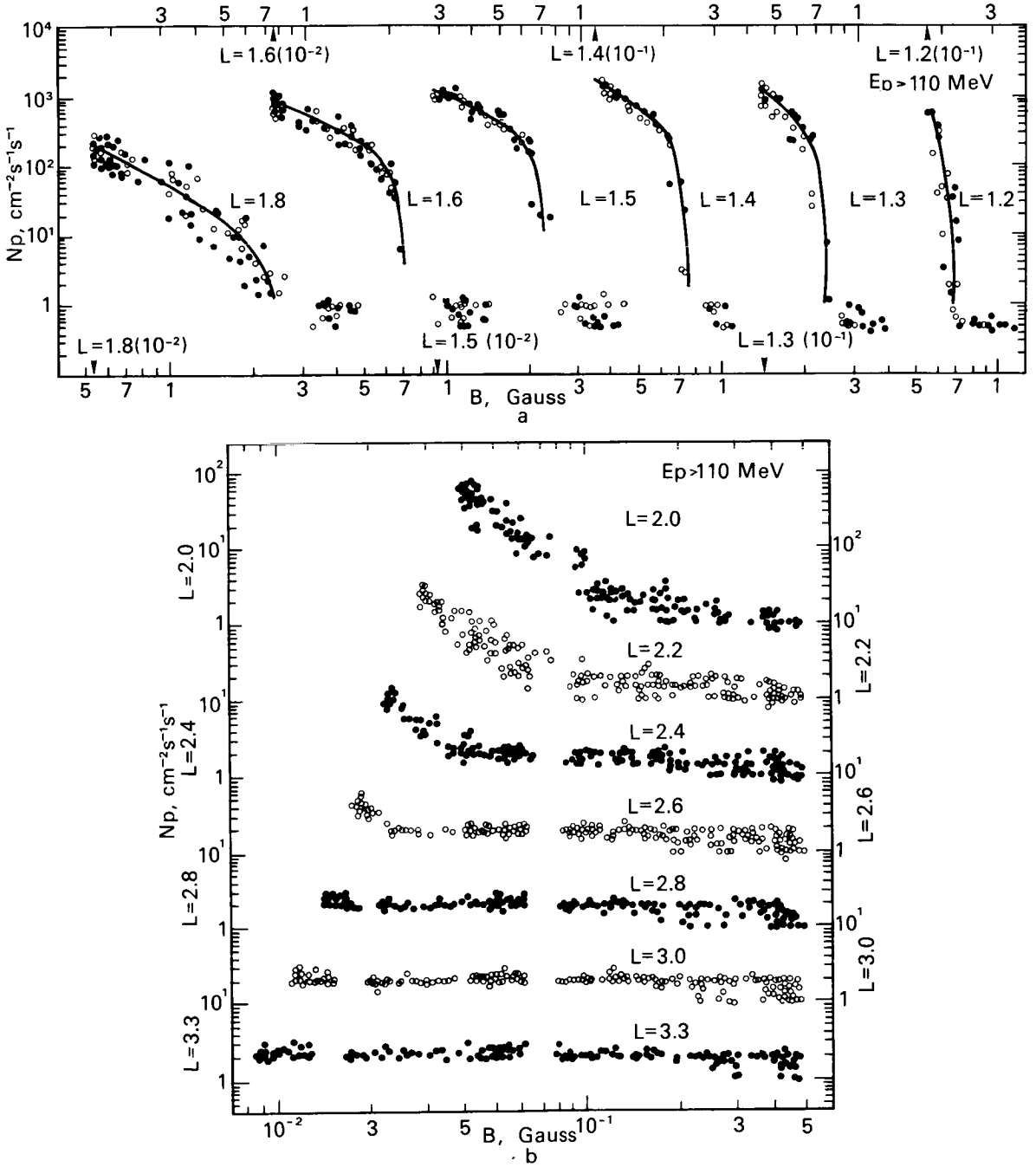

FIGURE 46.—Distribution of protons with energies $\geqslant$ to 110 MeV with respect to B in various L envelopes (from $L=1.2$ to $L=3.3$) according to data from electron satellites. Light points—February; dark points—July 1964. (a) Area $1.2 \leqslant L \leqslant 1.8$; (b) area $2.0 \leqslant L \leqslant 3.3$.

almost completely disappeared. The altitude course of electrons in the inner belt can be approximated by the expression $N \approx B^{-1}$.

The distribution of electron fluxes with energy $E_e \gtrsim 150$ keV in the outer radiation belt in the plane of a meridian is presented in Figure 52 [137]. The electrons of the solar wind are the sources of electrons for the outer radiation belt whose maximum intensity is at $L = 4-5$.

The altitude course of the electrons in the outer belt becomes weaker with transition from the outer boundary to the gap. As L changes from 6 to 4, the mean altitude course changes from $N \approx B^{-1}$ to $N \approx B^{-0.3}$. If a magnetically quiet situation is retained for 4–5 days, at $L \sim 4$ the altitude course disappears and $N = \text{const}$ with variations in altitude of ~6000 km to the Equator.

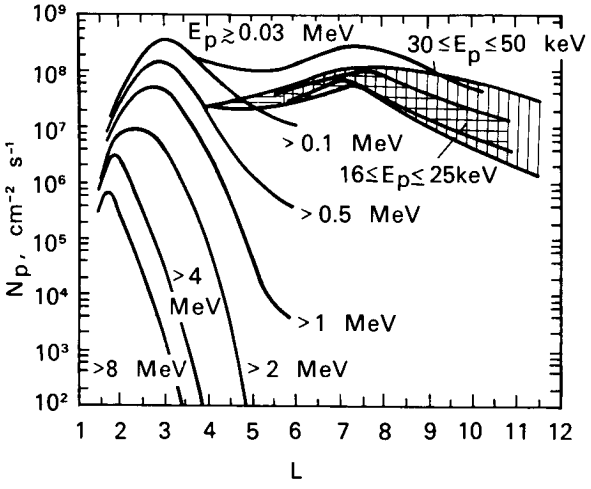

FIGURE 47.—Radial profiles of equatorial omnidirected flux of low-energy protons.

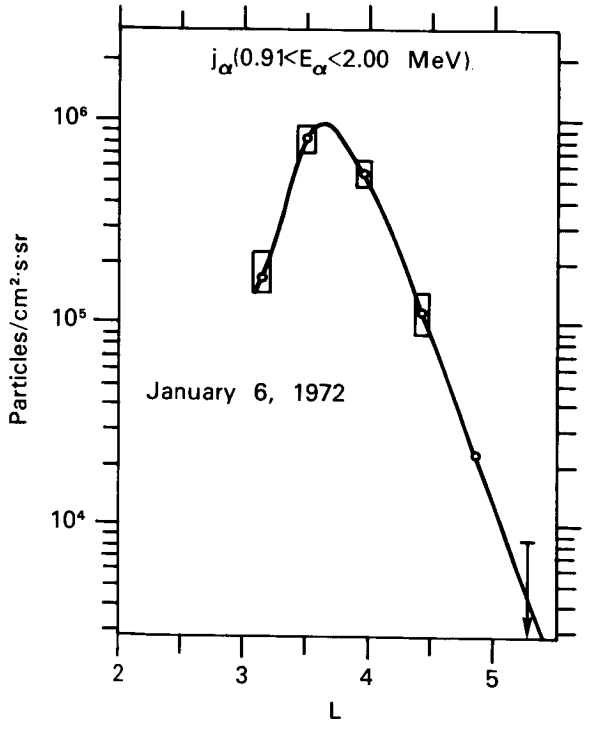

FIGURE 48.—Equatorial cross section of belt of low-energy α-particles.

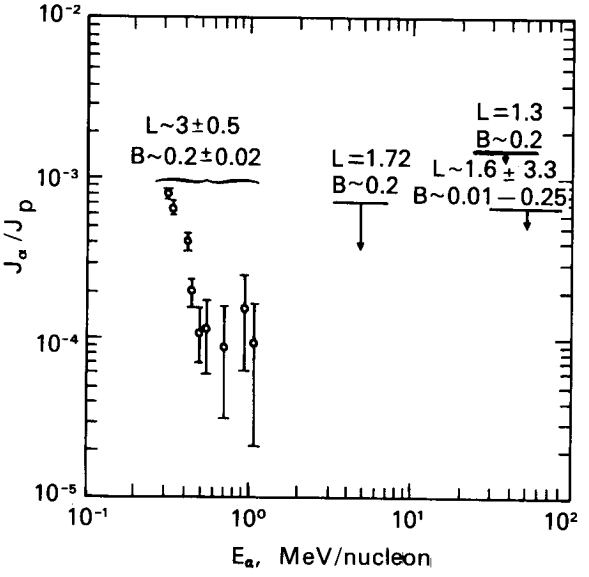

FIGURE 49.—Data on energy spectrum of α-particles in radiation belts.

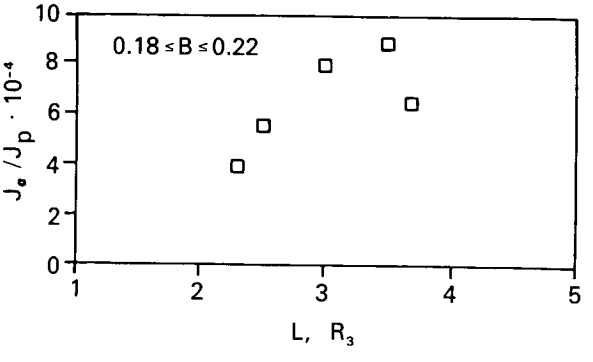

FIGURE 50—Relative intensity of α-particles with energies over 0.31 MeV/nucleon as a function of L.

Sources of Particles in Radiation Belts

The particles causing the Earth's radiation belts have already been noted; consideration will be given to the mechanisms by which the radiation belts of the Earth are filled, and these can be divided into two groups:

slow continuous filling of the radiation belts with particles;
rapid "impulse" injection of particles.

The slow, continuous filling of the radiation belts with high-energy particles occurs as neutrons of the cosmic ray albedo interact with the atmosphere of the Earth. This process is the source of particles for the proton belt with energies $E > 30$ MeV and the electron belt at $L \leqslant 2$–3. Many calculations have been made of the intensity of protons in the inner radiation belt, the source of which is the albedo neutrons [68, 130]. The actual altitude course of intensity differs significantly from the calculated course. Apparently, neither the change or flux of neutrons with altitude, nor the mechanism of proton death (usually only ionization losses are considered) is well-known.

This filling also occurs in the process of diffusion of particles from the outer areas of the magnetosphere to its core. The theory of the process has been well-developed [40, 106, 130]. It is assumed that the diffusion of particles occurs during sudden impulses of the geomagnetic field, frequently recorded by magnetic observatories. The diffusion of particles may also occur during magnetic substorms. This process leads to acceleration of the diffusion of electrons at low L ($L < 2$).

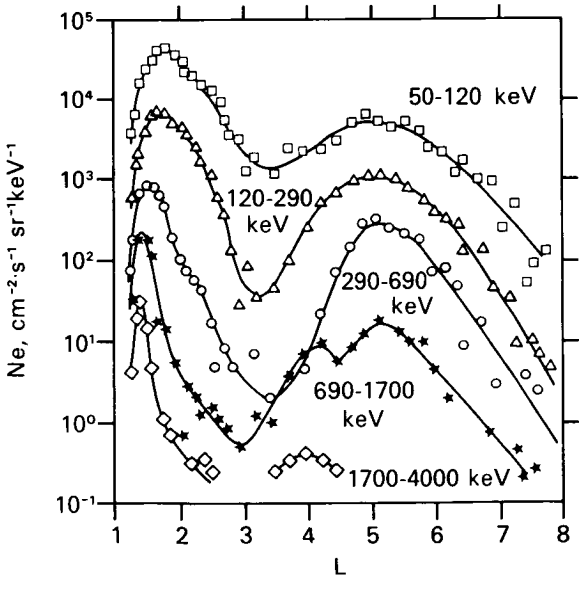

FIGURE 51.—Radial profiles of electron intensity at $L \geqslant 1.75$.

The change in the profile of the electron belt with $E_e > 1.6$ MeV in the process of diffusion is shown in Figure 53 [50]. The leading edge of the belt during the process of diffusion moves at $v = 33 \cdot 10^{-7} L^9 R_e$ per day. The rate of movement of the maximum of the belt is approximately one-fourth as great. This figure shows the dependence of the rate of diffusion of electrons with energies of 0.15–5 MeV on L [139].

During the process of diffusion, the proton belts of the Earth with $E_p < 30$ MeV and the outer electron belt are formed. The maximum intensity of particles of various energies is formed at the L for which diffusion time for the boundary of the belt is approximately equal to the lifetime of the particles.

Rapid increases in the intensity of particles in the belt occur during magnetospheric substorms, and involve strengthening of the large-scale electric field in the terrestrial magnetosphere. Three modifications of the acceleration mechanism can be noted.

First, particles are injected from the tail of the magnetosphere under the influence of a strengthened electric field. Higher energy particles in this case appear in more distant drift envelopes; electrons with $E_e \gtrsim 40$ keV appear at $L \geqslant 4.0$. Drift orbits of accelerated particles under the influence of the reinforced electric field are open, become closed only when it weakens.

Second, particles of the belt are redistributed under the influence of relatively weak electric fields, changing with time. The drift orbits of the particles remain closed in this case, but rapid diffusion of the particles occurs to the L envelope, for which the period of rotation of the particles around the Earth τ_3 is equal to the period of influence of the electric field, since $\tau_3 \sim \frac{1}{E_k L}$ so that high-energy particles increase their intensity less than lower energy particles.

Third, at the beginning of any magnetospheric substorm, the field in the tail of the magnetosphere is increased by transition of lines of force from the core of the magnetosphere into the tail. Upon completion of a storm, the lines of force return. The field at the tip of a line of force increases and the energy of particles located on a given line of force increases correspondingly ($E/B = \text{const}$). At the end of a magnetospheric substorm, an accelerating induction electric field appears in the tail of the magnetosphere [146].

The mechanism of development of the quasi-stable electric field is not yet clear. Possibly, charges separate at the boundary of the magnetosphere. They may arise in the region of the proton belt, where the current responsible for the D_{st} variation of a magnetic storm is formed (to be discussed later).

Death of Particles in the Earth's Radiation Belts

The general picture of the intensity of particles in the radiation belts drawn above reflects the state of dynamic equilibrium between the death of particles and their arrival. The mechanisms of death for particles of various types are different.

For protons and α-particles, the basic mechanism of death is a decrease in the energy of the particles due to ionization losses upon interaction with the traces of atmosphere at high altitudes. The disruption of the first adiabatic invariant is significant only for protons with $E_p \geqslant 100$ MeV.

For electrons, Coulomb scattering is more effective than ionization losses. It defines the lifetime of electrons at less than 1.5. For higher L, the lifetime decreases, indicating that there is a new, more effective mechanism leading to departure of electrons from the belts. This mechanism is scattering of electrons on low-frequency waves such as whistling atmospherics and natural cyclotron radiation.

The decrease in intensity of electrons in various L envelopes during magnetically quiet periods can be approximated by a function such as:

$$N \approx \exp(-t/\tau) \qquad (23)$$

where τ is called the lifetime of the electrons. A summary of the lifetime of electrons in various L envelopes is presented in Figure 54, which shows the dependence of lifetime of electrons with $E_e \geqslant 1.2$ MeV and $E_e \geqslant 300$ keV on L [144].

The intensity at which the flux of particles is reduced by a factor of 2 in 1 day is called the limiting intensity. At intensities near N_{np}, the lifetime of electrons with $E_e > 40$ keV and $E_e > 300$ keV drops sharply. The decrease in intensity is not exponential, but a power function: $N \approx t^{-1}$ [81]. When the intensity reaches the value $N \approx \frac{N_{np}}{0.69}\tau$, the power drop in intensity becomes exponential with lifetime τ. The decrease in the lifetime of electrons with an increase in intensity is related to the development of cyclotron instability and scattering of electrons on their own cyclotron radiation. The ionosphere in this case has a stabilizing influence on the belt, since it absorbs the cyclotron radiation of electrons with a frequency near the low-frequency radio radiation band. The death of particles occurs primarily on the night side of the Earth, where the ionization density is less and the absorption of cyclotron radiation is weaker.

The scattering of electrons can be conveniently observed on the basis of the accumulation of particles in forbidden drift trajectories, which descend into the denser layers of the atmosphere or to the Earth.

Figure 55 shows the change in intensity of electrons with $E_e \gtrsim 400$ keV at $L = 2$ at the drift trajectory with $h_{min} = 100$ km. It can easily be seen that at the departure from the anomaly, the flux of such particles is slight and increases with drift around the Earth.

The peculiarities of the pouring of electrons with $E_e \sim 100$ keV around the entire Earth can be seen in Figure 56, likewise the increased pouring of electrons during the night hours at $L \gtrsim 2$ to the east of the Brazilian anomaly (0°–60° W), a phenomenon which is related to conical instability. This pouring and death of particles occurs constantly even under quiet geomagnetic conditions. In addition to this stable death of particles, sporadic pourings of electrons and protons are observed in the belts. These phenomena are related to geomagnetic, ionospheric, and solar disturbances and will be described in the section on Sun-Earth connections.

SUN-EARTH CONNECTIONS

Geomagnetic Activity—Storms and Ionospheric Disturbances

Most geophysical phenomena in the upper atmosphere of the Earth are directly or indirectly related to active phenomena on the Sun. The most characteristic manifestations of this connection are geomagnetic storms, arising as a result of interaction of streams of solar plasma from flares with the magnetic field of the Earth. Geomagnetic storms, together with the geomagnetic and ionospheric disturbances accompanying these storms, form a complex group of phenomena called geomagnetic activity. Typical manifestations of geomagnetic activity are phenomena such as the polar auroras, absorption of cosmic noise in the polar caps, and atmospheric reduction and disturbances in the F layer of the ionosphere.

Ionospheric disturbances and polar auroras are among the outstanding phenomena related to geomagnetic storms. Study of the behavior of the ionosphere relates directly to determination of

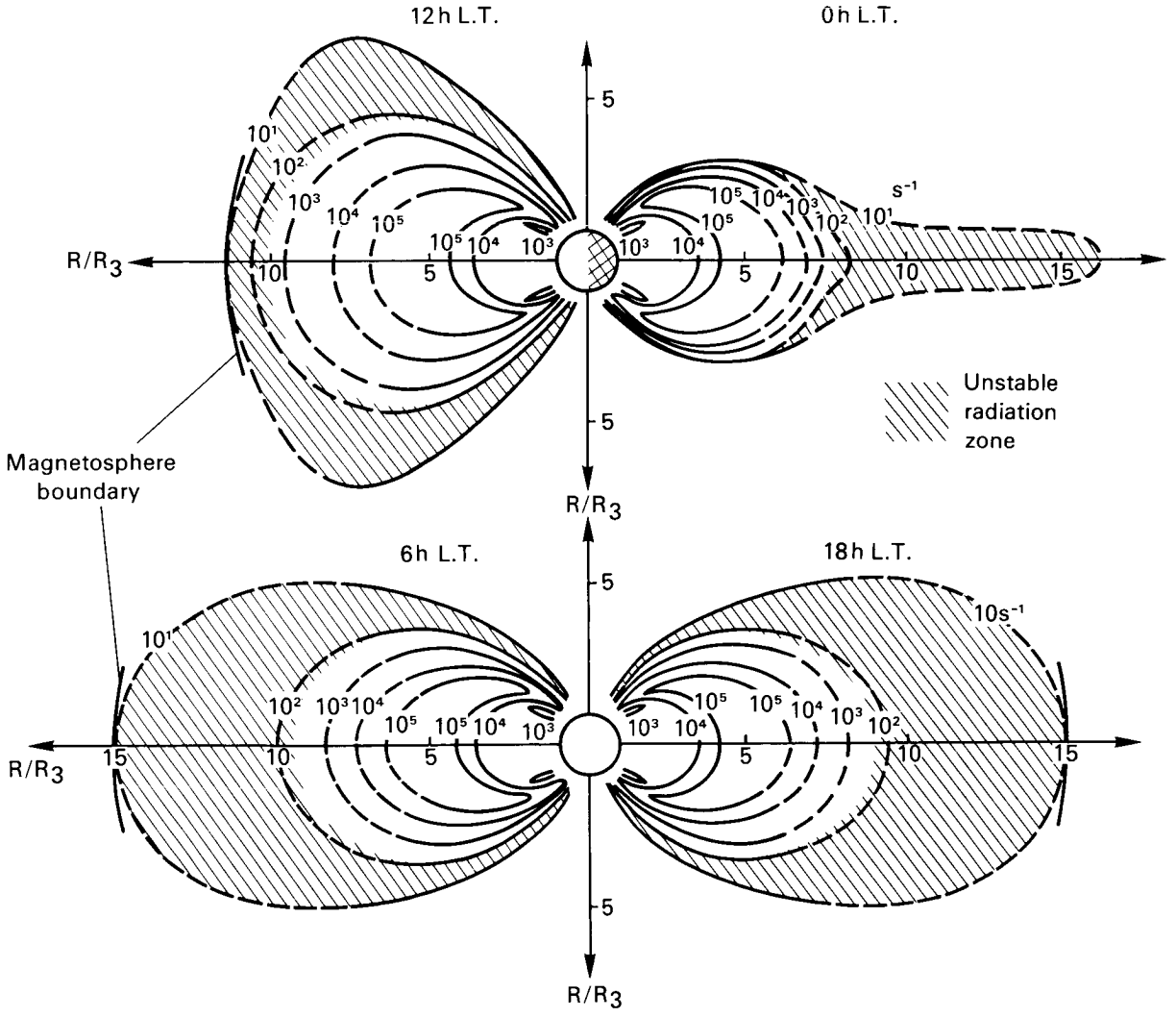

FIGURE 52.—Distribution of electrons with energies $E_e \geq 150$ keV in the terrestrial magnetosphere. To produce flux of electrons per cm² · s, figures by curves must be multiplied by a factor of about 100. Zone of unstable radiation shaded. Top—cross section through day-night line; bottom—morning-evening.

the mechanism of geomagnetic storms, since the primary current systems responsible for magnetic disturbances apparently lie in the ionosphere, while study of the auroras provides unique information on pouring of particles from the magnetosphere.

Geomagnetic activity is complexly dependent on a number of parameters of the interplanetary medium, the magnetosphere, and the ionosphere, and on the physical processes which occur in them. Its most common measure is the magnetic index, represented as K or A (depending on the

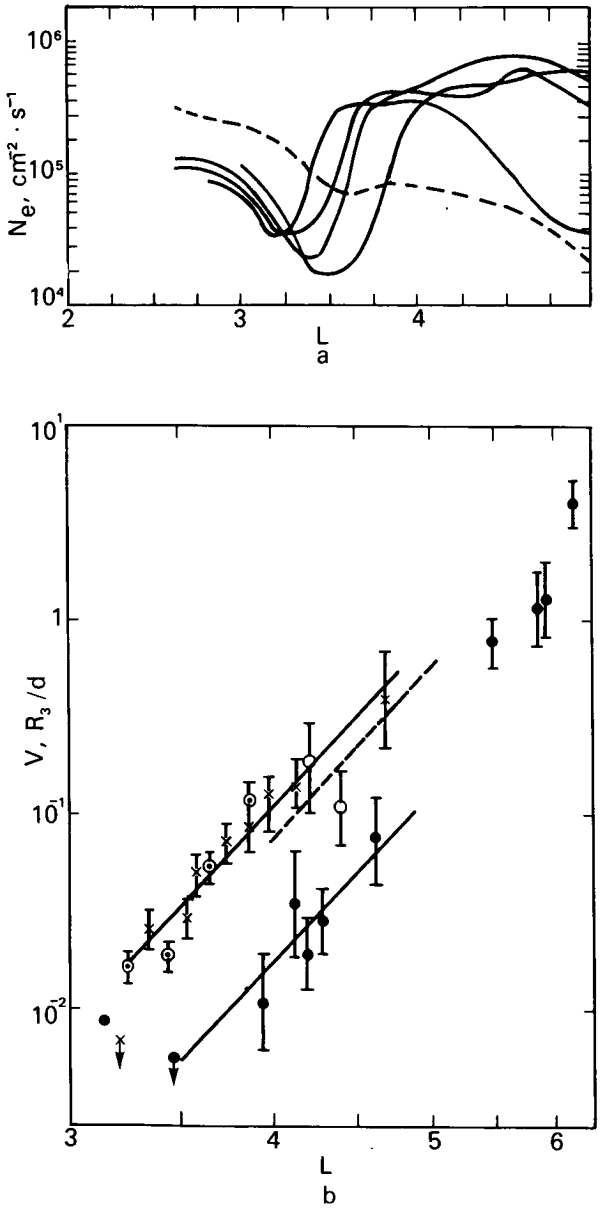

FIGURE 53.—(a) Change in profile of intensity of electrons with $E_e > 1.6$ MeV as a result of radial diffusion [39]. (b) Velocity of radial diffusion of electrons with energy $E \sim 0.15+50$ MeV as a function of L [81].

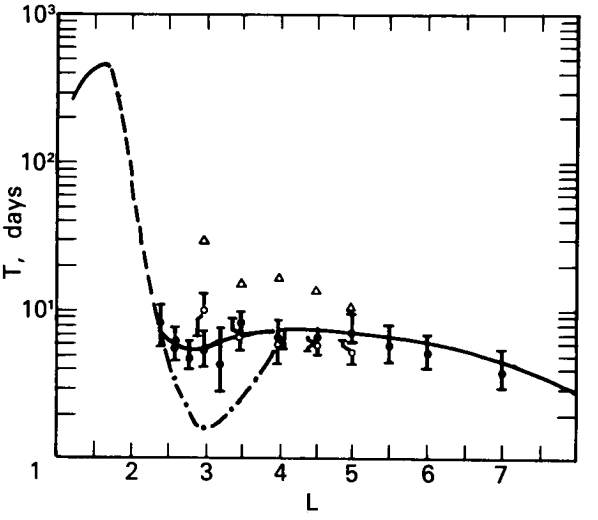

FIGURE 54.—Lifetime of electrons with $E_e > 300$ keV and $E_e > 1.2$ MeV as a function of L. △ > 1.2 MeV; ○ > 300 keV (Explorer 26); ● > 300 keV (1963—38°C). Dot-dash line, possible reduction in lifetime; solid line, lifetime of electrons with $E_e > 300$ keV; dashed line, no data available.

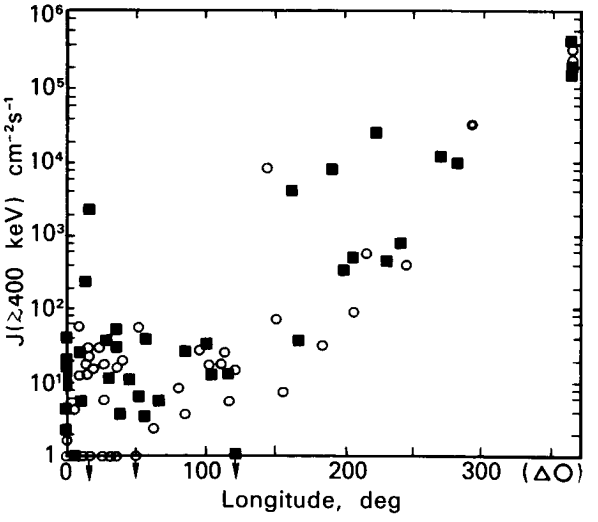

FIGURE 55.—Flux of electrons with $E_e > 400$ keV at $L = 2.0$ as a function of longitude, to east of Brazilian anomaly. △○, longitude interval between point of measurement and point h_{min}=100 km, ○—$T_m \sim 12$, ■—$T_m \sim 0h$.

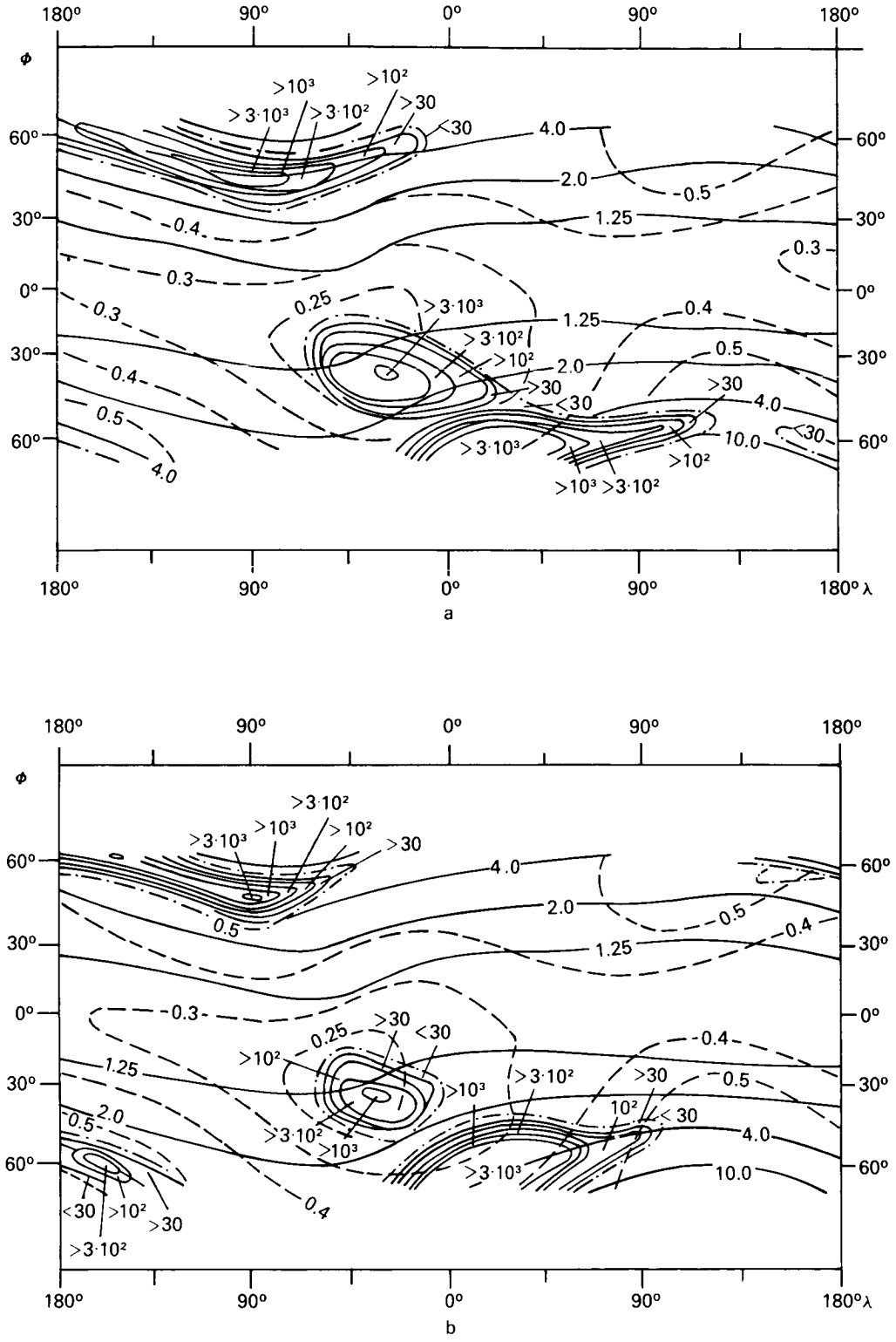

FIGURE 56.—Distribution of precipitation of electrons with $E_e >_1$ 100 keV for local time. (a) LT 18:00–5:00 (night); (b) LT 6:00–17:00 (day). Intensity is expressed in particles/cm · s.

use of the quasi-logarithmic or linear scale), characterizing the maximum change in the geomagnetic field over 3 hours.

Variations in geomagnetic activity observed are both periodic (27-day and 11-year variation) and sporadic in nature. The 11-year variation is closely related to the cycle of solar activity and correlates well with it; the 27-day variation indicates a relationship between the phenomena observed and certain active areas on the Sun. The perturbing agent may be either recurrent corpuscular streams from the active areas, or hard electromagnetic radiation. Increases in geomagnetic activity are observed as the Earth intersects streams of high-velocity solar plasma. Some increase in activity is observed as the Earth crosses the boundary of the sector of the interplanetary magnetic field where the velocity of the solar plasma frequently reaches values of 700–850 km/s. As the sector boundary is passed, a change is recorded in the intensity of cosmic rays, the index of magnetic activity A increases, and the intensity of captured electrons in the outer radiation belt changes. This represents the influence of the quasi-stable sectorial structure of the interplanetary magnetic field on geomagnetic activity. Study of the interaction of the solar wind with the magnetic field of the Earth has been reviewed [26, 208].

Interaction of the Solar Wind with the Earth's Magnetic Field

The solar wind and clouds of solar plasma, striking the magnetic field of the Earth as they propagate from the Sun, deform it in a way so that on the Sun side it is somewhat compressed, while on the opposite (shadow) side it extends outward, forming a long, geomagnetic tail. The particles of the solar plasma are partially deflected by the geomagnetic field. Flowing around the magnetosphere, they continue farther into interplanetary space, and are partially captured by the field, forming belts of charged particles or zones of captured radiation around the Earth.

Near-Earth space can be divided into three areas with regard to its physical characteristics:

(1) interplanetary space, where the properties of the interplanetary medium are not disturbed by the Earth and its magnetic field;
(2) the transition region or magnetosheath resulting from interaction of the solar wind with the geomagnetic field;
(3) the magnetosphere—the area of space occupied by the geomagnetic field.

The magnetosphere can in turn be divided into two parts: the portion of the magnetosphere which encompasses primarily the zones of captured radiation, and the remaining portion, including the magnetic tail (magnetotail) of the Earth with a magnetic neutral plasma layer.

These three areas of space are separated by two characteristic boundaries: the collisionless head shock wave and the magnetopause. The collisionless shock wave separates the unperturbed interplanetary medium from the magnetosheath; the magnetopause (boundary of the magnetosphere) separates the magnetosheath from the magnetosphere (see Fig. 37).

A boundary of the geomagnetic field and its motion were first discovered by the Explorer 10 satellite. The first measurements of captured particles, the magnetic field, and the plasma at the boundary of the geomagnetic field were made in 1961 by Explorer 12 [30, 52]. The geomagnetic field is compressed by the stream of the solar wind on the Sun side at a distance of about $8.2\,R_0$ along the Sun-Earth line. In addition to the limitation of the regular geomagnetic field, a limitation of the quasi-thermalized plasma was discovered, which was interpreted as the leading edge of a collisionless shock wave.

Further investigations finally established that there is an area which serves as a division boundary between the strong, regular geomagnetic field within the magnetosphere and the rapidly fluctuating weak magnetic fields of interplanetary origin in the transition area (Fig. 37). In the transition area, the low-energy solar plasma is retained and thermalized upon transition through the area of the collisionless shock wave. In both the shock wave and the magnetosphere, significant fluctuations of the magnetic field are observed. Later measurements of the magnetosphere boundary indicated a slightly higher value than the first measurements for its distance

from Earth, and showed that the position of both boundaries may change, displacements reaching 20% of the nominal values of the boundary distances. These variations in position of the boundary surfaces result from time variations in the density and velocity of the solar wind and related interplanetary fields.

The boundary of the magnetosphere on the Sun side is assumed to be approximately spherical in shape with a radius of curvature of about 14 R_0, and its center displaced by 3.5 R_0 toward the night side along the Earth-Sun line. The shock wave is approximately parabolic in shape and intersects the Sun-Earth line at a distance of 14 R_0. The axis of symmetry of the magnetosphere boundary in the plane of the ecliptic is rotated relative to the Sun-Earth direction by a slight angle (5°), a result of the effect of aberration due to the orbital motion of the Earth around the Sun.

The head shock wave is recorded by sharp change in physical properties of the plasma medium (appearance of low-energy plasma in the transition area). Observations on satellites such as Vela [39] have shown that the flux of electrons recorded by satellites in the area of the assumed head shock wave undergoes sudden and sharp changes. The general nature of the change in proton and electron fluxes agrees with the idea that turbulence results from interaction of the solar wind plasma with the shock wave. Protons of the solar wind lose some of their energy, while the electrons of the solar wind increase their energy and the direction of motion of the particles becomes more chaotic. The global flux of electrons with $E_e > 350$ eV, upon transition from interplanetary space to the transition area, increases from not more than 10^7 to about $5 \cdot 10^8$ cm^{-2} s^{-1}. The temperature of the protons increases from about $10^5 \cdot$ (typical value for interplanetary space) to about 10^6 °K. The electron temperature behind the leading edge of the shock wave is about 10^6 °K, although higher values are frequently observed (up to about $5 \cdot 10^6$ °K).

In the transition area approximately between 10 and 15 R_0, near-isotropic but varying streams of protons and electrons have been observed with intensities of 10^9 cm^{-2} s^{-1}. A significant increase in the ion temperature and a sharp decrease in the intensity of streams of protons and electrons have also been observed near the magnetopause ($R_m \approx 10.5\ R_0$). Measurements have shown that the concentration of protons in the transition area is 8 to 10 times higher than in the solar wind. The magnetopause is easily detected not only by the change in the magnetic field, but also by the sharp decrease in the flux of protons with $E_p < 10$ keV and the appearance of electrons with $E_e > 40$ keV within the magnetosphere. Both boundaries (the head shock wave and the magnetopause) sometimes diffuse, making identification more difficult.

On the night side of the Earth, the lines of force of the geomagnetic field are extended far away from the Sun, forming a long loop, extending to a distance over 80 R_0, i.e., beyond the orbit of the Moon [43, 44, 61].

A tail is indicated as far out as $R \simeq 1000\ R_0$ [101]. The diameter of the tail of 30 R_0 is about 40 R_0, at the geocentric distance of 80 R_0 about 50 R_0. The geomagnetic tail is assumed to form as a result of extension of the lines of force of the geomagnetic field from the polar areas by the solar wind. It is shaped like a slightly flattened cylinder with a θ-shaped cross section, consisting of two individual magnetic force tubes. In the southern tube, the magnetic lines of force from the south polar area are directed away from the Earth; in the northern tube the magnetic lines of force, connected to the north polar area, are directed toward the Earth. These tubes are separated by a magnetically neutral layer with very low field intensity, almost coinciding with the layer of hot plasma, balancing the pressure upward and downward from the neutral layer.

The neutral layer, according to observations [16, 17], is very thin; its thickness is not over the radius of the Earth (changes within limits of 500–5000 km have been recorded). When a satellite crosses the neutral layer, the sign of the field reverses; thus the existence is presumed of a layer of plasma and an equivalent electrical current, connected to the field gradient. Measurements made by the IMP–1 satellite show the neutral layer to be frequently in motion; the lines of force have a small component connecting the lines of force on opposite sides of the neutral layer. During magnetic storms, the magnetic tail is strongly deformed and changes [144].

574-269 O - 76 - 8

The intensity of the magnetic field in the tail (H_x) decreases with increasing geocentric distance r_{se} according to the rule $H_x \approx (r_{se})^{-\gamma}$, γ 0.5 ± 0.2. At the distance $r_{se} = 10$–$15\ R_0$, $H_x = 20$–$30\ \gamma$. At $r_{se} = 40\ R_0$, $H_x \sim 10$–$18\ \gamma$, while at $r_{se} = 80\ R_0$, $H_x \approx 6$–$12\ \gamma$. The value of the component perpendicular to the neutral layer is $H_z \approx 1$–4γ [129]. According to measurements by Explorer 33 [100], the field intensity of the geomagnetic loop at the orbit of the Moon is 10–18 γ; the direction of the field is almost parallel to the Earth-Sun line. The form of the geomagnetic tail depends largely on the flux of plasma at its surface and, like the mechanism of the tail formation, is still debated [15].

Geomagnetic Disturbances

The instability of solar plasma fluxes leads to fluctuations in the position of the outer boundary of the magnetosphere, which can be recorded on Earth as pulsations of the geomagnetic field. Comparison of variations in parameters of the solar wind flux, made from observations by Venera 2, 4, and 6, with pulsations of the geomagnetic field [66], show that the primary parameter of the solar wind, determining the nature of geomagnetic field pulsations, recorded on the Earth, is the concentration of the proton component.

The stronger geomagnetic disturbances are caused by high-energy fluxes of solar plasma from solar flares and recurrent fluxes of solar plasma. These disturbances may be periodic (smooth and regular) or sporadic; the most intensive are called geomagnetic storms. The intensity of the geomagnetic field, equal to about 0.3 Oe (30 000 γ) at the surface of the Earth near the Equator, may vary as much as 1%–2% during the strongest geomagnetic storms.

A geomagnetic storm usually passes through three phases of development: the initial phase, a smooth or sudden change of field; the main phase, a significant decrease in the horizontal component of the field in the middle and low latitudes; and a phase of gradual recovery, developing approximately 1 day after the beginning of a storm and continuing for several days (Fig. 57).

Correlation of the time variation of the field of a storm D_{st} with the position of the magnetopause on the day side, shows that in the initial phase of a magnetic storm, the magnetosphere is compressed, apparently due to an increase in the solar plasma flux, while during the recovery phase there is general expansion. In geomagnetic

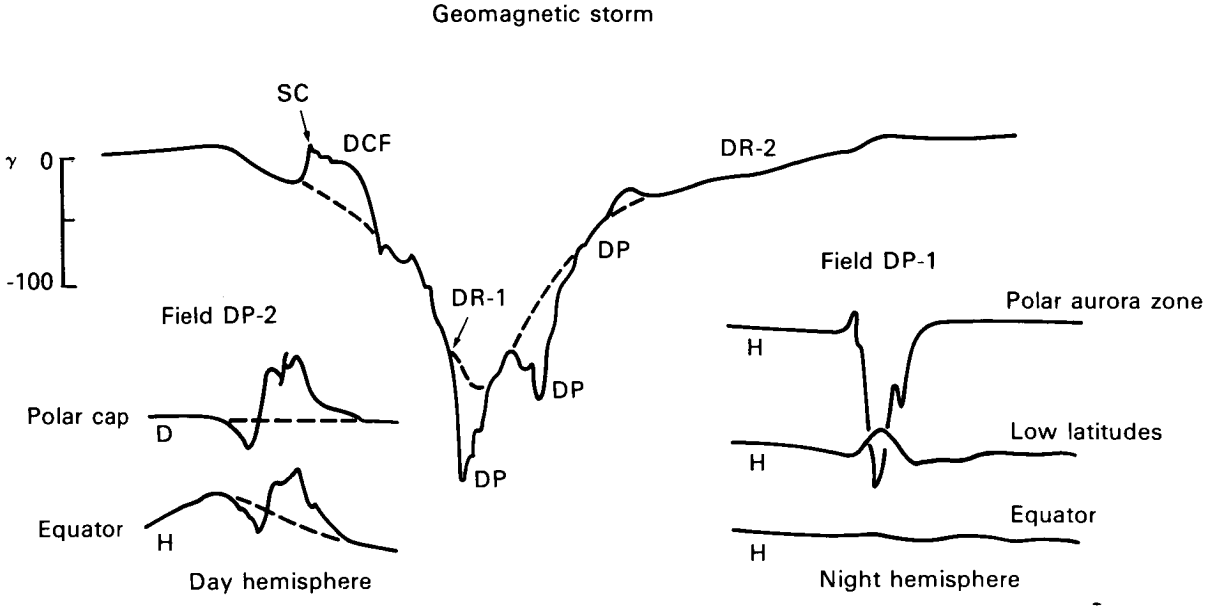

FIGURE 57. – Change of magnetic field during a geomagnetic storm.

storms with a clearly expressed main phase, there are great increases in the distance to the head shock wave and in the thickness of the transition, and a tendency toward increased storm intensity with increasing transition area thickness. Formation of the broader transition area may facilitate generation and transmission of magnetohydrodynamic waves into the magnetosphere, causing an increase in the viscous interaction and subsequent transfer of magnetic lines of force into the Earth tail, which increases the intensity of the storm.

There is a relationship between the position of the flare responsible for a storm on the solar disk and the nature of the storm. Storms caused by central flares are usually more sudden in onset SC and show a well-developed main phase; flares near the edges of the solar disk cause storms with milder, more extended initial phases; the development of the main phase is not always the same during such storms. The flux of energy responsible for geomagnetic storms can be assumed to be concentrated in a narrow cone, with an axis directed radially outward from the area of the flare. The appearance of flares responsible for storms with sudden onset at any point on the solar disk also shows that the leading edge of the plasma flow expands almost hemispherically as it propagates, and forms an extended envelope. These concepts can be combined into a single picture, presumably, of the distortion of the shock wave generated, as plasma is thrown outward from the area of a solar flare [59].

Morphology of Geomagnetic Disturbances

The analysis of the morphology of geomagnetic disturbances presented here is based largely on the detailed review by Obayashi [102]. Chapman suggested that the field of a disturbance D be formally divided into two areas to describe the rather complex nature of a geomagnetic storm: the axisymmetrical area D_{st} and the asymmetrical area DS:

$$D = D_{st} + DS \qquad (24)$$

The field D_{st} corresponds to variations during the storm. For a typical geomagnetic storm, this portion begins with a sharp change in the field at the moment of the sudden onset SC and continues with the longer initial phase (Fig. 57). The main phase of the storm shows a significant decrease in the horizontal component of the field D_{st} in the middle and lower latitudes. Field DS is disturbed, depending on local time; the average of DS is called the disturbed solar-diurnal variation DS. Field DS predominates, generally, in the high latitudes and is most active during the main phase of the storm [33].

In the polar auroral areas, particularly along the auroral belt, the magnetic disturbances are very intense. These disturbances, polar substorms or geomagnetic bays, usually last no more than a few hours and may reach several hundred gammas. They may appear during planetwide geomagnetic storms, or under quiet magnetic conditions. The most significant feature of these disturbances is the development of strong stream currents in the ionosphere along the night side of the auroral belt, the auroral electric streams. These disturbances are represented as field DP–1 (Fig. 57).

With the auroral electric stream DP–1, another ionospheric current system, responsible for the DP–2 field, consists of two current vortices with opposite directions, located in the polar area, with centers approximately along the morning-evening meridian. The field of DP–2 disturbances arises and exists over the entire Earth (from the pole to the Equator), i.e., has a wider distribution in space than field DP–1. The frequency of current systems DP–2, excluding cases of SC and SI, is comparable to the frequency of DP–1 polar magnetic substorms.

Upper Atmosphere of the Earth—the Ionosphere

Short-wave radiation from the Sun carries sufficient energy to cause significant photoionization of the terrestrial atmosphere at high altitudes, creating a partially ionized area in the upper atmosphere, the ionosphere. The ionosphere extends from about 50 km to the boundary of the magnetosphere. It is usually divided into several parts: the D area (50 to 90 km), E area (90 to 120–140 km), F area (120–140 to 600–1500 km), and protonosphere (1200–5000 km to the

boundary of the magnetosphere). The F area is divided into the F_1 and F_2 layers, the E area is sometimes divided into the E_1 and E_2 layers. The separation into areas is defined by the processes of their formation and composition of ions they contain. The D, E, and F areas are primarily molecular ions O_2^+ and O^+, the F_2 area consists of O^+, and the protonosphere consists of H^+.

Atmospheric conditions in areas of the ionosphere differ greatly. The temperature varies from about 200 to 1000–2000° K, the concentration of neutral particles n varies by a factor of a million: from 10^{15} cm^{-3} in the D area to 10^9 cm^{-3} in the F area. The electron concentration n_e depends on the phase of the solar cycle and the time of day. The maximum concentration of ions and electrons is reached in the uppermost layer, in the F_2 layer above 300 km altitude. At altitudes over 110 km, the degree of ionization n_e/n in the daytime is about 10^{-7}, while at altitudes of about 300 km it reaches 10^{-3}. Upon transition from day to night, the electron concentration in the F_2 area decreases by about 3–10 times, whereas in the E and D area it drops by 1.5 and 2.5 orders of magnitude. The time and geographic variations of the day E layer are quite regular. The maximum ion concentration in the E layer depends almost entirely on the activity and zenith distance of the Sun. The E layer has almost no sharp disturbances, such as those observed in the D and F layers.

Ionization by solar radiation dominates throughout the ionosphere over $h \approx 80$ km, with the primary portion of shortwave solar radiation absorbed at altitudes of 100–200 km. Over 85 km at the minimum of solar activity and over 70 km at the maximum of solar activity, the primary source of ionization is x-radiation with $\lambda \leq 10$ Å. Radiation in L_α is also significant at $70 \leq h \leq 90$ km. Below 65–70 km, at the middle latitudes, the effect of cosmic rays predominates even in the daytime. The flux of cosmic rays increases by a factor of 3 from the minimum to the maximum of solar activity. In the 65–80 km area in the daytime and ≥ 80 km at night, ionization by corpuscular streams of particles, pouring into the lower portion of the atmosphere, predominates. During magnetic disturbances, the flux of poured particles increases and ionization correspondingly increases (even at 100–110 km on the day side).

The total flux of ionizing radiation from the Sun varies between 2.5 and 8 $erg \cdot cm^{-2} \cdot s$. Cosmic rays expend $3 \cdot 10^{-3}$ $erg \cdot cm^{-2} \cdot s$ on ionization of the terrestrial atmosphere in the middle latitudes. Of this energy, over 90% goes to ionization of the atmosphere below 40 km. Particles poured in during periods of high solar activity expend up to 1 $erg \cdot cm^{-2} \cdot s$ on ionization during the daytime and 10^{-2} $erg \cdot cm^{-2} \cdot s$ at night.

The most significant changes in parameters of the Earth's upper atmosphere are related to changes in the flux of shortwave solar radiation. Dependence of ionospheric parameters on solar shortwave radiation is manifested as periodic (27-day and 11-year) changes and sporadic disturbances, a result of sharp increases in the flux of x-ray and ultraviolet radiation during active phenomena on the Sun.

A change is observed in the parameters of the ionosphere during the course of the day from day to night. The temperature changes most strongly in the 100–200 km altitude range. Over $h \approx 250$–300 km is an area of isothermy. The daily maximum temperature T_{ex} in this area is at 14:00–16:00, the minimum at 4:00–5:00 local time, indicating the inertial properties of the temperature of the atmosphere. Upon transition from day to night, T_{ex} decreases by 20%–40% with low activity and 1.5–2 times with high activity of the Sun, from 1000° to 800° K and 1800° to 1100° K respectively. At altitudes less than 200–250 km, the change in temperature is much more complex. As solar activity increases, the density of the atmosphere increases significantly. The overall atmospheric density at 200 and 300 km increases by 2 and 3–4 times respectively upon transition from minimum to maximum activity. Atmosphere temperature also correlates well with the planetary geomagnetic index A_p. The increase in the geomagnetic index during geomagnetic storms corresponds to an increase in pressure, i.e., density and temperature changes (in the upper atmosphere) are generally recorded 5–7 h after a magnetic storm begins. The upper atmosphere of the Earth and the ionosphere have been widely studied [75, 96, 111].

Ionospheric Disturbances

Disturbances in the ionosphere include processes of two main types: reinforcement of ionization in the lower ionosphere (*D* and *E* areas) and complex aerochemical and dynamic processes relating to the *F* area (Fig. 58 [102]). That the anomalous ionization in the lower ionosphere results from bursts of solar radiation or outpouring of energetic particles is generally accepted.

The plan of disturbances in the *E* area, including the auroras, is shown in Figure 59 from [102]. During solar flares, ionization of the atmosphere, particularly below 100 km, increases sharply. In the *D* layer, following intensive solar flares, it increases by 10^2-10^4 times as a function of the altitude in the atmosphere and the intensity of the flare. This increase in ionization, a sudden ionospheric disturbance (SID), is determined primarily by increase in intensity of solar x-radiation in the 0–20 Å range. The increase in electron density at various altitudes is determined by the increase in the flux of radiation in the 0–20 Å range, and change in spectral distribution of this radiation. The duration of SID is a few minutes to a few hours.

Sudden ionospheric disturbances encompass the lower portion of the ionosphere in the *D* area, although an increase in n_e sometimes occurs in the *E* and *F* layers. Recording of sudden increase in ionization in an area is based on sudden phase anomalies in reflected radio signals (SPD), sudden increases in atmospherics and atmospheric whistles (SEA and SES) at altitudes below 70 km, fading of shortwave signals (SWF), and sudden absorption of cosmic radio radiation (SCNA) between 60 and 100 km.

The strong increase in the Sun's ultraviolet and x-radiation during a flare leads, in a few minutes, to an increase in the system of electrical currents in the ionosphere, responsible for the daily variations in the magnetic field, and is noted on magnetograms as sudden slight excursions—"crumbs." Crumbs are observed on the sunlit side of the Earth and are most clearly expressed near the subsolar point. Almost all crumbs have been observed during periods of increasing x-radiation. The beginning of radio bursts in the centimeter range and the beginning of crumbs usually coincide.

Perturbations in the *F* area, related to geomagnetic storms, have been studied for many years. Analysis of data from the world network of ionospheric sounding stations has revealed many important peculiarities of variations in the elec-

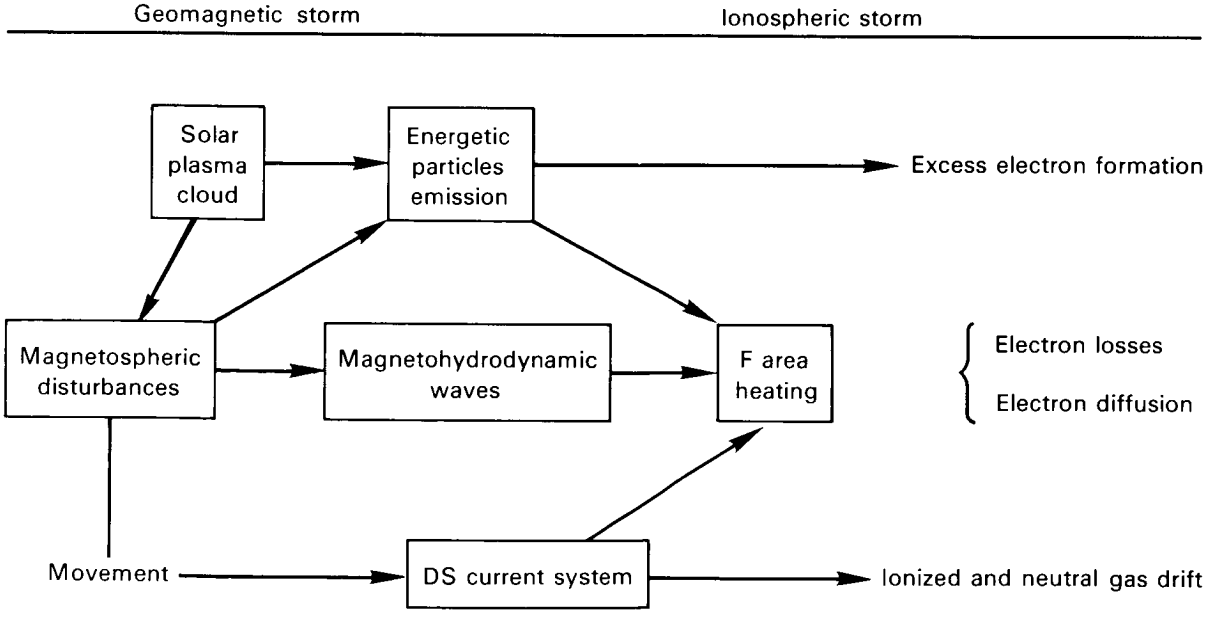

FIGURE 58.—Possible mechanism of ionospheric storm in *F* area.

tron concentration in the ionosphere. However, the theories set forth to explain the mechanism of these disturbances in the F area are debatable; there is still no satisfactory explanation for the main peculiarities of the storms. This situation is caused by the complex processes of formation of the F layer and poor understanding of the electrodynamics of the upper atmosphere. Nevertheless, two factors should be important in solving the problem: the change in the temperature of the ionosphere during magnetic disturbances and the drift electrodynamic motions of electrons under the influence of electric fields arising in the ionosphere.

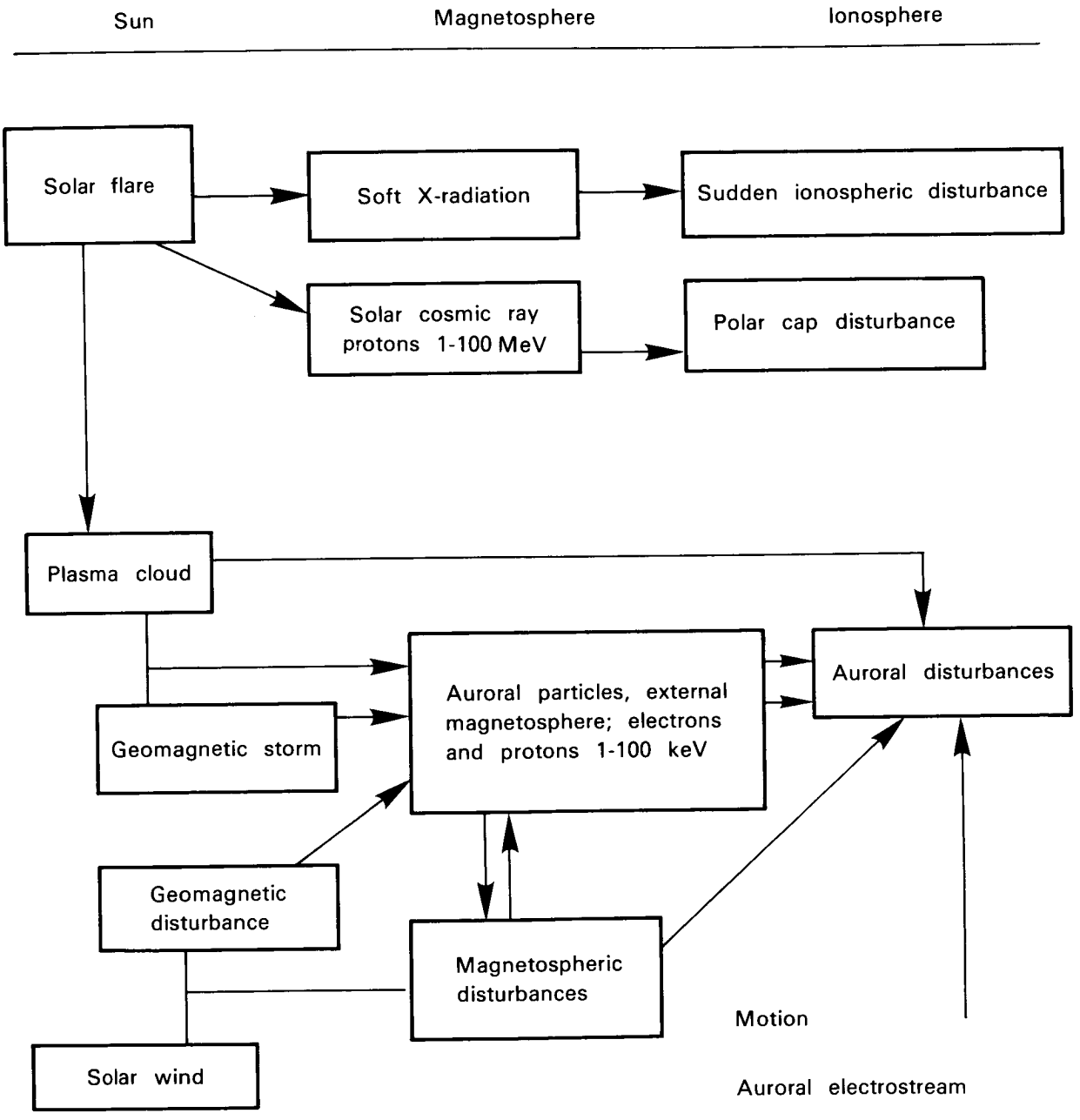

FIGURE 59.—Sources and mechanism of development of primary disturbances in the F area.

The temperature in the F area obviously increases during geomagnetic storms. Observations of the atmospheric braking of satellites have shown that general heating of the ionosphere occurs in altitudes 200 to 700 km; the temperature rise correlates well with the rise in geomagnetic activity. Increased temperature in the F layer leads to significant changes in equilibrium as a result of the electrodynamic drift motion of electrons, caused by interaction of the geomagnetic and electrical fields, related to the currents flowing in the ionosphere.

Polar Auroras and Auroral Phenomena

One manifestation of the Sun-Earth connection is the polar auroras, the only visible manifestation of the interaction of charged particles with the upper atmosphere and ionosphere. This phenomenon varies in the form of the glowing areas and their brightness, color, mobility, and duration (Fig. 60 [31]). The polar aurora has been the subject of many works [2, 12, 31, 32, 74, 76, 77, 80, 96, 111].

All auroras are divided into two structural classes: ray type and homogeneous. The first includes forms of individual rays coinciding in direction with the geomagnetic lines of force; the second, of a homogeneous diffuse glow. Auroras with ray structure are usually very mobile, while homogeneous forms stay at rest.

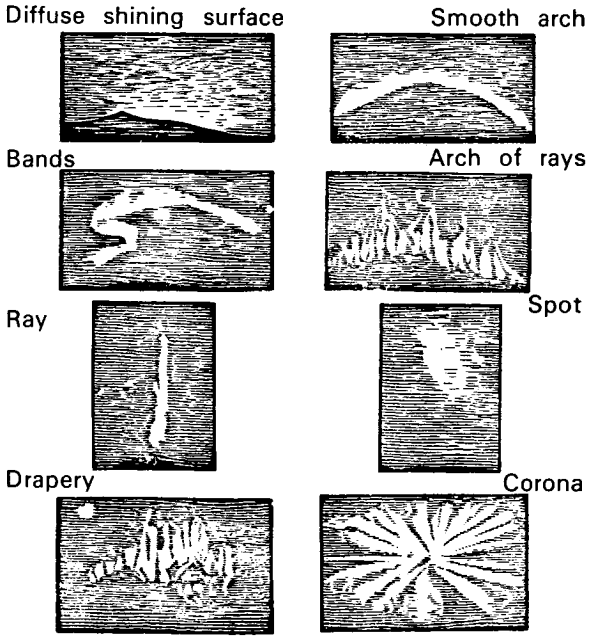

FIGURE 60. – Primary forms of polar auroras.

Study of the polar auroras, closely related to ionospheric and geomagnetic disturbances, can produce indirect information about parameters of the magnetosphere and its charged particles. The timespan of individual forms of auroras varies from a few seconds (ray forms) to several hours (homogeneous forms). The thickness (width) of the arcs falls within 1.5 to 23 km, with a mean value of 10 km; as the geomagnetic disturbance increases, the thickness of the arcs increases. The thickness of the rays amounts to a few hundred meters. The vertical extent of homogeneous arcs is about 30 km, arcs of rays $\gtrsim$40 km, and individual rays about 100 km, sometimes up to several hundred km. The altitude of an aurora is usually the altitude of the lower boundary of the glow (Fig. 61 [147]). Several arcs may be present simultaneously in the sky. The minimum distance observed between them is about 10 km, the maximum distance about 200 km, and the most probable distance, 30–40 km.

Arcs have been observed repeatedly stretching over 180° of longitude, i.e., extending about 7000 km, which is apparently not the limit, since the length of individual forms in the longitude interval $>180°$ has never been studied. As the level of geomagnetic disturbance increases, the length of the arcs decreases and their regular form is disrupted.

Auroras become visible to the naked eye when their brightness exceeds the night sky glow. The brightest auroras are 1000 times as bright as the glow of the night sky. The international 4-grade scale of brightness (see Table 8) is based on the

TABLE 8. – *Physical Properties of Auroras*

Brightness, arbitrary grades	I	II	III	IV
Intensity of 5577 Å (kR)	1	10	100	1000
Light flux (erg/cm² · s)	0.01	0.1	1	10
Flux energy of particles (erg/cm² · s)	3–5	30–50	300–500	3000–5000

absolute intensity [2] of the 5577 Å emission. The Rayleigh is used as a unit of measurement. An auroral intensity of 1 Rayleigh corresponds to the emission of 10^6 quanta/s in a column of atmosphere with a cross section of 1 cm^2.

The overall spectra of electrons (shown in Fig. 62 [77]) is according to the data from rockets and satellites for the high and middle latitudes. In both cases, electrons with $E = 1-10$ keV carry the primary energy of the stream, although at the auroral latitudes their intensity is significantly higher. These electrons are most effective in formation of the polar auroras and ionization at the altitude of the E layer.

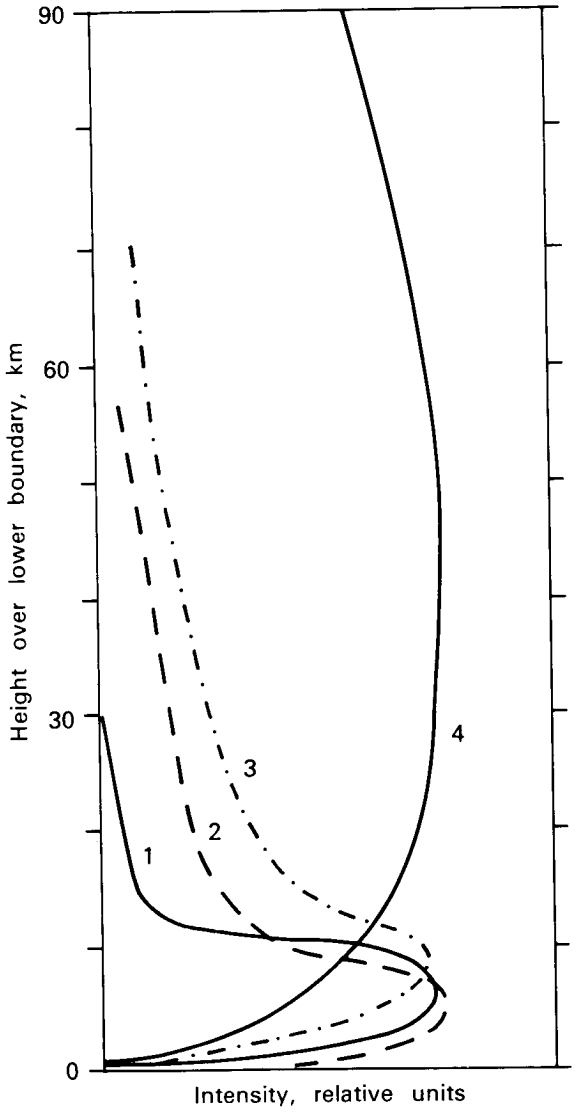

FIGURE 61.—Vertical cross section of intensity of glow of various types of polar auroras: 1, smooth arches; 2, arches of rays; 3, bands of rays; 4, rays.

The area in space in which polar auroras can be observed at a given fixed moment in time is an irregular circle, asymmetrical relative to the magnetic pole; on the night side of the Earth, the circle passes over latitudes $\phi \sim 67°-68°$; on the day side—over $\phi \sim 75°-77°$ (Fig. 63a). The radius of the circle is 18°–19° latitude. The probability of appearance of auroras at local times along the entire circle is almost constant and at its maximum, equal to about 0.8 (slightly decreasing toward the day meridian [79]).

The area of latitudes lying within the circle of auroras is called the *polar cap*. The probability of appearance of auroras in the polar cap is not over 0.2. Usually, a weak diffuse glow or weak, short, and short-lived homogeneous arc which arises and develops separately from the glow of the polar oval may be seen. Figure 63b shows typical distribution of the form of auroras in the polar oval and the polar cap during a moderate substorm. During quiet times, the auroras do not disappear completely, but only one fine arc may remain on the night portion of the oval, with groups of separate rays on the day portion.

The altitude of the auroras changes along the oval: the most probable altitudes are 100 km, 125, and 150 km in the night, evening, and day portions respectively. No data are yet available concerning the altitudes in the morning sector; there is reason to assume that it is even lower than at night.

The spatial position of the polar oval is shown in Figure 63a, which is for the winter hemisphere, the geographic axis combined with the geomagnetic axis. The probability is about 0.8 of this glowing ring appearing. The brightness of the auroras in the day portion of the oval is always less, apparently a result of their greater altitude; the auroras here arise in the less dense layers of the atmosphere.

All that has been stated is true of electron auroras. Much less information is available about proton auroras. It can only be said that they are also located in an asymmetrical ring, but it is

somewhat displaced relative to the ring of the electron auroras; during the evening hours, proton auroras are found in lower latitudes, during the morning, in higher latitudes. Around midnight, these two rings cross.

The most active and brightest manifestations of the polar auroras arise in the midnight sector of the auroral belt [3]. This system of manifestations is subject to repeated large-scale expansions and contractions, which may go beyond the limits of the field of vision of an individual station. These large-scale auroral activities, which arise during development of a single phenomenon, have been called auroral substorms.

Auroral substorms are closely related to magnetic disturbances. Akasofu and Chapman [4] have shown that intensive auroral substorms frequently appear during the stage of development of the main phase of a storm, not during the quiet initial phase. Significant displacement of auroral arcs toward the Equator is observed during the large main phases of geomagnetic storms.

In addition to the ordinary polar auroras, two other types, which are not visible, have been discovered: subauroral red arcs, and a glow in the area of the polar caps. The stable red arcs (6300 Å), which cannot be seen by eye, appear in the zone of middle latitudes during geomagnetic storms. These arcs are located in the F area of the ionosphere, extend over about 500 km of latitude and form magnetic continuous bands, at least for the night half of the Earth. The intensity of the arcs increases with increasing geomagnetic activity.

Observations of emissions in the oxygen line at 6300 Å in the upper atmosphere of the Earth ($h > 200$ km) during geomagnetic disturbances have shown that emissions on the 6300 Å line are closely related to solar activity. In particular, a close relationship has been observed between the intensity of the 6300 Å line and the flux of solar radio radiation at $I_{10.7\text{-cm}}$ wavelength. For sufficiently large geomagnetic disturbances ($D_{st} > 100$ γ), the logarithm of intensity of the emission line is linearly related to the indices D_{st} and $I_{10.7\text{-cm}}$.

The glow in the area of the polar caps is observed in close connection with absorption in the polar caps (PCA). This form of polar aurora is usually an intense glow, covering the entire polar cap; the intensity of the glow changes according to changes in the flux of solar cosmic rays. The polar auroras of this type arise at altitudes of 60–100 km, and their spectrum characteristically shows radiation in the bands of molecular nitrogen, blending with weak hydrogen radiation with broad Doppler profile of the line. These peculiarities show that the glow in the area of the polar caps results primarily from the protons of solar cosmic rays with energies of 1–10 MeV.

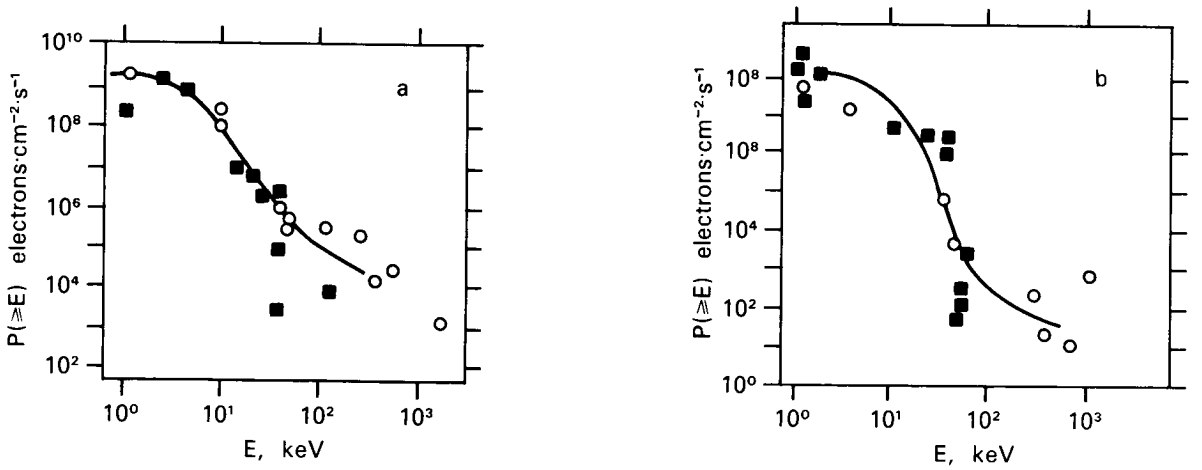

FIGURE 62.—Generalized spectrum of electron precipitation: (a) at latitudes of auroral zone; (b) at middle latitudes. Circles show satellite data; squares show rocket data.

Absorption in the Polar Caps

When the stream of high-energy particles enters the terrestrial atmosphere from solar flares, one of the first results is the absorption of cosmic radio noise in the polar caps (PCA) or, as it is sometimes called, polar cap blackout [49]. This absorption results from anomalously great ionization of the ionosphere in the area of the polar caps by the flux of high-energy particles with energies of 1–30 MeV. Absorption in the polar cap begins approximately 1 hour after a flare and may continue for several days. The main ionizing agent responsible for PCA during a grade 2B flare on May 13, 1967, was protons with energies of 10–20 MeV during the day and protons with energies of 5–10 MeV at night. The stream of protons had an energy spectrum $N(E) = k \cdot E^{-\gamma}$, $\gamma = 2.2$–3.5, $k = 2.7 \cdot 10^4$–$2 \cdot 10^6$, and reached a maximum value at the Earth at all energies 40 hours after the flare. In addition to absorption in the polar caps, auroral absorption (auroral blackout) is also observed, caused by auroral particles (particles poured into the auroral area during strong geomagnetic disturbances).

Distribution of the PCA is in the form of a circle with its center at the geomagnetic pole. Distribution of the auroral absorption differs slightly, depending on the specific conditions of geomagnetic activity. During a strong geomagnetic storm, distribution of anomalous ionization is in the form of a spiral, falling along the belt of polar auroras; the greatest intensity of ionization relates to the morning and midnight sectors. However, during the time of an isolated bay-shaped disturbance (polar substorm), the greatest increase in ionization relates to the midnight section of the polar auroral belt. The auroral blackouts, as a rule, are associated with visible manifestations of polar auroras and localized influx of electrons and protons with energies on the order of keV. An intensive sporadic *E* layer, known as the auroral *E* layer, frequently appears in the ionosphere along with the auroral blackouts. During the sudden onset of a storm, there is a brief, sudden increase in ionization resulting from the x-ray bremsstrahlung of the energetic electrons, which penetrate into the denser layers of the atmosphere along the polar auroral belts [24].

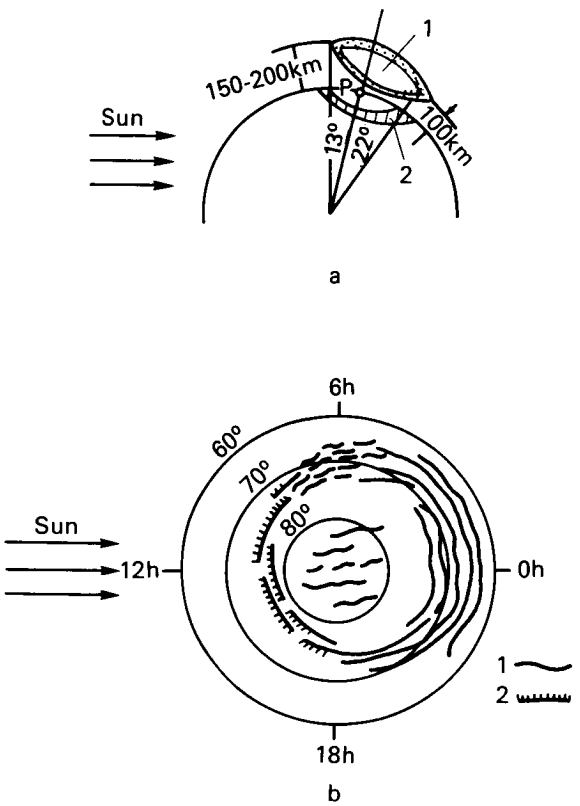

FIGURE 63.–Form on Earth from evening side. (a) 1–auroral ring; 2–projection of the ring on Earth's surface, and distribution of aurora forms along the instantaneous zone. (b) 1–homogeneous arcs; 2–rayed arcs.

Influx of Particles in the Upper Atmosphere

The main part of the auroral phenomena results from the influx of energetic particles, usually called auroral, i.e., responsible for the polar auroras and associated phenomena. Since the discovery of radiation belts, there have been extensive studies of the relationships between the auroral and captured energetic particles. In this respect, there is significant interest in the zone of pouring of particles.

In a review of satellite results relating to the pouring of particles [103], it was concluded that two pouring zones existed. Zone 1 occupies the area of geomagnetic latitudes between 60° and 70°. In this zone, electrons with energies primarily over 10 keV are poured out, with a broad maximum of pouring in the morning-noon sector. Zone

2, in the night sector, overlaps zone 1, but is displaced near noon to the latitude 75°–80°. Electrons entering this zone have lower energies than in zone 1.

The pouring of particles in zone 1 is diffuse and stable and encompasses a broad area; pouring in zone 2 is discrete and impulselike, usually localized in space, and subject to rapid, strong fluctuations. All this information, produced by direct measurement of particle fluxes and indirect methods (altitudes of development of various phenomena in the atmosphere), indicates that the phenomena in zone 1 result from streams of relatively hard electrons, in zone 2, from streams of soft electrons.

The line of intersection of the captured radiation belt outer boundary with the ionosphere roughly coincides with the oval of polar auroras and the division boundary between zones 1 and 2. Comparison of the position of the outer boundary of the radiation belt to the boundary according to the model of the geomagnetic field in the magnetosphere [145] shows that zone 2 corresponds to the entry of the lines of force or the set of closed and open lines of force directly related to the division boundary, or passes very close to it. In other words, this zone is directly related to the magnetically neutral layer in the geomagnetic tail of the Earth.

During geomagnetic storms, the position of the pouring zones generally shifts toward the Equator. Changes in zone 2 are particularly noticeable during auroral substorms accompanied by repeated expansion, with subsequent contraction, of the width of the belt.

Auroral particles, intensive bursts of streams of electrons with energies primarily less than 10 keV, are assumed to be responsible for the visible auroral substorms. These streams may correspond to the "islands" of electrons discovered in the geomagnetic tail.

High energy particles, 10–100 keV, are poured out in addition to low-energy auroral particles, energies less than 10 keV; this pouring is usually related to the active polar auroras along the 60°–70° latitude band. Some of these particles may be high-energy particles from the solar plasma, but most are a result of acceleration in the magnetosphere rather close to the Earth. The acceleration might possibly be due to fluctuating electrostatic fields along the lines of force of the geomagnetic field.

In smaller scales, the pouring of particles occurs (constantly and sporadically) in the moderate latitudes as well. Streams of electrons with energies of 1–10 keV at altitudes of 200–500 km in the daytime reach about 0.3 erg/cm²·s, a significant (up to 10%) share of the energy flux from shortwave solar radiation. At altitudes below 150–200 km, the flux of poured electrons begins to weaken. The full energy of the flux of electrons with $E \geq 1$–3 keV, measured during the Soviet "Sun-atmosphere" experiment of April 18–23, 1969, at altitudes of ≥ 125 km, varied from 0.07 to 0.01 erg/cm²·s·sr [78]. Many scientists consider these data elevated by 1 to 2 orders of magnitude. At altitudes of about 100 km, the recorded radiation flux was 3–4 times less than at ~125 km. The energy spectrum can be approximated by the exponent $N \approx \exp(-E/E_0)$, $E_0 =$ 10–12 keV. The flux of electrons with $E > 40$ keV in the area of altitudes around 85 km varied significantly, within limits of 1–1.5 orders of magnitude, as well as varying in the energy spectrum, particularly in the 40–60 keV energy range.

Fast reductions (less than 3 h) in the intensity of electrons and protons in the outer radiation belt also result from dumping of particles during magnetospheric substorms. The death of particles in this case occurs during magnetic disturbances type DP-1 in the area where the current responsible for the D_{st} variation is formed, during the beginning of formation of the current. This is indicated by one condition being necessary for rapid death of particles: good development of the evening ionospheric electrojet and a strong reduction in the field at low latitudes in the evening sector of the Earth (18:00–24:00 local time). During magnetic storms, when D_{st} variations are increased, the rapid reduction in intensity encompasses L envelopes closer to the Earth.

The polar magnetic and auroral substorms are related to sudden decreases in the field of the geomagnetic tail, according to observations. This led to hypothesizing that the auroral phenomena are caused by particles accelerated in the neutral layer of the geomagnetic tail. The decrease in the geomagnetic tail field can be represented as

attachment (contact) of the tail's lines of force through the neutral layer. The conversion of magnetic energy to kinetic energy which occurs in this case can cause heating of the particles to about 1 keV, and acceleration to about 1–10 keV.

There is still no quantitative theory of annihilation of the magnetic field of the tail applicable to details of the effects of auroral storms. The quietness of conditions during periods between successive phenomena apparently indicates that the process of annihilation of the field in the tail is relatively brief. This process may be caused by macroinstability developing in the plasma of the tail, with conversion defined by changes in the parameters of the solar wind. Another possibility might be realized with a change in direction of the outer magnetic field, leading to disruption of the equilibrium of the system [124]. Observations of the intensity of streams of low-energy electrons with $E_e \geq 100$ eV on the Luna–1, Luna–2 [65], Mars–1 [63] spacecraft and the Explorer 12 satellite at distances of over 8 R_0 show that the position of the streams of high-intensity electrons corresponds to the beginning of strong deformation of the field of the tail in the direction away from the Sun, measured by the IMP–1 and Explorer 14 satellites. The observed electron energy flux of some tens of erg/cm^2 · s (energy density on the order of 10^{-8} erg/cm^3, if E_e is on the order of several keV), is sufficient for maintenance of the neutral layer if the intensity of the field in neighboring areas is about 30 γ. The high intensities of streams of electrons of such energies might indicate that the area of the tail is, at least partially, a reservoir or area for acceleration of particles producing the polar auroras.

Sources and Transmission of Energy in the Magnetosphere

The flux of solar plasma is the primary source of energy responsible for large-scale disturbances in the magnetosphere. The effects of the flux of solar plasma on the magnetosphere can be represented by normal and transverse components. The normal components lead to general compression or a return to the initial state of the magnetospheric cavity in the stream of solar plasma and, consequently, is a field source [32]. The transverse components influence the general form of the magnetosphere, primarily by leading to formation of a tail.

Dissipative effects in the magnetopause lead to transverse stresses in the magnetosphere plasma, causing formation of a geomagnetic tail with a neutral layer and a plasma convection system in the magnetosphere [10]. The *DP* fields and related disturbances are believed to result primarily from processes in the geomagnetic tail. Theories explaining the field depression during the period of the main phase of storms (*DR* field) are still in question. Essentially, the mechanism for transmitting the energy of the solar plasma to circular current located deep within the magnetosphere remains unknown.

The total energy of an average geomagnetic storm has been estimated as 10^{22}–10^{23} erg [51]. Dissipation of energy occurs in three forms: (a) formation of polar auroras about 10^{18} erg/s; (b) heating of the ionosphere about 10^{18} erg/s; and (c) swelling of the magnetosphere (circular currents) about 10^{18}–10^{19} erg/s.

The energy of circular currents in the final analysis is dissipated during the phase of restoration, which may last several days, but the energy must be injected in a few hours. Thus, any theory of magnetic storms and polar auroras must be capable of explaining a transfer through the magnetopause of at least 10^{18}–10^{19} erg/s. On the other hand, since the solar plasma energy flux is assumed to be 1–10 erg · cm^2 · s, the total influx of energy throughout the surface of magnetosphere ($R \approx 20\ R_0$) is estimated as 10^{22} erg/s. Therefore, approximately 10^{-3}–10^{-4} of the entire influx of energy must be transmitted from the solar plasma to the magnetospheric plasma.

The inward transmission of energy to the magnetosphere can be achieved by:

(1) deformation of the magnetosphere, a result of the pressure of the medium (causing generation of magnetohydrodynamic waves and heating of the thermal magnetic plasma);
(2) direct injection of energy;
(3) a mechanism of reconnecting magnetic force lines of the interplanetary and geomagnetic fields with subsequent

formation of the magnetic tail of the Earth, believed responsible for many magnetic disturbances;

(4) the mechanism of viscous interaction of the solar wind with the magnetosphere.

A great contribution to geomagnetic activity may be made by fluctuations in the magnetospheric circular current and currents of the ionosphere as well as by the instability of the magnetopause and instability and accelerating processes within the magnetosphere itself [10, 14, 123]. It must be noted that present experimental data and theoretical analysis do not yet warrant giving definite preference to any given theory or mechanism of transmission of energy of the interplanetary medium into the magnetosphere.

RADIATION CONDITIONS NEAR OTHER PLANETS OF THE SOLAR SYSTEM

Radiation conditions near the planets of the solar system are determined, to a significant extent, by the presence or absence of an internal magnetic field of the planet. This field, if it exists, determines the nature of interaction of the solar wind with the planet.

The characteristics of the planets of the solar system and the Moon, along with certain characteristics of the solar wind near these planets, are listed in Table 9. In this table, the radius of the heliosphere is assumed to be about 40 AU, the convective velocity of the solar wind about 400 $km \cdot s^{-1}$.

When the magnetic field or properties of the ionosphere of the planet were unknown, the dimensions of the magnetopause were taken to be equal to the diameter of the planet. For Venus and Mars, the effective diameter of the magnetopause was determined by measurements of the shock wave and is the upper limit of the measured quantity. For Jupiter, this quantity was based on radio astronomy observations.

Moon. There are no radiation belts near the Moon, according to observations. Attempts to measure the constant magnetic field have indicated that the magnetic moment of the Moon is 10^{-6} of the magnetic moment of the Earth. This means that radiation conditions of the Moon's surface are completely determined by the radiation in interplanetary space considering the geometric shielding provided by the body of the Moon. There is no shock wave near the Moon, and the flow of the solar wind around it is well-described by hydrodynamic equations. The Moon has no significant influence on the characteristics of the solar wind [142]. Similar interactions might be expected between solar wind and the planets Uranus, Pluto, and Neptune.

Venus. There is also no radiation field around Venus, indicating a weak internal magnetic

TABLE 9.—*Characteristics of Planets of the Solar System, Moon, and Solar Wind*

Physical properties	Celestial body									
	Mercury	Venus	Earth	Moon	Mars	Jupiter	Saturn	Uranus	Neptune	Pluto
Radius in km[3]	2.42	6.08	6.38	1.74	3.38	71.35	60.40	23.80	22.20	3.00
Distance from Sun, AU	0.39	0.72	1.0	1.0	1.52	5.2	9.5	19.2	30.0	39.4
Dipole moment, M_{planet}/M_z	?	$2 \cdot 10^{-3}$	1	$1 \cdot 10^{-6}$	$2 \cdot 10^{-4}$	$4 \cdot 10^{5}$	—	?	?	?
Solar wind velocity, km/s	300	350	400	400	400	400	400	400	400	400
Density of protons, m^{-3}	34.0	9.5	5.0	5.0	2.1	0.19	0.055	0.018	0.006	0.003
Mean temperature of protons, T, $10^4 \cdot K°$	6.9	4.7	4.0	4.0	3.2	1.8	1.3	0.92	0.73	0.64
Magnetic field, gammas	24.7	8.26	5.0	5.0	3.12	1.72	0.39	0.19	0.12	0.09
Angle of Archimedes spiral, deg.	30°	42°	47°	47°	59°	80°	84°	87°	88°	89°
Magnetopause diameter, km[3]	4.84	30.4	268.0	1.74	18.0	34 000	120.8	47.6	44.4	6.00

field [62, 135]. Detailed study of data about the magnetic field shows that the field, down to an altitude of about 200 km over the surface of the planet, is the interplanetary magnetic field; that the magnetic moment of Venus is $\bar{M}_v \lesssim 10^{-4}$ of the magnetic moment of the Earth. However, a shock wave is observed near Venus which apparently is related to a dense ionosphere around this planet. The high conductivity of the ionospheric plasma does not allow the interplanetary magnetic field to penetrate to the surface of the planet. Therefore, an obstacle is produced, causing a shock wave in the stream of the solar wind.

Mars. Radiation belts are not around this planet. An estimate of the magnetic moment of Mars indicates a value of $2 \cdot 10^{-4}$ of the moment of the Earth. A shock wave is observed near the planet in the solar wind, apparently, as is true for Venus, a result of a small ionosphere [132].

Jupiter. Strong sources of decimeter and decameter radio radiation have been detected near this planet. Analysis has shown that the decimeter radiation is polarized and reminiscent of synchrotron radiation from relativistic electrons. Numerical estimates have led to these values: if the magnetic field has a value of about 1 gauss, and the energies of electrons of 2.5–25 MeV the flux should be about $5 \cdot 10^7$ electrons $\cdot$ cm$^2 \cdot$ s; with a field of 0.1 G and energies of 10–100 MeV, the flux of electrons should be about $5 \cdot 10^8$ electrons $\cdot$ cm$^2 \cdot$ s [95]. Analysis of the decameter radiation has led to an estimate of the magnetic moment of Jupiter as 10^4 times the magnetic moment of Earth. Thus, the radiation belts and magnetosphere around this planet should be the strongest in the solar system. The dynamics of the radiation belts apparently are the same as around the Earth, although they may be complicated by interaction of the planets with its satellites. The magnetosphere of Jupiter is apparently reminiscent of that of the Earth with a distance to the magnetopause of about $4 \cdot 10^6$ km [114].

The space probe Pioneer 10 approached the planet in December 1973 and found a magnetosphere which extends to distances of $96R_s$ (the angle of approach to the planet was formed along the Jupiter-Sun line at about 35°) [36]. A standing shock wave and the transition field were observed from distances of $109R_s$. Within the magnetosphere a disklike distribution of charged particles was observed in a magnetic field resembling the field in the tail end of the Earth magnetosphere. At distances from 96–$25R_s$, the field has the value of $\sim 5\ \gamma$ and does not change significantly. It increases in the part from 50 to $25R_s$, where its intensity reaches values of about 20 γ. In this case, electron fluxes with an energy of 0.4–1.0 MeV reach values from 10^3 to 10^5 $v \cdot$ cm$^2 \cdot$ s. Proton fluxes with E from 5.6 to 21 MeV amount to a value of 1–10^2 $v \cdot$ cm$^2 \cdot$ s. Particles are within a thin layer close to the equator.

Beginning with distances R about $20R_s$, the magnetic field starts to increase essentially as it approaches the planet and has a bipolar character. Its intensity increases up to values of about 0.2 gauss for R at $2.8R_s$. Within this field, which essentially represents the radiation belts of Jupiter, the intensity of the particle fluxes increases rapidly: at distances of about $5R_s$ the intensity of electron fluxes with $E > 3$ MeV reaches $5 \cdot 10^8$ cm$^2 \cdot$ s^{-1}, and with an energy $E > 50$ MeV $= 10^7 \cdot$ cm$^2 \cdot$ s^{-1}, proton fluxes $E > 50$ MeV at these distances amount to $4 \cdot 10^6 \cdot$ cm$^2 \cdot$ s^{-1}. The distribution in space of various spectral components of particles is fairly complicated and seems to be connected with the interaction of these particles with the satellites of Jupiter, Io, Europa, and Ganymede.

REFERENCES

1. Anon. Surprises for Pioneer 10 in the asteroid belt. *Aerosp. Dly* 58(8):62, 1972.
2. AKASOFU, S. I. *Polar and Magnetospheric Substorms.* Dordrecht, Holl., D. Reidel; New York, Springer, 1968.
3. AKASOFU, S. I. The development of the auroral substorm. *Planet. Space Sci.* 12:273–282, 1964.
4. AKASOFU, S. I., and S. CHAPMAN. Magnetic storms: the simultaneous development of the main phase (DR) and of polar magnetic substorms (DP). *J. Geophys. Res.* 68(10):3155–3158, 1963.
5. ALFVÉN, H., and G. G. FÄLTHAMMAR. *Cosmical Electrodynamics,* 2nd ed. Oxford, Clarendon, 1963.
6. ANDERSON, K. A. Electrons and protons in long-lived

streams of energetic solar particles. *Solar Phys.* 6:111–132, 1969.

7. ANTONOVA, A. E., and V. P. SHABANSKIY. The structure of the geomagnetic field at great distances from the Earth. *Geomagn. Aeron.* 8:801–811, 1968.
8. ARNOLDY, R. L., S. R. KANE, and J. R. WINCKLER. Energetic solar flare x-rays observed by satellite and their correlation with solar radio and energetic particle emission. *Astrophys. J.* 151(2, Pt. 1):711–736, 1968.
9. ATHAY, R. G. Sources of solar ultraviolet radiation. *J. Geophys. Res.* 66(2):385–390, 1961.
10. AXFORD, W. I. Viscous interaction between the solar wind and the Earth's magnetosphere. *Planet. Space Sci.* 12:45–53, 1964.
11. BAME, S. J., A. I. HUNDHAUSEN, J. K. ASBRIDGE, and I. B. STRONG. Solar wind ion composition. *Phys. Rev. Lett.* 20:393–395, 1968.
12. BARBIER. D. Introduction to the study of the aurora and airglow. *In,* DeWitt, C., J. Hieblot, and A. Lebeau, Eds. *Geophysics, The Earth's Environment,* pp. 301–368. New York, Gordon & Breach, 1963.
13. BAROUCH, E., J. ENGELMANN, M. GROS, L. KOCH, and P. MASSE. Observations of the spectra and time history of protons in interplanetary space, February 25–28, 1969. *In,* Manno, V., and D. E. Page, Eds. *Intercorrelated Satellite Observations Related to Solar Events;* Proc., 3rd ESLAB/ESSRIN Symp., Noordwijk, Neth., Sept., 1969 (Astrophysics and Space Science Library), Vol. 19, pp. 448–459. Dordrecht, Holl., Reidel, 1970.
14. BEARD, D. B. The interaction of the terrestrial magnetic field with the solar corpuscular radiation. *J. Geophys. Res.* 65:3559–3568, 1960.
15. BEHANNON, K. W. Mapping of the Earth's bow shock and magnetic tail by Explorer 33. *J. Geophys. Res.* 73:907–930, 1968.
16. BERNSTEIN, W., R. W. FREDERICKS, and F. L. SCARF. A model for a broad disordered transition between the solar wind and the magnetosphere. *J. Geophys. Res.* 69(7):1201–1210, 1964.
17. BIERMANN, L. Kometenschweife und Solare Korpuskularstrahlung. (Transl: Comets' tails and solar corpuscular radiation). *Zs. Astrophys.* 29:274–286, 1951.
18. BIERMANN, L. Über den Schweifes Kometen Halley in Jahre, 1910. (Transl: The tail of Halley's Comet in 1910). *Zs. Naturforsch.* 7(Pt. A):127–136, 1952.
19. BISWAS, S., C. E. FICHTEL, and D. E. GUSS. Study of the hydrogen helium and heavy nuclei in the Nov. 12, 1960 solar cosmic event. *Phys. Rev.* 128:2756–2771, 1962.
20. BISWAS, S., C. E. FICHTEL, D. E. GUSS, and C. J. WADDINGTON. Hydrogen, helium and heavy nuclei from the solar event in Nov. 15, 1960. *J. Geophys. Res.* 68:3109–3122, 1963.
21. BONETTI, A., H. S. BRIDGE, A. S. LAZARUS, B. ROSSI, and F. SCHERB. Explorer 10 plasma measurements. *J. Geophys. Res.* 68(13):4017–4063, 1963.
22. BONNET, R. M. Stigmatic spectra of the Sun between 1800 Å and 2800 Å. *In,* Mitra, A. P., L. G. Jacchia, and W. S. Newman, Eds. *Life Sciences and Space Research* (Proc. 10th Plenary COSPAR Meet., London, July 1967), Vol. 8, pp. 458–472. Amsterdam, North-Holland, 1968.
23. BRANDT, J. C., and P. W. HODGE. *Solar System Astrophysics.* New York, McGraw-Hill, 1964.
24. BROWN, R. R. Electron precipitation in the auroral zone. *Space Sci. Rev.* 5:311–387, 1966.
25. BRYANT, D. A., T. L. CLINE, U. D. DESAIR, and F. B. MCDONALD. Studies of solar protons with Explorers XII and XIV. *Astrophys. J.* 141:478–499, 1965.
26. BRYUNELLI, B. Ye. Processes in near-Earth space and geomagnetic disturbances. *In, Trudy 5-y Vsesoyuznoy Yezhegodnoy Zimney Shkoly po Kosmofizike* (Transl: *Works of Fifth All-Union Annual Winter School on Astrophysics*), p. 212. Apatity, 1968.
27. BURLAGA, L. F. Anisotropic diffusion of solar cosmic rays. *J. Geophys. Res.* 72(17):4449–4466, 1967.
28. BURLAGA, L. F. Nature and origin of directional discontinuities in the solar wind. *J. Geophys. Res.* 76:4360–4365, 1971.
29. BURLAGA, L. F., and N. F. NESS. Macro and micro structure of the interplanetary magnetic fields. *Can. J. Phys.* 46:S962–S965, 1971.
30. CAHILL, L. F., and P. G. AMAZEEN. The boundary of the geomagnetic field. *J. Geophys. Res.* 68(7):1835–1843, 1963.
31. CHAMBERLAIN, J. W. *Physics of the Aurora and Airglow.* New York, Academic, 1961.
32. CHAPMAN, S. Solar plasma, geomagnetism and aurora. *In,* DeWitt, C., J. Hieblot, and A. Lebeau, Eds. *Geophysics, The Earth's Environment,* pp. 371–502. New York, Gordon & Breach, 1963.
33. CHAPMAN, S., and V. C. A. FERRARO. A new theory of magnetic storm. *Terr. Magn. Atmos. Electr.* 36:77–97, June 1931.
34. CHARAKHCH'YAN, A. N., V. F. TULINOV, and T. N. CHARAKHCH'YAN. The energy spectrum and time dependence of the intensity of solar cosmic ray protons. *Zh. Eksp. Teor. Fiz.* 41(3):735–746, 1961. (Transl: *Sov. Phys. JETP*) 14:530–537, 1962.
35. CLINE, T. L., and F. B. MCDONALD. *Relativistic Electrons from Solar Flares.* Greenbelt, Md., Goddard Space Flight Cent., 1968. (NASA TM–X–63210)
36. [Collected reports on Pioneer 10 mission to Jupiter.] *Science* 183(4122, Jan. 25):301–324, 1974.
37. COLOMBO, G., D. A. LAUTMAN, and I. I. SHAPIRO. The Earth's dust belt: fact or fiction? 2. Gravitational focusing and Jacobi capture. *J. Geophys. Res.* 71:5705–5717, 1966.
38. COLOMBO, G., I. I. SHAPIRO, and D. A. LAUTMAN. The Earth's dust belt: fact or fiction? 3. Lunar ejecta. *J. Geophys. Res.* 71:5719–5731, 1966.
39. COON, J. H. Vela satellite measurements of particles in the solar wind and the distant geomagnetosphere. *In,* McCormac, B. M., Ed. *Radiation Trapped in the Earth's Magnetic Field,* pp. 231–255. Presented

at Adv. Stud. Inst., Bergen, 1965. Dordrecht, Holl., D. Reidel, 1966.

40. DAVIS, L., Jr., and D. B. CHANG. On the effect of geomagnetic fluctuations on trapped particles. *J. Geophys. Res.* 67:2169–2179, 1962.
41. DE JAGER, C. Structure and dynamics of the solar atmosphere. *In*, Flügge, S., Ed. *Handbuch der Physik, (Astrophysik III: Das Sonnensystem)*, Vol. 52, pp. 80–362. Berlin, Springer, 1959.
42. DOHNAHYI, J. S. On the origin and distribution of meteoroids. *J. Geophys. Res.* 75:3468–3493, 1970.
43. DOLGINOV, Sh. Sh., Ye. G. YEROSHENKO, L. N. ZHUZGOV, and N. V. PUSHKOV. Measurements of the magnetic field in the area of the Moon by the Luna 10 satellite. *Dokl. Akad. Nauk SSSR* 170(3):574–577, 1966.
44. DOLGINOV, Sh. Sh., Ye. G. YEROSHENKO, L. N. ZHUZGOV, and I. A. ZHULIN. Possible interpretation of results of measurements performed by the lunar satellite Luna 10. *Geomagn. Aeron.* 7(3):436–441, 1967. (Transl: *Geomagn. Aeron.*) 7(3):352–356, 1967.
45. DORMAN, L. I. *Variatsii Kosmicheskikh Luchey i Isslednovaniye Kosmosa* (Transl: *Variations in Cosmic Rays and Space Studies*). Moscow, Akad. Nauk SSSR, 1963.
46. ELLISON, M. A. *The Sun and Its Influence*. London, Routledge, 1955.
47. ERICKSON, J. E. Mass influx and penetration rate of meteor streams. *J. Geophys. Res.* 74:576–585, 1969.
48. FAIRFIELD, D. H. Average magnetic field configuration of the outer magnetosphere. *J. Geophys. Res.* 73:7329–7338, 1968.
49. FISK, L. A. and W. I. AXFORD. Anisotropies of solar cosmic rays. *Solar Phys.* 7:486–498, 1969.
50. FRANK, L. A. Inward radial diffusion of electrons of greater than 1.6 million electron volts in the outer radiation zone. *J. Geophys. Res.* 70:3533–3540, 1965.
51. FRANK, L. A. On the extraterrestrial ring current during geomagnetic storms. *J. Geophys. Res.* 72:3753–3767, 1967.
52. FREEMAN, J. W., J. A. VAN ALLEN, and L. J. CAHILL. Explorer 12 observations of the magnetospheric boundary and the associated solar plasma on September 13, 1961. *J. Geophys. Res.* 68(8):2121–2130, 1963.
53. FRITZ, T. A., and D. J. WILLIAMS. *Initial Observations of Geomagnetically Trapped Alpha Particles at the Equator*. Boulder, Colo., Nat. Oceanic Atmos. Adm., Space Environ. Lab., 1972. (NOAA-TM-ERL-SEL-20)
54. FROMAN, M. A. The equilibrium anisotropy in the flux of 10 MeV solar flare particles and their convection in the solar wind. *J. Geophys. Res.* 75(16):3147–3153, 1970.
55. GINZBURG, V. L., and S. I. SYROVATSKIY. *Proishkhozhdeniye Kosmicheskikh Luchey* (Transl: *The Origin of Cosmic Rays*). Moscow, Akad. Nauk SSSR, 1963.
56. GLEESON, L. J., and W. I. AXFORD. The Compton-getting effect. *Astrophys. Space Sci.* 2(4):431–437, 1968.
57. GNEVYSHEV, M. N. On the 11-year cycle of solar activity. *Solar Phys.* 1(1):107–120, 1967.
58. GNEVYSHEV, M. N. The 11-year cycle of solar activity. *Usp. Fiz. Nauk* (Transl: *Successes Phys. Sci.* 90(2):291–301, 1966.
59. GOLD, T. Plasma and magnetic fields in the solar system. *J. Geophys. Res.* 64:1665–1674, 1959.
60. GRINGAUZ, K. I. Some results of experiments in interplanetary space by means of charged particle traps on Soviet space probes. *In*, Van de Hulst, H. C., C. de Jager, and A. F. Moore, Eds. *Life Sciences and Space Research* (Proc., 2nd COSPAR Int. Space Sci. Symp., Florence, 1961), Vol. 2, pp. 539–553. Amsterdam, North-Holland; New York, Interscience, 1961.
61. GRINGAUZ, K. I., V. V. BEZRUKIKH, M. Z. KHOKHLOV, L. S. MUSATOV, and A. P. REMIZOV. Indications of intersection of the Earth's magnetospheric tail by the Moon according to charged particle traps on the first artificial satellite of the Moon. *Dokl. Akad. Nauk SSSR* 170(3):570–573, 1966.
62. GRINGAUZ, K. I., V. V. BEZRUKIKH, L. S. MUSATOV, and T. K. BREUS. Plasma measurements performed near Venus by Venera 4. *Kosm. Issled.* 6:411–419, 1968.
63. GRINGAUZ, K. I., V. V. BEZRUKIKH, J. S. MUSATOV, R. Ye. RYBCHINSKY, and S. M. SHERONOVA. Measurements made in the Earth's magnetosphere by means of charged particle traps aboard the Mars 1 probe. *In*, Muller, P., Ed. *Life Sciences and Space Research* (Proc., 4th COSPAR Int. Space Sci. Symp., Warsaw, June 1963), Vol. 4, pp. 621–626. Amsterdam, North-Holland; New York, Wiley, 1964.
64. GRINGAUZ, K. I., V. V. BEZRUKIKH, V. D. OZEROV, and R. Ye. RYBCHINSKIY. Study of interplanetary ionized gas, energetic elements and corpuscular radiation of the Sun using three electrode charge particle traps on the second Soviet space rocket. *Dokl. Akad. Nauk SSSR* 131(6):1301–1304, 1960.
65. GRINGAUZ, K. I., V. G. KURT, V. I. MOROZ, and I. S. SHKLOVSKIY. Results of observations performed with charge particle traps on Soviet space rockets up to about 100 000 km. *Astron. Zh.* 37:716–735, 1960. Transl. in *Sov. Astron. AJ* 4:680–695, Jan./Feb. 1961.
66. GRINGAUZ, K. I., V. A. TROITSKAYA, E. K. SOLOMATINA, and R. V. SHCHEPETNOV. Variations of the solar wind flux observed with Venera 2, 4, 5, and 6, and pulsations of the geomagnetic field connected with them. Presented at Int. Symp. on Solar Terrestrial Physics, Leningrad, May 1970. Also, Variations of solar wind flux observed by several spacecraft and related pulsations of the Earth's electromagnetic field. *J. Geophys. Res.* 76:Feb. 1, 1065–1069, 1971.
67. HAFFNER, H. W. *Radiation and Shielding in Space*. New York Academic, 1967.
68. HESS, W. N. *Radiation Belt and Magnetosphere*. Waltham, Mass., Bleisdell, 1968.
69. HINTEREGGER, H. E., and L. A. HALL. Solar extreme ultraviolet emission in the range 260–1300 Å observed

from OSO–111. *Solar Phys.* 6(12):175–182, 1969.

70. HIRSHBERG, J., A. ALKSNE, D. S. COLBURN, S. J. BAME, and A. J. HUNDHAUSEN. Observations of a solar flare, induced interplanetary shock and helium-enriched driver gas. *J. Geophys. Res.* 75:1–15, 1970.
71. HUNDHAUSEN, A. J. Composition and dynamics of the solar wind plasma. *Rev. Geophys. Space Phys.* 8:729–811, 1970.
72. International Astronomical Union. *Quarterly Bulletin on Solar Activity.* Zurich, Eidgenossische Sternwarte, 1932–
73. International Astronomical Union. *Report.* Zurich, Eidgenossische Sternwarte, Aug. 1966.
74. ISAYEV, S. I. *Morfologiya Polyarnykh Siyanyy* (Transl: *The Morphology of Polar Auroras*). Leningrad, Nauka, 1968.
75. IVANOV-KHOLODNIY, G. S., Ed. *Fizika Verkhney Atmosfery* (Transl: *Upper Atmosphere Physics*). Leningrad, Gidrometizdat, 1971.
76. IVANOV-KHOLODNIY, G. S., T. V. KAZACHEVSKAYA, G. A. KOKIN, and V. V. MIKHNEVICH. *In*, Mikhnevich, V. V., and A. D. Danilov, Eds. *Issledovaniya Atmosfery i Ionosfery v Period Povyshennoy Solnechnoy Aktivnosti* (Transl: *Studies of the Atmosphere and Ionosphere During a Period of Increased Solar Activity*), pp. 143–153. Leningrad, Gidrometeo, 1970.
77. IVANOV-KHOLODNIY, G. S., and G. M. NIKOL'SKIY. *Solntse i Ionosfera* (Transl: *The Sun and the Ionosphere*). Moscow, Nauka, 1969.
78. JOKIPII, J. R., and E. N. PARKER. Stochastic aspects of magnetic lines of force with application to cosmic-ray propagation. *Astrophys. J.* 155:777–798, 1969.
79. KHOROSHEVA, O. V. Space-time distribution of polar auroras. *In, Mezhduvedomstvennyi Komitet po Provedeniyu Mezhdunarodnogo Geofizicheskogo Goda.* IV. *Razdel Programmy MGG: Polyarnyye Siyaniya.* Moscow, Nauka, 1967.
80. KRASOVSKIY, V. I. *Shtili i Shtormy v Verkhney Atmosfere* (Transl: *Calms and Storms in the Upper Atmosphere*). Moscow, Nauka, 1971.
81. KUZNETSOV, S. N., and B. A. TVERSKOY. Monotonic decrease of the intensity of electrons in the radiation belts of the Earth. *Geomagn. Aeron.* 11(1):3–10, 1971. (Transl: *Geomagn. Aeron.*) 11(1):1–6, 1974.
82. LAUTMAN, D. A., I. I. SHAPIRO, and G. COLOMBO. The Earth's dust belt: fact or fiction? 4. Sunlight-pressure air-drag capture. *J. Geophys. Res.* 71:5733–5741, 1966.
83. LIN, R. P. The emission and propagation of ~40 keV solar flare electrons. I. The relationship of ~40 keV electron to energetic proton and relativistic electron emission by the Sun. *Solar Phys.* 12:266–303, 1970.
84. LIN, R. P., S. W. KAHLER, and E. C. ROELOF. Solar flare injection and propagation of low energy protons and electrons in the event of July 7–9, 1966. *Solar Phys.* 4(3):338–360, 1968.
85. MALITSON, H. H. The solar energy spectrum, *Sky Telesc.* 29(3):162–165, 1965.
86. MAZETS, E. P. Cosmic dust and meteor showers. *In*, Kondratyev, K. Ya., M. J. Rycroft, and C. Sagan, Eds. *Life Sciences and Space Reasearch* (Proc., 13th COSPAR Plenary Meet., Leningrad, May 1970), Vol. 11, pp. 363–369. Berlin, Ger. (E.), Akademie, 1971.
87. MCCRACKEN, K. G., and N. F. NESS. The collimation of cosmic rays by the interplanetary magnetic field. *J. Geophys. Res.* 71:3315–3318, 1966.
88. MCCRACKEN, K. G., R. A. R. PALMEIRA, R. P. BUKATA, U. R. RAO, F. R. ALLUM, and E. P. KEATH. A co-rotating solar cosmic ray enhancement observed by Pioneer 8 and Explorer 34 on July 13, 1968. Presented at 11th Int. Conf. on Cosmic Rays, Budapest, 1969.
89. MCCRACKEN, K. G., U. R. RAO, and R. P. BUKATA. Cosmic ray propagation processes. I. A study of the cosmic-ray flare effect. *J. Geophys. Res.* 72:4293–4324, 1967.
90. MCCRACKEN, K. G., U. R. RAO, R. P. BUKATA, and E. P. KEATH. The decay phase of solar flare events. *Solar Phys.* 18:100–132, 1971.
91. MCILWAIN, C. E. Coordinates for mapping the distribution of magnetically trapped particles. *J. Geophys. Res.* 66:3681–3691, 1961.
92. MCKINNON, J. A. *August 1972 Solar Activity and Related Geophysical Effects.* Boulder, Colo., Nat. Oceanic Atmos. Adm., Space Environ. Lab., 1972. (NOAA–TM–ERL–SEL–22)
93. MENZEL, D. H. *Our Sun.* Cambridge, Mass., Harvard Univ. Press, 1959.
94. MEYER, P. Cosmic rays in galaxy. *In*, Goldberg, L., Ed. *Annual Review of Astronomy and Astrophysics*, pp. 1–38. Palo Alto, Calif., Annual Reviews, 1969.
95. MICHAUX, C. M. *Handbook of the Physical Properties of the Planet Jupiter.* Washington, NASA, 1967. (NASA SP–3031)
96. MITRA, S. K. *The Upper Atmosphere*, 2nd ed. Calcutta, Asiatic Soc., 1952.
97. NESS, N. F. Measurements of the magnetic fields in interplanetary space and the magnetosphere. *In, Proceedings, 9th International Conference on Cosmic Rays*, London, Sept. 1965, Vol. 1, pp. 14–25. London, Inst. Phys. Phys. Soc., 1966.
98. NESS, N. F. Observations of the interaction of the solar wind with the geomagnetic field during quiet conditions. *In*, King, J. W., and W. S. Newman, Eds. *Solar Terrestrial Physics*, pp. 57–89. (Presented at Inter-Union Symp. on Solar-Terrestrial Physics, Belgrade, Aug. 1966.) London, Academic, 1967.
99. NESS, N. F. Simultaneous measurements of the interplanetary magnetic field. *J. Geophys. Res.* 71(13):3319–3324, 1966.
100. NESS, N. F., K. W. BEHANNON, S. C. CANTARANO, and C. S. SCEARCE. Observations of the Earth's magnetic tail and neutral sheet at 510 000 kilometers by Explorer 33. *J. Geophys. Res.* 72(3):927–933, 1967.
101. NESS, N. F., and J. M. WILCOX. Extension of the photospheric magnetic field into interplanetary space. *Astrophys. J.* 143:23–31, 1966.
102. OBAYASHI, T. The interaction between solar wind and geomagnetic field during active periods. *In*, King,

J. W., and W. S. Newman, Eds. *Solar Terrestrial Physics*, pp. 107–167. (Presented at Inter-Union Symp. on Solar-Terrestrial Physics, Belgrade, Aug. 1966.) London, Academic, 1967.

103. O'BRIEN, B. J. Rocket and satellite observations of energetic particles during P. C. A. events. *In*, Smith-Rose, R. L., Ed. *Life Sciences and Space Research* (Proc., 7th COSPAR Int. Space Sci. Symp., Vienna, May 1966), Vol. 7, Pt. 2, pp. 806–818. Amsterdam, North-Holland, 1967.
104. PALMEIRA, R. A. R., F. R. ALLUM, K. G. MCCRACKEN, and U. R. RAO. Low energy solar proton and electron propagation in interplanetary space. *In, Trudy Mezhdunarodnogo Seminara po Probleme Generatsiya Kosmicheskikh Luchey na Solntse* (Transl: *Proceedings, International Seminar on Solar Cosmic Ray Generation*), pp. 75–151. Moscow, 1971.
105. PARKER, E. N. Dynamics of the interplanetary and magnetic fields. *Astrophys. J.* 128:664–676, 1958.
106. PARKER, E. N. Geomagnetic fluctuations and the form of the outer zone of the Van Allen radiation belt. *J. Geophys. Res.* 65:3117–3130, 1960.
107. PARKER, E. N. *Interplanetary Dynamic Processes*. New York, Interscience, 1963.
108. PARKER, E. N. Solar wind interaction with the geomagnetic field. *Rev. Geophys.* 7(7):3–10, 1969.
109. POUNDS, K. A. Recent solar x-ray studies in the United Kingdom. *Ann. Astrophys.* (Paris) 28(1):132–145, 1965.
110. *Radioizlucheniye Solntsa* (Transl: *Radio Radiation of the Sun*), Collect. No. 1. Leningrad, Leningrad State Univ., 1969.
111. RATCLIFFE, J. A., Ed. *Physics of the Upper Atmosphere*. New York, Academic, 1960; Moscow, Fizmatizdat, 1963.
112. ROEDERER, J. G. *Dynamics of Geomagnetically Trapped Radiation (Physics and Chemistry in Space)*, Vol. 2. Berlin, New York, Springer, 1970.
113. ROEDERER, J. G. Quantitative models of the magnetosphere. *Rev. Geophys.* 7:77–96, 1969.
114. SCARF, F. L. Characteristics of the solar wind near the orbit of Jupiter. *Planet. Space Sci.* 17:595–608, 1969.
115. SCHATTEN, K. H., J. M. WILCOX, and N. F. NESS. A model of interplanetary and coronal magnetic fields. *Solar Phys.* 6:442–455, 1969.
116. SHAPIRO, I. I., D. A. LAUTMAN, and G. COLOMBO. The Earth's dust belt: fact or fiction? 1. Forces perturbing dust particle motion. *J. Geophys. Res.* 71:5695–5704, 1966.
117. SHAPIRO, M. M., and R. SILBERBERG. Heavy cosmic ray nuclei. *In*, Segre, E., Ed. *Annual Review of Nuclear Science*, Vol. 20, pp. 323–392. Palo Alto, Calif., Annual Reviews, 1970.
118. SIMPSON, J. A. Galactic sources and the propagation of cosmic rays. *In, Invited and Rapporteur Papers, 12th International Conference on Cosmic Rays*, Hobart, Aust., Aug. 1971, pp. 324–355. Hobart, Univ. Tasmania, 1972.
119. SLYSH, V. I. Observations of radio radiation of the Sun at long wave lengths by the Luna 11 and Luna 12 artificial lunar orbiters. *Kosm. Issled.* 5(6):897–910, 1967.
120. SMITH, F. G. *Radio Astronomy*. London, Penguin, 1960.
121. SMITH, H. J., and E. VAN P. SMITH. *Solar Flares*. New York, Macmillan, 1963.
122. *Solnechnyye Dannye* (Transl: *Solar Data*). Leningrad, Nauka, 1954– (Monthly)
123. SONETT, C. P., P. J. COLEMAN, Jr., and J. M. WILCOX, Eds. *Solar Wind*. Washington, D.C., NASA, 1972. (NASA SP–308)
124. SONNERUP, B. U. Ö. On the stability of the closed magnetosphere. *J. Geophys. Res.* 70(5):1051–1060, 1965.
125. SPEISER, T. W., and N. F. NESS. The neutral sheet in geomagnetic tail; its motion, equivalent currents and field line connection through it. *J. Geophys. Res.* 72:121–141, 1967.
126. SVESTKA, Z. PCA events and forbush effects. Presented at Inter-Union Symp. on Solar-Terrestrial Physics, Belgrade, Aug. 1966.
127. SYROVATSKIY, S. I. The development of current layers in the plasma with frozen magnetic lines of force. *Zh. Eksp. Teor. Fiz.* 60:1727–1741, 1971. (Transl: *Sov. Phys.-JETP*) 33:933–940, 1971.
128. SYROVATSKIY, S. I. The formation of polar and equatorial condensations of plasma in the proximity of a changing magnetic dipole. *Astrophys. Space Sci.* 4:240–251, 1969.
129. TOUSEY, R. Ultraviolet spectroscopy of the Sun. *In*, Liller, W., Ed. *Space Astrophysics*, pp. 1–16. New York, McGraw-Hill, 1961.
130. TVERSKOY, B. A. *Dinamika Radiatsionnykh Poyasov Zemli* (Transl: *Dynamics of the Radiation Belts of the Earth*). Moscow, Nauka, 1968.
131. U.S. Environmental Science Service Administration. *Solar Geophysical Data*. Boulder, Colo., ESSA Res. Labs., 1966–1970.
132. VAISBERG, O., and A. BOGDANOV. About structure and variation solar wind–Mars interaction region. *J. Geophys. Res.* (In press)
133. VAN ALLEN, J. A. Dynamics, composition and origin of corpuscular radiation trapped in the Earth's magnetic field. *In*, LeGalley, D. P., Ed. *Space Science*, pp. 226–274. New York, Wiley, 1963.
134. VAN ALLEN, J. A., and S. M. KRIMIGIS. Impulsive emission of ~40 keV electrons from the Sun. *J. Geophys. Res.* 70(23):5737–5751, 1965.
135. VERNOV, S. N., S. N. CHUDAKOV, P. V. VAKULOV, E. V. GORCHAKOV, P. P. IGNATIEV, N. N. KONTOR, S. N. KUZNETSOV, et al. A study of solar and cosmic radiation from the Venus 4 space probe. *In*, Champion, K. S. H., P. A. Smith, and R. L. Smith-Rose, Eds. *Life Sciences and Space Research* (Proc., 11th COSPAR Plenary Meet., Tokyo, May 1968), Vol. 9, pp. 203–214. Amsterdam, North-Holland, 1969.
136. VERNOV, S. N., A. E. CHUDAKOV, P. V. VAKULOV, E. V. GORCHAKOV, N. N. KONTOR, Yu. I. LOGACHEV, G. P. LYUBIMOV, N. V. PERESLEGINA, and G. A. TIMOFEEV. Propagation of solar and galactic cosmic rays of low energies in the interplanetary medium.

In, Somogyi, A., Ed. *Acta Physica, Acad. Scient. Hung., Proceedings, 11th Conference on Cosmic Rays*, Budapest, 1969, Vol. 29, Suppl. 2, pp. 459–469. Budapest, Akademiai Kiado, 1970.

137. VERNOV, S. N., E. V. GORCHAKOV, S. N. KUZNETSOV, Yu. I. LOGACHEV, E. N. SOSNOVETS, and V. G. STOLPOVSKIY. Particle fluxes in the outer geomagnetic field. *Rev. Geophys.* 7:257–280, 1969.
138. VERNOV, S. N., P. V. VAKULOV, E. V. GORCHAKOV, V. G. KURT, Yu. I. LOGACHEV, G. P. LYUBIMOV, and G. A. TIMOFEEV. The nature of propagation of fast particles in interplanetary space at various stages of increases in solar cosmic ray fluxes. *In, Trudy Mezhdunarodnogo Seminara po Probleme Generatsiya Kosmicheskikh Luchey na Solntse, 1970.* (Transl: *Proceedings, International Seminar on Solar Cosmic Ray Generation*), pp. 64–74. Moscow, 1971.
139. VERNOV, S. N., P. V. VAKULOV, and Yu. I. LOGACHEV. The radiation belts of the Earth. *In*, Blagonravov, A. A., Ed. *Uspekhi Sovetskogo Soyuza v Issledovanii Kosmicheskogo Prostranstva* (Transl: *Successes of the Soviet Union in Space Studies*), pp. 106–148. Moscow, Nauka, 1968.
140. WEBBER, W. R. Review of solar cosmic ray events. *In*, Hess, W. N., Ed. *NASA Symposium on the Physics of Solar Flares*, pp. 215–255. Washington, D.C., NASA, 1963. (NASA SP–50)
141. WEBBER, W. R. The spectrum and charge composition of the primary cosmic radiation. *In*, Flügge, S., Ed. *Handbuch der Physik (Kosmische Strahlung II)*, Vol. 46, pp. 181–264. Berlin, Springer, 1967.
142. WHANG, Y. C., and N. F. NESS. Observations and interpretation of the lunar Mach cone. *J. Geophys. Res.* 75:6002–6010, 1970.
143. WHIPPLE, F. J. A comet model. II. Physical relations for comets and meteors. *Astrophys. J.* 113:464–474, 1951.
144. WILLIAMS, D. J. Sources, losses, and transport of magnetospherically trapped particles. *In, Solar Terrestrial Physics, 1970. The Magnetosphere* (Proc., Int. Symp., Leningrad, May 1970), Pt. 3, pp. 66–130. Dordrecht, Holl., D. Reidel, 1972.
145. WILLIAMS, D. J., and G. D. MEAD. Nightside magnetosphere configuration as obtained from trapped electrons at 1100 kilometers. *J. Geophys. Res.* 70(13):3017–3029, 1965.
146. WILLIAMS, D. J., and N. F. NESS. Simultaneous trapped electrons and magnetic tail field observations. *J. Geophys. Res.* 71(21):5117–5128, 1966.
147. WINCKLER, J. R. The origin of energetic electrons in the Earth's environment. *In, Proceedings, International Seminar on Space Research*, p. 130. Leningrad, 1969.
148. ZHELEZNYAKOV, V. V. *Radioizlucheniye Solntsa i Planet* (Transl: *Radio Radiation of the Sun and Planets*). Moscow, Nauka, 1964.